CERN-ATS Report-2023-0004

gianluigi.arduini@cern.ch

LHC Triplet Task Force Report

G. Arduini, B. Bradu, K. Brodzinski, R. Bruce, F. Cerutti, A. Ciccotelli, G. Deferne, S. Fartoukh, P. Fessia, C. Garion, M. Karppinen, S. Le Naour, M. Liebsch, E. Page, T. Persson, D. Prelipcean, S. Roesler, M. Sabate Gilarte, C. Scheuerlein, M. Solfaroli Camillocci, H. Thiesen, P. A. Thonet, Y. Thurel, D. Tommasini, A. Verweij

Abstract

The excellent performance of the Large Hadron Collider (LHC) and the extension of Run 3 by one year have led to a significant increase of the expected integrated luminosity by the end of its operation and before the start of the High Luminosity LHC (HL-LHC), exceeding the design LHC integrated luminosity of 300 fb^{-1} for which the final focus region has been designed. The radiation dose accumulated by the components close to the Interaction Points (IPs) and resulting from the collision debris might approach or exceed the radiation limits that have guided the selection of the materials in the design of these components. A task force has been set-up to analyse the potential impact on machine performance and availability and identify mitigation measures. The results of the studies conducted by the Task Force are summarized in this report.

CERN-ACC-2023-0004
29/11/2023

Geneva, Switzerland

November 29, 2023

Contents

1 Executive Summary

The LHC is expected to deliver an integrated luminosity of at least 250 fb^{-1} during Run 3 in IR1 and IR5, significantly surpassing the total integrated luminosity of 300 fb^{-1} for which the final focus region has been designed. Initial estimates of the Run 3 performance conducted at the end of 2022 had shown that operation at high intensity and high availability could allow to approach a total integrated luminosity of $\approx$500 fb^{-1} before LS3 and the start of the High-Luminosity LHC. The radiation dose accumulated by the components close to the Interaction Points (IPs) and resulting from the collision debris might approach or exceed the radiation limits that have guided the design of these components. For 500 fb^{-1}, peak radiation doses of more than $\approx$30 MGy are expected in the coils of the triplet quadrupoles, $\approx$10 MGy in those of the IT skew quadrupoles (MQSX), $\approx$25 MGy in the coils of the non-linear (NL) IT correctors and up to 120 MGy in the coil of the warm D1 magnets (MBXW). During the same period, LHCb is expected to accumulate up to 30 fb^{-1} leading to peak radiation doses of up to $\approx$6 MGy in the coils of the triplet quadrupoles, less than 1 MGy in those of the IT skew quadrupoles, less than 2 MGy in the coils of the non-linear IT correctors, and up to $\approx$3 MGy in the super-conducting (SC) D1 magnets (MBX), all well below the design limits for the radiation resistance. The warm compensator magnets MBXWH amd MBXWS, installed on each side of the LHCb spectrometer dipole, are expected to reach up to $\approx$4 MGy and $\approx$11 MGy, respectively. The peak dose to the IR2 magnets of the long straight section is estimated to remain below 1 MGy by the end of Run 3, including the lead ion programme.

The statistical error of the results of the simulations is typically of the order of 5 % and the 3D dose distribution has been validated by means of absolute comparisons with BLM signals and dosimetry measurements as well as code inter-comparisons. However the measurement points are localized outside the coils and in significantly lower radiation fields and a precise quantification of the systematic uncertainty of peak dose values is currently out of reach. It must be highlighted that no additional safety factors have been added differently from the energy deposition estimates used to guide the mitigation measures against quenches.

The main magnet components affected by the radiation degradation are the polymers and polymer composites that are used to build the insulating system of the conductors or mechanical components, generally designed to transfer forces. The choice of the materials used has been made taking into account their radiation hardness at the design phase. The IT quadrupoles and the SC separation dipoles D1 (in IR2 and IR8) are expected to withstand accumulated doses of 30 MGy considering the well documented radiation effects on epoxy and epoxy-glass (coil-end spacers and collets). The IT correctors have been designed with a target of at least 7 MGy, likely a conservative estimate in the absence of precise experimental data for the insulator used. The warm magnets installed in the IRs (separation dipoles and spectrometer compensation dipoles) share the design concept and technologies of the MBW magnets installed in IR3 and IR7 and moderate damage is expected for radiation doses in the range of 75–90 MGy.

While the degradation of room temperature irradiated components is a continuous incremental process, it is not the case for irradiation in cryogenic conditions, because of the absence of diffusion and of oxygen. Both processes are suddenly activated when the magnets are warmed-up and exposed to oxygen as in case of a warm-up of the triplet. **Thermal cycles and venting to air of the IT coils should be therefore avoided, in particular in IR1 and IR5.** The possibility of preventing warming-up the triplets in case of an intervention on a magnet in the corresponding sector has been studied, though a full risks analysis should be performed. Although it might be

possible to maintain an inert atmosphere in the triplet, its temperature might approach the ambient one, depending on the length of the intervention.

It is quite improbable that radiation-induced magnet failure could appear as a result of the degradation of the electrical properties of the organic insulators, as the electrical properties start to degrade after the mechanical ones. It is therefore likely that a radiation-induced mechanical failure will provoke, as secondary effect, an electrical failure. This could occur as a result of a quench if the stored energy is sufficiently high (e.g. for the MQSX and MCBX circuits when operated at close to nominal currents). This suggests also that the early detection of polymer degradation via electrical testing is unlikely. Mechanical damage is linked to the failure of a component in a specific load configuration. Therefore, while mechanical tests at various levels of radiation exposure will provide a hint of how the material behaves, these must be complemented by an extremely precise knowledge of the construction details of the individual components and mechanical loads during operation, e.g. fibres orientation with respect to the main loads. The above considerations, together with the variability in the composition of commercial composites and the inevitable stochastic nature of the radiation effects, make a prediction of the doses at which failure would take place extremely difficult.

A series of irradiation tests have been launched to qualify the properties of polymers used in the MCBC and MCBY corrector magnets. These materials are also used in the fabrication of the IT corrector magnet coils. Most of the tests have been performed in ambient conditions, so far. First results indicate that the irradiation environment (e.g. temperature, atmosphere) have a significant influence on the effect of radiation on the thermo-mechanical, mechanical and electrical properties of these materials. It appears that aging effects inferred from these irradiation tests are likely pessimistic. Additional tests are planned though the results are expected mainly in 2024.

The continuation of the above tests is recommended in order to gather additional information on the behaviour of the materials used in the fabrication of the IR magnets in view of the operation of the IR2 and IR8 triplets during HL-LHC and as input for the design of magnets for future accelerators.

A softening of the coil impregnation resin at ambient temperature might change the magnet training performance after a thermal cycle. So far this behaviour has been observed in the MCBX magnets, mainly in the *high-radiation regions* (IR1 and IR5), and for the MQSX magnets though, for the latter, the difference between *high-radiation regions* and *low-radiation regions* is less marked. The estimated accumulated radiation doses for the MCBX and MQSX magnets are by at least a factor two lower than the design radiation levels. In all cases, the increase in the number of training quenches has been observed only after a thermal cycle and in no case during operation, while radiation dose is accumulated in cryogenic conditions. Almost no training quench has been observed in the MCBX magnets below 300 A, so far. In the other triplet circuits and in the D1 magnets in IR2 and IR8 no clear statistical sign of degraded quench performance has been noted since the start of the LHC. The existing non-conformities in the IT circuits are not related to the accumulated radiation dose during operation.

The degradation of the training performance of the MCBX magnets is not correlated with appreciable variations in the results of High Voltage (HV) tests or Transfer Function Measurements (TFM). The QPS has insufficient resolution and sampling rate to provide meaningful data. The accuracy of all the above measurements is significantly affected by the changing environmental conditions to which the warm part of the circuits are subject and for that reason they do not promise to provide a reliable tool for early detection of circuit degradation due to irradiation.

Different failure scenarios have been briefly studied to assess their impact on machine performance and possible mitigation measures:

- failure of one of the main IT quadrupoles will not allow operation at low–β^* and will likely prevent operation if occurring in IR2 or IR8. Some possible optics solutions, allowing to operate, at least in degraded mode, in case of an IT main quadrupole failure in IR1 and/or IR5, have been sketched but their study and evaluation would require additional time. **Further optics design work in this direction is recommended**.
- High-intensity low-β^* operation in case of failure of up to 2 MCBX orbit correctors per plane and side of the IP should be possible but will require the operation of the remaining MCBX at currents of $\approx$ 400 A. In case the available circuit is MCBX3, possible beam-based realignment might be required with transverse offsets of the IT quadrupoles of up to $\pm 100 - 150$ µm to be applied. In case of failure of the three MCBX in the same plane and side of the IP more complex configuration of the crossing bumps extending further in the IR could be feasible but would require additional studies.
- The failure of a MQSX magnet on one side of IP1 or IP5 will have an impact on the luminosity performance on that IP with a potential reduction of the integrated luminosity of $\approx$25 % in the worst case (failure of MQSX.3L1) assuming the present optics and machine configuration[1]. The same applies for a failure of a MQSX magnet on one side of IP2 during ion operation. In case of failure of the MQSX on both sides of an IP, operation will be likely limited to $\beta^* \approx$85 cm or larger in that IP. Compensation by a tilt of the triplet quadrupoles has been considered but it would require the warm-up of the triplet to minimize the risk of W-bellow buckling and for that reason it is not considered a viable option. Installation of a warm skew quadrupole in the affected IR appears to be the only possible action able to mitigate the effect of the failure of one of the MQSX providing the largest corrections in IR1, IR2 (for ion operation) and IR5.
- No evident show-stopper has been identified to continue operation at β^* down to 30 cm in case of failure of one or more of the NL IT correctors, though lower beam lifetime and possibly more complex operational procedures might be required (e.g. to compensate for the dependence of tune and coupling on crossing angle or for the dependence of the amplitude detuning on β^*).
- Operation with 5 out of 6 MBXW magnets composing the D1 separation dipoles in IR1 and IR5, in case of a failure of one of the MBXW appears to be possible at 6.8 TeV. This would require operating the D1 dipoles, left and right of the IP to 900 A by swapping the present power converters with the previous thyristor-bridge power converters that are still installed as "hot spares". A larger b_3 error is expected because of saturation. **The possibility to operate the magnet and the power converter at** 900 A **should be validated with a heat run and the impact on dynamic aperture and possible correction should be further studied.**

One complete set of IT cryo-magnets is available at CERN, one of them (LQXB-01 — Q2 magnet) is being consolidated following the damage that occurred during the pressure test performed in 2007 in the tunnel. Additional spare magnets are stored at CERN to build Q1 or Q3 cryo-magnets. This process would take approximately 2 years. There are no MQXB magnets

[1]MQSX corrections have been reproducible so far. A polarity reversal of the triplet quadrupoles might require different corrections as the exact localization of the quadrupole misalignments within the triplet is not known.

available to build an additional Q2 cryo-magnet. The replacement of any of the SC magnets in the IT will require a significant time (up to 1 year) and a detailed procedure for the replacement of a IT SC magnet does not exist but it is being defined by TE/MSC. **The Task Force fully support the documentation of a procedure for the replacement of an IT SC magnet with high priority.**

The deterioration of the mechanical properties of polymers used in the construction of the coils can lead to a degradation of the magnet training performance. Radiation-induced embrittlement of the cable insulation in the magnet coils, combined with mechanical load, can lead to electrical failure in case of a quench if the magnet stored energy is sufficiently high. **It is recommended to reduce as low as reasonably possible the HWC and pre-cycle currents of the IT corrector circuits in the *high-radiation regions* IR1 and IR5, compatibly with the operational requirements.** Below 300 A the energy stored in the corrector magnets is considered to be sufficiently low to avoid damage in case of a quench, in addition the probability of quench at these currents is considered to be low, from present experience. Minor changes can be implemented for the HWC current of the IT quadrupoles taking into account that the machine is going to be operated at 6.8 TeV during Run 3 while the pre-cycle currents were already limited to 3.5 TeV equivalent values and cannot be further reduced to preserve cycle-to-cycle magnetic reproducibility. **These measures have already been implemented for the 2023 Run with no visible impact on operation. It is proposed to apply the reduction of the HWC and pre-cycle currents also in IR2 and IR8 in 2024, compatibly with the operational requirements.**

The radiation dose is not distributed uniformly in the triplet and D1 coils and the position of its maxima depends on:

- the plane and sign of the crossing angle;
- the beam-screen orientation;
- the triplet polarity, presently FDF for the quadrupoles Q1/Q2 and Q3 (i.e. Q1 is focussing in the horizontal plane for the beam outgoing from the IP).

The sign of the crossing angle at the IP can only be changed in the vertical plane and this feature has already been used during Run 2 to redistribute the radiation dose and lower its peak value in IR1.

A significant redistribution of the radiation dose can be obtained by reverting the polarity of the triplet and swapping the crossing angle plane from V/H in IR1/5, respectively, to H/V (so-called RP — Reverse Polarity — configuration). The implementation of such optics starting from 2024 onward would allow to reduce the peak radiation dose to the triplet quadrupoles by close to 25 % with respect to the dose expected with the present optics configuration and maintain the maximum value at 24 MGy for an integrated luminosity of 500 fb^{-1}, assuming a crossing angle decrease along the fill and crossing angle polarity change in IR1 after the production of half of the luminosity target for 2023. An important reduction of the dose at the coil heads of the first MBXW magnet (IP side) is also expected (from 120 MGy to 80 MGy in IR1). In the absence of a crossing angle polarity change during 2023, the peak radiation dose in the triplet quadrupoles will increase to 25 MGy, still providing a significant reduction. An optics compatible with the aperture requirements for high intensity operation, has been designed with a squeeze down to 60/18 cm and potentially to 50/15 cm. The design of the Van der Meer (VdM) optics and the beam dynamics validation studies are ongoing showing extremely good results for beam-beam effects.

The studies performed so far indicate that the crossing angle plane rotation required to minimize the peak radiation dose with the RP configuration is incompatible with the AFP programme in

IR1 and it requires the rotation of some of the CMS-PPS roman pots in IR5 to maintain acceptable sensitivity.

The inversion of the polarity of the triplet quadrupoles can be achieved by inverting the output of the corresponding power converters. This HW modification requires the fabrication and installation of dedicated connection pieces. HWC is then necessary to verify the correct functionality of the circuit. The HW modification and the corresponding HWC should be performed at least in IR1 (both sides of the IP) to confirm the feasibility of operating the triplet with reverse polarity. A series of beam tests is also necessary for validating aperture requirements and optics correction capability.

The implementation of the Reverse Polarity configuration, starting from the 2024 Run is recommended as the most effective action allowing to minimize the peak radiation dose to the IR magnets for a given luminosity, pending the HW modification validation in IR1, the results of the additional beam dynamics simulations above mentioned and the beam tests with at least IR1 operated with reversed polarity. The reduction of the dose to the IT magnets will minimize the risks of performance degradation in case a sector warm-up is required (e.g. to replace an arc magnet) and it would preserve the magnets as possible spares (in particular for the Q2 quadrupole) for the IR2 and IR8 triplets during HL-LHC operation. A possible stepwise implementation of the RP configuration, including an intermediate stage, being validated with beam-beam simulations, compatible with Forward Physics in IR1 and IR5, not requiring crossing plane rotation and therefore based on a round optics, has been analyzed in detail in terms of peak radiation dose in Section 11, also considering the reduced luminosity production in 2023. The corresponding peak radiation doses by the end of 2025 and after a possible extension of the run to 2026 are summarized in Table 1, compared to the ones obtained with an earlier implementation of the full RP configuration as well as to those reached without the RP configuration implementation. The considered stepwise approach is neutral in terms of radiation increase, with respect to a direct implementation of the RP configuration in 2024, for IR1 already at the end of 2025 and for both IR1 and IR5, should Run 3 be extended by an additional year.

Configuration	Peak dose [MGy] at the end of 2025 ($430\,\mathrm{fb}^{-1}$)	Peak dose [MGy] for extended operation ($530\,\mathrm{fb}^{-1}$)
Present	26.5–27 (Q2A in IR1) 26.5–27 (Q2B in IR5)	33–33.5 (Q2A in IR1) 33–33.5 (Q2B in IR5)
RP configuration	20.5 (Q2A in IR1) 20.5 (Q2A in IR5)	25 (Q1 in IR1) 26 (Q2A in IR5)
Stepwise implementation	20.5 (Q2A in IR1) 22.5 (Q2B in IR5)	23 (Q1 and Q2A in IR1) 25.5 (Q2A in IR5)

Table 1: Peak radiation doses expected by the end of 2025 and after an additional hypothetical run in 2026.

While the proposed implementation of the RP optics allows to maintain the peak radiation doses in the main triplet quadrupoles below the expected radiation dose limit of 30 MGy, the radiation dose at the MQSX approaches the expected radiation limit and the failure of one of these magnets, in particular at the left of IP1 or at the right of IP5 (for proton operation in the present configuration) and at the left of IP2 (for ion operation), would limit significantly the performance of the LHC. **It is recommended to prepare the necessary HW (LQS with inserted stainless steel a-C coated vacuum chamber, transition chambers, the corresponding power converter) and**

perform some preparatory work (e.g. tracing of equipment position, installation of supports, preparation of water connections, etc...) for the possible installation of at least two LQS magnets on the non-IP side of D1 in a reduced time.

2 Introduction

The excellent LHC performance and the extension of Run 3 by one year have led to a significant increase of the expected integrated luminosity by the end of LHC operation and before the start of HL-LHC, exceeding the design LHC integrated luminosity of $300\,\mathrm{fb}^{-1}$ for which the final focus region has been designed. The radiation dose accumulated by the components close to the Interaction Points (IPs) and resulting from the collision debris might approach or exceed the radiation limits that have guided the selection of the materials in the design of these components. A task force has been set-up to analyse the potential impact on machine performance and availability and identify mitigation measures.

2.1 Mandate

This task force is mandated by the LHC Machine Committee (LMC) to carry out a full analysis of the impact of radiation on the lifetime of equipment in the LHC Inner Triplet (IT) regions and to propose possible mitigation measures. This shall include:

- a review of the damage limits currently assumed for all magnetic components;
- a review of how these damage limits are calculated to determine confidence limits for Run 3 operation;
- possible tests and measurements that could be made to validate these limits;
- identification of all weak components;
- a study of measurement methods that could give an early warning on potential failure;
- a study of possible mitigation measures, including:
  - beam optics choices;
  - operation modes;
  - how to limit the stresses on these magnets;
  - compensation with additional warm magnets;
  - installation of shielding;
- a review of the spares situation and implications for the HL-LHC era (LHCb/ALICE).

2.2 Deliverables

The task force shall deliver a final report on its findings and present a summary to the LMC. In addition to summarising the analysis described above the Task Force shall put forward a proposal for optimising the triplet lifetime during Run 3 and report on the expected lifetime of the triplets in Insertion Region (IR)2 and IR8 during the High Luminosity LHC era. An intermediate report shall be presented at Chamonix 2023 [1].

The presentations and minutes of the meetings are available in [2].

2.3 Structure of the report

Section 3 of this report summarizes the expected Run 3 LHC integrated luminosity as estimated at the end of 2022 and Section 4 the corresponding radiation levels in the IT regions (including the D1 — separation — magnets). After a review of the expected radiation effects on the magnet components (Section 5) the IT magnets' training performance is reviewed in Section 6 together with the evolution of the measured magnet electrical parameters. The possibility of early detection of radiation-induced degradation based on these measurements is also discussed. Section 7 describes the possible magnet failure scenarios, their implications for operation and performance and conceivable mitigation measures, when available. Section 8 outlines a series of preventive actions that can be envisaged to minimize the risk of occurrence or the impact of the above magnet failures. Section 9 illustrates the expected radiation levels in IR2 and IR8 during HL-LHC operation, considering also the possible upgrade scenarios for ALICE and LHCb, and the implications for magnet performance. The IT and D1 magnet spare inventory is presented in Section 10. An updated luminosity and radiation evolution estimate, considering the 2023 LHC performance, is presented in Section 11 together with its possible implications, including the case of an extension of the operation to 2026. A summary of the findings and the main recommendations of the Task Force are presented in Section 1.

3 Expected performance during LHC Run 3

The main parameters impacting on the yearly performance of the LHC when operating at a small β^* in the range of 30 cm are essentially the following:

- the number of days of scheduled physics time, namely $T_{\mathrm{OP}} = 97$ days rounded up to 100 days for 2023, and expected to be 16 and 19 weeks, rounded to 110 and 130 days, for 2024 and 2025, respectively [3].
- the so-called Stable Beam (SB) efficiency, namely $\eta_{\mathrm{SB}} = T_{\mathrm{SB}}/T_{\mathrm{OP}}$, which is the ratio between the time actually spent in stable beam and the scheduled physics time. The average η_{SB} efficiency was 32 % in 2022, but with a peak of 50 % in the last 32 days of operation [4].
- the maximum possible levelled luminosity, namely L_{Lev}, depending on the cryogenic limit of the inner triplet ($L_{\mathrm{cryo}} = 2.0 \times 10^{34}\,\mathrm{cm}^{-2}\mathrm{s}^{-1}$ in 2022, it could be increased to $2.2 \times 10^{34}\,\mathrm{cm}^{-2}\mathrm{s}^{-1}$ in the future), but also on the average pile-up limit per bunch crossing ($\langle\mu\rangle_{\mathrm{max}} = 54$ in 2022, 60 in 2023, with the possibility to reach 65 during Run 3). The pile-up limit implies a limit in the levelled luminosity:

$$L_{\mathrm{Lev}} \leq L_{\mu} \overset{\mathrm{def}}{=} \frac{N_b f_0}{\sigma_{\mathrm{tot}}} \times \langle\mu\rangle_{\mathrm{max}} \,, \tag{1}$$

  with $\sigma_{\mathrm{tot}} = 81$ mb denoting the total inelastic cross-section, $f_0 = 11.25$ kHz the LHC revolution frequency, and N_b the number of collision pairs at IP1 and IP5. The levelled luminosity can therefore be optimized when the IT cryogenic limit and the pile-up limit coincide, namely $L_{\mathrm{Lev}} \equiv L_{\mathrm{cryo}} \equiv L_{\mu}$. As illustrated in Figure 1, this is actually the case for

$L_{\mathrm{Lev}} = 2.0\,(2.2) \times 10^{34}\,\mathrm{cm}^{-2}\mathrm{s}^{-1}$, $\langle\mu\rangle_{\mathrm{max}} = 60\,(65)$, and $N_b \sim 2400$ (limited in Run 3 by the heat-load from electron cloud in the arcs [5]).

- the bunch population, limited to $Q_b = 1.8 \times 10^{11}$ p/b in Run 3 by a series of existing LHC sub-systems [6], is presently maintained below $Q_b = 1.6 \times 10^{11}$ p/b because of a recently observed abnormal beam-induced RF heating being investigated [7].

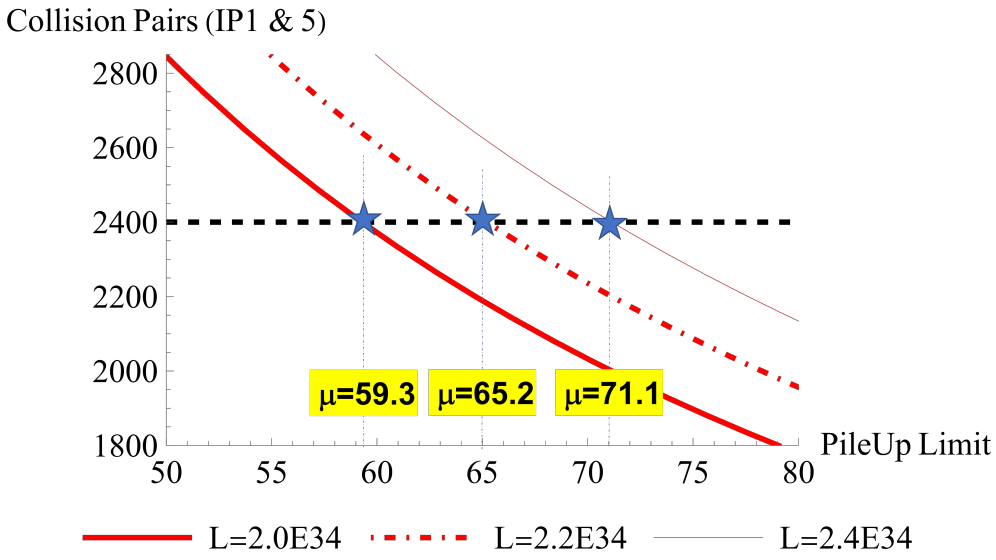

Figure 1: Best possible matching between the pile-up limit and the cryo-cooling capacity of the inner triplet, as a function of the number of collision pairs at IP1 and IP5, regardless of any optics or other beam parameters.

On the other hand, the yearly performance of the LHC mildly depends, at the level of a few permil, on the bunch length (levelled in SB to about 1.25 ns to mitigate the injection kicker — MKI — heating), and on the transverse normalized beam emittances (over the range of 2–3 µm).
The expected yearly integrated luminosity, normalised to 50 days of SB (e.g. $T_{\mathrm{OP}} = 100$ days and $\eta_{\mathrm{SB}} = 50$ %), is plotted in Figure 2(a) as a function of the bunch charge, for various possible combinations of IT cryogenic limit ($L_{\mathrm{cryo}} = 2.0 \rightarrow 2.2 \times 10^{34}\,\mathrm{cm}^{-2}\mathrm{s}^{-1}$), pile-up limit ($\langle\mu\rangle_{\mathrm{max}} = 60 \rightarrow 65$), and different numbers of collision pairs at IP1 and IP5: $N_b = 2452$, which is the upper theoretical limit for the 36b-8b4e hybrid filling scheme [8], and $N_b = 2345$ corresponding to the 2023 pre-Technical Stop (TS)1 LHC filling scheme to cope with the losses at injection and the LHCb request for isolated nominal bunches. Figure 2(b) shows the yearly performance for very different optics parameters corresponding to the so-called Reversed Polarity (RP) optics which will be introduced in section 8.2, namely a rather aggressive flat optics with $\beta^* = 50$ cm in the (rotated) crossing plane of ATLAS and CMS, $\beta^* = 15$ cm in the other plane, and a half crossing-angle $\Theta_X/2$ of 145 µrad. Although these optics parameters would lead to an increase of the virtual luminosity by about 35 % (and to a sizeable lengthening of the levelling time and optimal fill length), the increase of yearly performance is quite modest at constant stable beam efficiency.

The integrated luminosity expected for ATLAS and CMS till the end of Run 3 is summarised in Table 2, in the worst and best case of a stable beam efficiency of $\eta_{\mathrm{SB}} = 32$ % and 50 %, respectively, clearly pointing towards an overall performance close to 500 fb^{-1} at the end of the

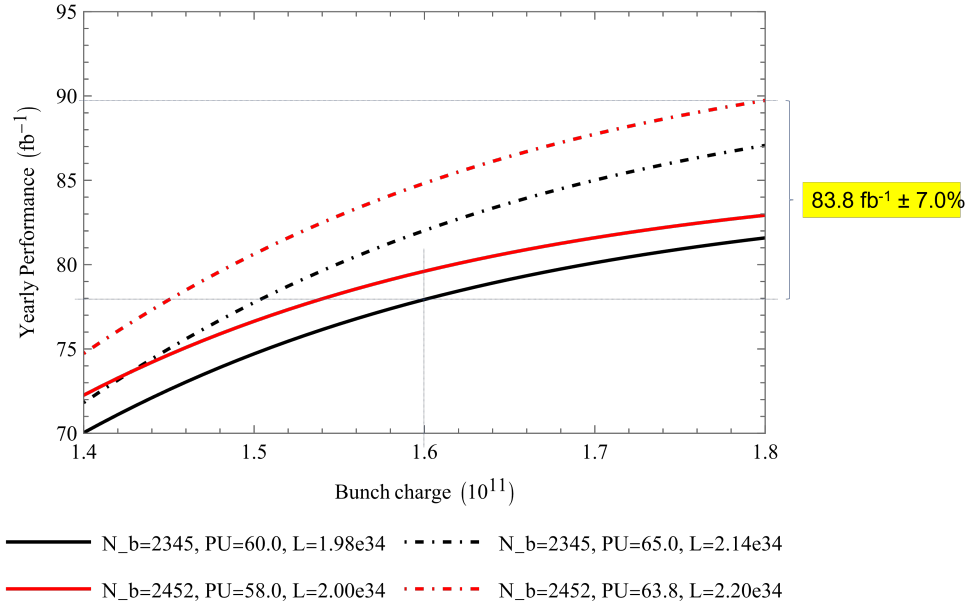

(a) $\beta^* = 30$ cm (nominal Run 3 collision optics) with $\Theta_X/2$=160 µrad at the end of β^*-levelling

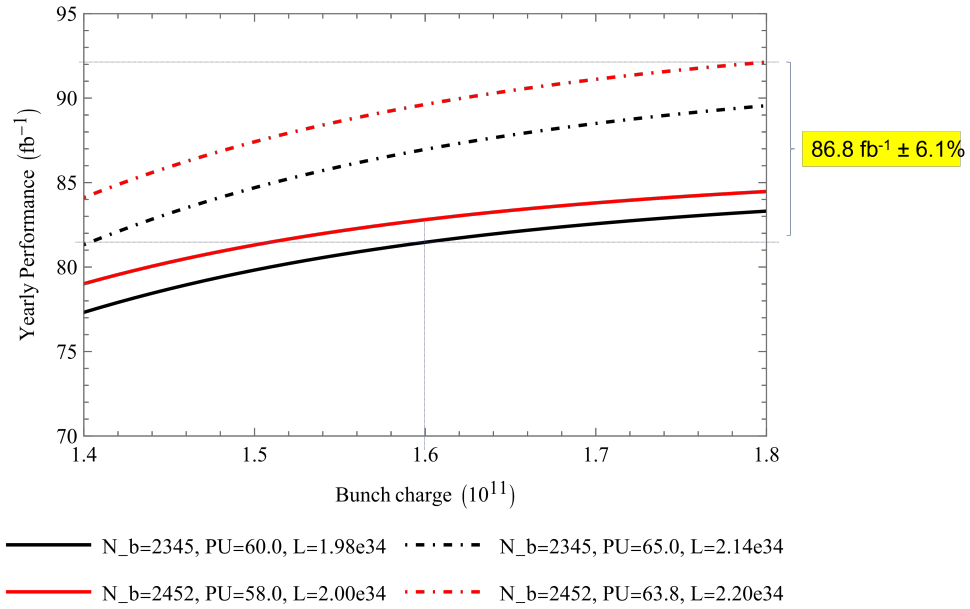

(b) $\beta^*_X = 50$ cm and $\beta^*_{||} = 15$ cm (flat optics), with $\Theta_X/2$=145 µrad at the end of β^*-levelling

Figure 2: LHC integrated performance for the nominal optics (top) and reversed polarity (RP) triplet optics (bottom) for 50 days of physics data taking (e.g. $T_{\mathrm{OP}} = 100$ days and $\eta_{\mathrm{SB}} = 50$ %), as a function of the bunch population, and its uncertainty for various combinations of number of bunches, pile-up limit and cryo-cooling capacity of the inner triplet. An effective cross-section of 100 mb has been assumed for the proton burn-off calculation, and the average turn-around time of 4.5 h has been considered for the calculation of the optimal fill length.

2025 run. For simplicity, a luminosity of 80, 90 and 100 fb^{-1} will be assumed in all the rest of the paper for 2023, 2024 and 2025, respectively, except in the last two sections 11 and 1 where the performance loss in 2023 will be duly considered.

LHC exploitation period	$\eta_{\text{SB}} = 32$ %	$\eta_{\text{SB}} = 50$ %
Run1+Run2+2022	233.2 (for CMS, and 224.4 for ATLAS [9])	
2023 (100 days)	53.6 ± 3.8	83.8 ± 5.9
2024 (110 days)	58.9 ± 4.2	92.1 ± 6.5
2025 (130 days)	69.7 ± 4.9	108.9 ± 7.7
Total	415 ± 13	518 ± 20

Table 2: Integrated luminosity $\left[\text{fb}^{-1}\right]$ estimate for ATLAS and CMS till the end of Run 3 (for the nominal 30 cm collision optics).

LHCb has collected an integrated luminosity of $11.2\,\text{fb}^{-1}$ [9], so far. While the levelled luminosity is presently limited following an incident affecting the VeLo detector [10, 11], it is expected to reach the target of $1.7 - 2.0 \times 10^{33}\,\text{cm}^{-2}\text{s}^{-1}$ (limited by a pile-up of $\langle\mu\rangle = 6 - 7$ for the $N_b = 2007$ collision pairs in LHCb which are expected for the 36b-8b4e hybrid filling scheme [8]) in 2024 and 2025. Neglecting the 2023 production, and accounting on a total 240 remaining scheduled physics days in 2024 and 2025 (see Table 2), the integrated luminosity delivered to LHCb by the end of Run 3 should then range in between 23.5 ± 1.0 fb^{-1} and 30.5 ± 1.5 fb^{-1}, when estimated with a stable beam efficiency of $\eta_{\text{SB}} = 32$ % and 50 %, respectively.

4 Expected radiation levels in the LHC Interaction Regions at the end of Run 3

Proton–proton collisions at 13.6 TeV center-of-mass energy, as taking place in the ongoing LHC Run 3, generate on average about 120 particles per collision, with large fluctuations from one collision to another. At an instantaneous luminosity of 2×10^{34} cm^{-2} s^{-1} – regularly reached in IP1 and IP5 – and owing to an inelastic cross section of 80 mb (including diffractive events), this particle debris carries 1.75 kW to either side of the IP. While the vast majority of the collision products is intercepted by the 4π high luminosity detector (ATLAS or CMS), most of the debris power is carried by few forward energetic particles that escape the experimental cavern through the aperture of the TAS absorber (protecting the first final focus quadrupole Q1) and impact the accelerator elements in the LHC tunnel. Such an impact poses important challenges, in particular in terms of total power absorbed by the cold triplet string and to be evacuated by the cryogenic system, as well as peak energy deposition in its superconducting (SC) coils. The latter has a twofold relevance. The steady power density (in mW/cm^3) corresponding to the levelled instantaneous luminosity should remain safely below the quench limit, such as not to induce a sudden and detrimental transition to the normal-conducting (NC) state. On the other hand, the maximum integrated dose (in MGy) corresponding to the integrated luminosity should not exceed the damage limit, which is determined by the coil insulator material. Dedicated Monte Carlo simulations have been carried out since the LHC design phase to evaluate these quantities and implement mitigation measures [12, 13, 6].

In the context of this report, we mainly focus on the accumulated dose in the SC coils of the Q1–Q3 quadrupoles and the various corrector magnets embedded in the triplet cryostats, as well as the NC (SC) separation dipole D1 that follows the triplet on the non-IP side of IR1 and IR5 (IR2 and IR8). The 3D dose distribution is calculated by FLUKA [14, 15, 16], thanks to a detailed IR model, which has been validated by means of absolute comparisons with the measured Beam Loss Monitor (BLM) signals [17, 18]. The IP collisions are simulated with the included DPMJET event generator [19, 20, 21] and subsequent particle showers are tracked down to low energies (typically 100 keV, except for electrons/positrons — 1 MeV — and neutrons — thermal energy) to produce energy deposition maps across the geometry. In particular, dose values in the coils are assessed with a radial resolution of 3 mm or not exceeding the cable thickness, an azimuthal resolution of 2°, and a longitudinal resolution of about 10 cm. Their statistical error is typically of the order of 5 %. On the other hand, the variety of uncertainty sources (such as the multiple physics models involved, the geometry and material description, the magnetic field implementation, the scoring algorithm, etc.) prevents a thorough quantification of the systematic error. While the accuracy achieved in the BLM signal reproduction, which is typically of few tens of percent, cannot directly apply to peak dose values in the magnet coils, it is worth recalling that the same degree of agreement was obtained for the latter ones from code inter-comparisons, namely between FLUKA and MARS [13, 22].

4.1 Inner Triplets and superconducting D1 (IR2/IR8)

Figure 3 displays, as a function of the distance from the IP, the peak dose in the coil transverse plane, on which the 2D dose distribution is strongly polarized along the vertical and horizontal axis, as reported in Figure 4 for the longitudinal maximum of the IR1 and IR5 triplet, respectively.

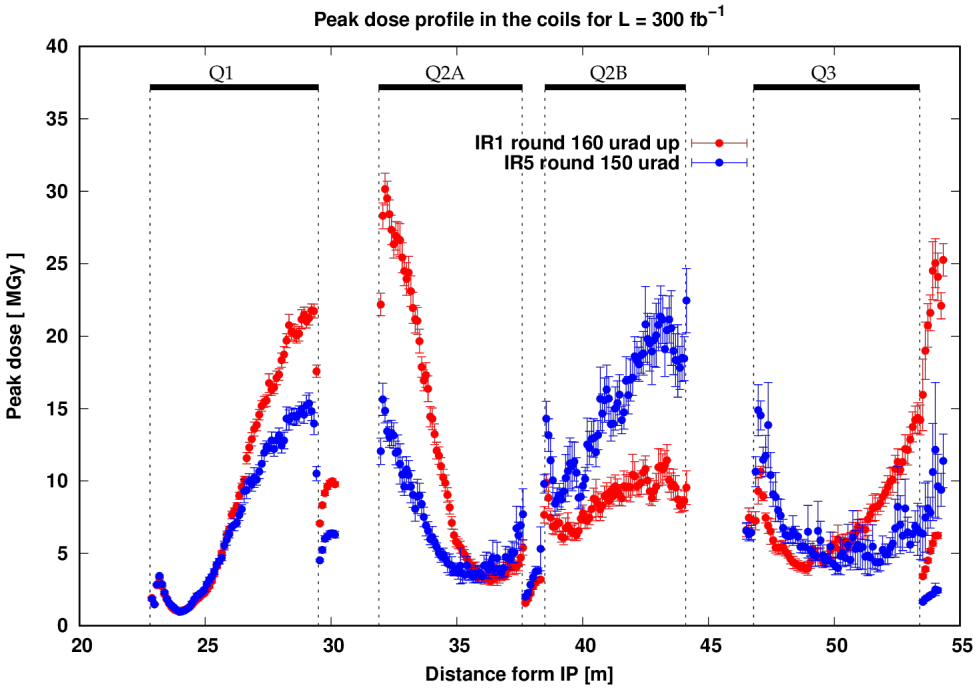

Figure 3: Longitudinal profile of peak dose in the coils of the IR1 (red) and IR5 (blue) triplet. Corrector magnets are included, outside the main quadrupole length (at the non-IP extremity of Q3, the lower curve corresponds to the dipole corrector and the higher curve to the innermost high order correctors). Error bars represent the statistical uncertainty. For illustration purposes, values refer here to 7 TeV proton beam operation with the indicated crossing angle and are normalized to a (slightly conservative) p–p inelastic cross section of 85 mb and an integrated luminosity of 300 fb^{-1}.

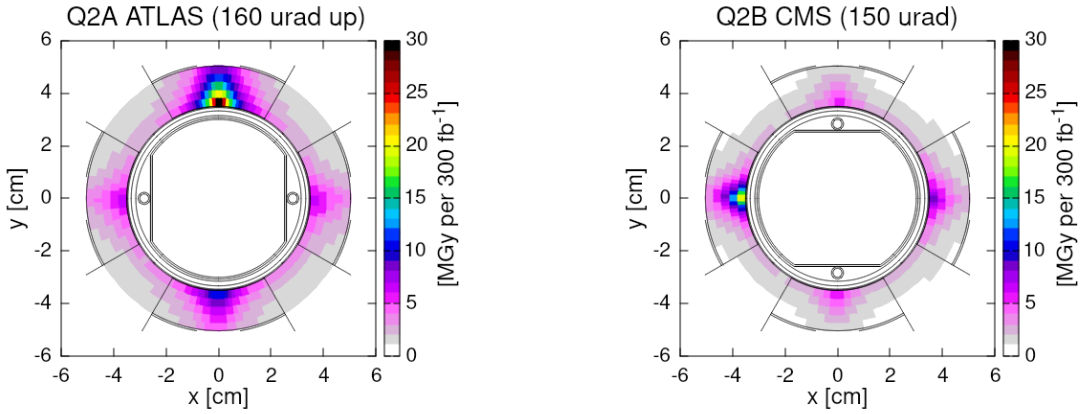

Figure 4: Transverse dose distribution at the maximum of the ATLAS (left) and CMS (right) profile of Figure 3.

Despite the identical magnetic configuration of the Q1-Q2-Q3 quadrupoles, which is focusing-defocusing-focusing (FDF) on the horizontal plane for the outgoing proton beam, the IR1 and IR5

curves are significantly different, because of the orthogonal crossing plane. In fact, the collision debris, which are mostly positively charged, preferentially travel on the crossing plane and, as a result, one can appreciate the steeper dose rise induced by Q1 on its defocusing vertical plane, which is the crossing plane in ATLAS. The same feature can be observed in Q3, where, however, the hot spot is no longer at the top (as in the left panel of Figure 4, reflecting the upward crossing) but moved to the bottom, due to the Q2 bending effect. In the case of the CMS horizontal crossing, the latter is equally responsible for the displacement of the hot spot from the external side (at positive x in Q1 and the first half of Q2A, again reflecting the outgoing beam direction) to the internal side (at negative x as in the right panel of Figure 4).

Contrary to horizontal crossing, vertical crossing allows for the inversion of the beam transverse direction, i.e. the alternate adoption of upward and downward crossing. This flexibility has been profitably exploited since the middle of Run 2, in order to equalize the dose spot at the top and at the bottom and to significantly reduce it, making the maximum dose of the ATLAS triplets quite close to the one of the CMS triplets [23]. This is apparent in Figure 5, where the maximum dose evolution in the most (and least) impacted quadrupoles is projected until the end of Run 3 in 2025 (see also Tables 18 and 19 in Appendix B for more details).

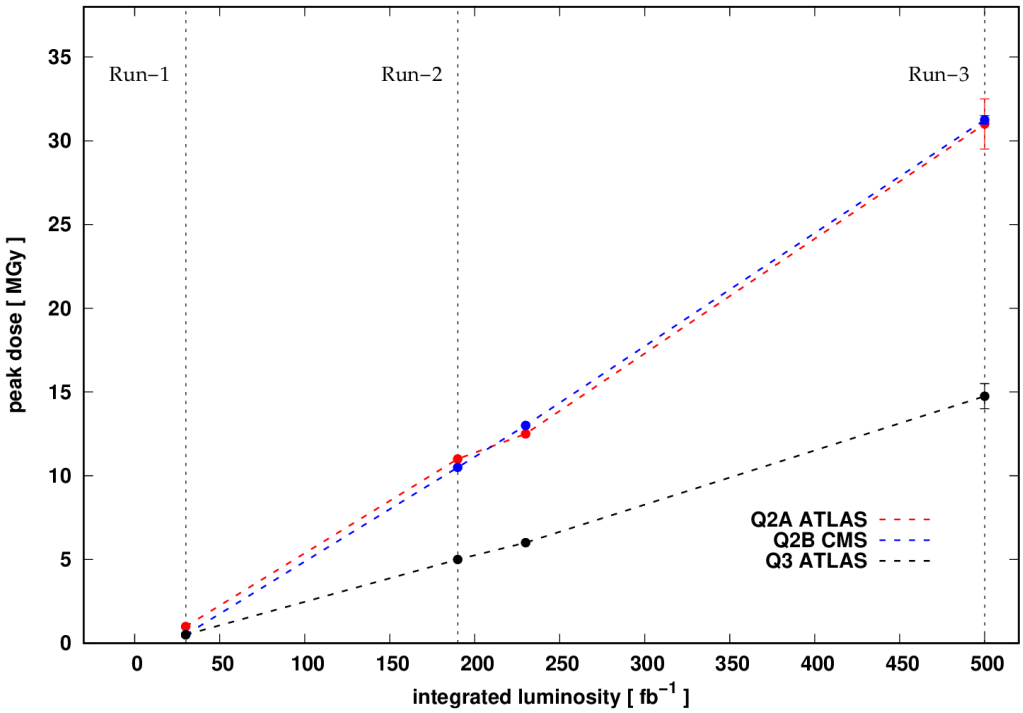

Figure 5: Maximum dose in the indicated most and least impacted quadrupoles as a function of delivered luminosity. Here realistic cross section values have been adopted as a function of the collision energy. The change of slope in the ATLAS triplet reflects the inversion of the angle sign for vertical beam crossing. A forecast of 80, 90 and 100 fb^{-1} is assumed for 2023, 2024 and 2025, respectively. The error bars at the end of Run 3 indicate the margin between the more favourable configuration, featuring a crossing angle decrease along the fill and – in ATLAS – the upward/downward swap in the middle of 2025, and the less favourable configuration, with constant crossing angle and ATLAS crossing swap only at the beginning of 2024.

The design limit of 30 MGy, corresponding to the assumed damage threshold of the employed insulator, turns out to be only slightly surpassed in both insertions after a total integrated luminosity of 500 fb^{-1}. In the absence of the regular upward/downward crossing inversion in ATLAS, it was originally predicted to reach it in IR1 already after 300 fb^{-1}, which was the considered luminosity target. It is worth pointing out that a safety factor of 3 was applied when defining the design limit in terms of instantaneous power density, such as to compensate for the systematic uncertainty of the energy deposition estimate and the quench limit. However, no safety factor has been applied for the accumulated dose.

Figure 6 shows the evolution for the short corrector magnets (see Section 5.1 for a description of the IT magnet layout). Dose values are significantly lower for the orbit corrector dipoles, thanks to their larger aperture, and the skew quadrupoles, where the coils sit outside the horizontal and vertical planes (see also Tables 18 and 19 in Appendix B for more details). They approach instead the main quadrupole levels for the innermost high order correctors at the non-IP extremity of the triplet, namely the dodecapole (MCTX) and the skew octupole (MCOSX) in IR1. Nonetheless, the design target for the radiation hardness of the insulator employed in the corrector coils is 7 MGy (see Section 5.1.2).

The dependence of the resulting peak dose on the magnetic configuration of the triplet (FDF in the present optics), the crossing plane, and the crossing angle sign and magnitude, was highlighted above. Among the ruling factors, one should mention in addition the beam energy as well as the (fixed) orientation of the beam screen. In fact, the rectellipse shape [24, 25] of the latter introduces an asymmetry, since the particle debris are more spread-out in the plane where flat parts of the beam screen are located (e.g., in the horizontal plane of the ATLAS insertion, where the beam screen has the H orientation, limiting the mechanical aperture horizontally), leading there to a lower peak dose, and conversely for the orthogonal plane. On the other hand, no substantial dependence on emittance, β^* and bunch-length was observed from simulations.

The LHCb insertion (IR8) is quite special, in view of its asymmetric layout and the presence of the detector spectrometer and the three associated NC compensator dipoles between the two ITs (two — MBXWH and MBXWS — on the left of the IP and one — MBXWS — on the right of the experimental cavern, on the IP side of the right triplet), featured also by the ALICE insertion (IR2). The spectrometer bump, combined with the external crossing angle, alters profoundly the collision debris propagation in the triplet and the resulting dose distribution, as recently published [26]. The LHCb upgrade carried out in the last Long Shutdown (LS) 2 has enabled the objective of collecting 25–30 fb^{-1} during Run 3 at an instantaneous luminosity of 2×10^{33} cm^{-2}s^{-1}, after the installation of a new absorber (TANB) protecting the recombination dipole D2, mostly from neutral particles emerging from IP8. Based on this expectation, assuming external vertical crossing, alternate LHCb spectrometer polarity, and taking into account the estimated dose accumulated so far, mainly produced with external horizontal crossing (which gives a different peak dose picture), a dose maximum of 6 MGy is predicted to be reached in the SC coils of the Q1 magnet at the right side of the IP, by the end of Run 3. This maximum is located on the IP side of the magnet, as a result of the TAS absence. The asymmetry of the vacuum chamber on the two sides of IP8 leads to only 4.5 MGy in the left Q1 at the same extremity. The most impacted high-order correctors would get less than 2 MGy, and 3 MGy is the maximum for the superconducting D1, at its non-IP extremity.

The ALICE luminosity targets pose no threat in terms of dose to the IR2 magnets of the Long Straight Section (LSS), which is estimated to remain below 1 MGy by the end of Run 3, including

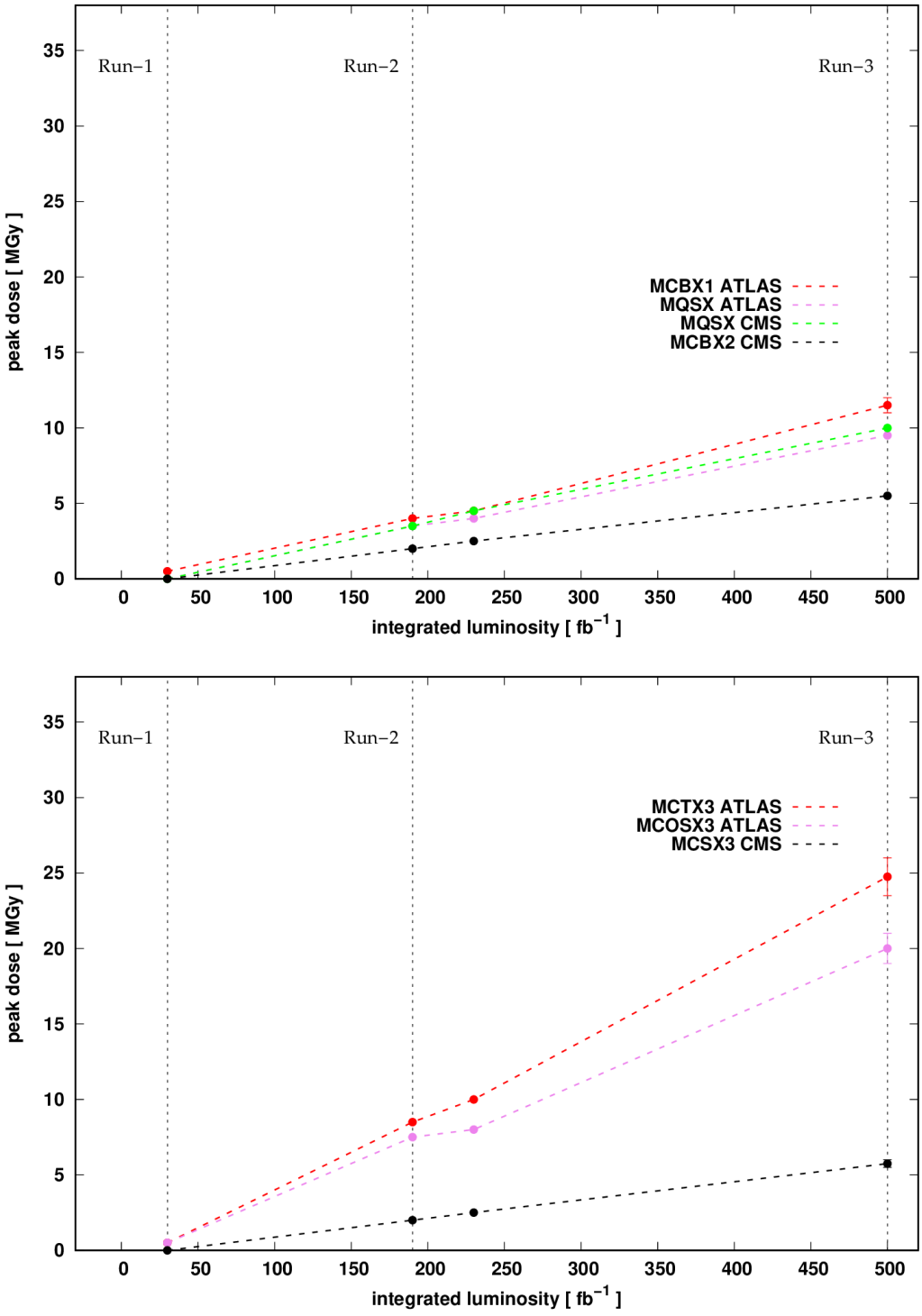

Figure 6: Maximum dose in the indicated skew quadrupoles and most and least impacted orbit correctors (top) and most and least impacted high order correctors (bottom) as a function of delivered luminosity. See the caption of Figure 5 for further details.

the lead ion programme.

4.2 Normal-conducting D1 and compensator magnets (IR2/IR8)

FLUKA simulations yield a hot spot of 120 MGy on the IP side of the first D1 module (MBXW.A4) after the electrical distribution feed-box for the IT circuits (DFBX) in IR1, for an integrated luminosity of 500 fb^{-1}. The following modules are significantly less exposed since they are protected by the previous MBXWs that act as shielding. The absorbed peak dose in the MBXW coil is positioned in the magnet heads, on the vertical axis as shown in the right panel of Figure 7, but not at the extremity close to the flange, rather deeper in proximity of the iron yoke. In IR5 the maximum value is lower, i.e. 80 MGy, because of the horizontal crossing.

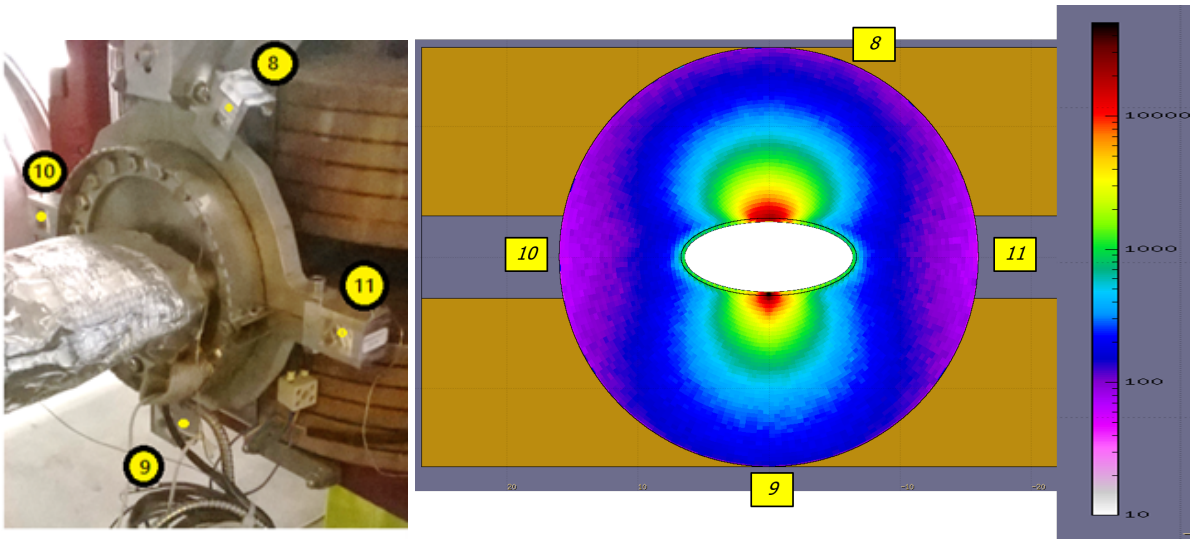

Figure 7: Image of the closer extremity of the D1 magnet string on the right side of IP1 (left panel) and respective radiation dose distribution at the position of the flange (right panel). The numbers in the yellow frames indicate the position of installed dosimeters, which were read after a two-year measurement period in the course of Run 2 (2017–2018) corresponding to an integrated luminosity of 115 fb^{-1}. The logarithmic color scale gives the calculated value in kGy for the latter, reaching on the coil surface about 10 MGy (per 115 fb^{-1}), which however are considerably surpassed at larger depths, on the head side close to the dipole yoke.

MBXW.A4L1 dosimeter #	Measured dose [kGy]	MBXW.A4R1 dosimeter #	Measured dose [kGy]	Simulated dose [kGy]
1	40	8	50	120–135
2	45	9	90	160–175
3	50	11	55	50–70
4	70	10	15	50–70

Table 3: 2017–2018 dose measurements by the dosimeters indicated in Figure 7 and the corresponding ones on the left of IP1 (1–4), together with respective FLUKA predictions. The interval of the latter reflects the statistical error and the position accuracy.

Installed dosimeters (see left panel of Figure 7) provide a benchmark at locations where the dose is two orders of magnitude lower than in the coil hot spot. Table 3 summarizes the results for the last two years of Run 2. The unexplained asymmetries between measures on the left and right of IP1 may indicate to some extent the related uncertainty, while the FLUKA calculation tends to conservatively overestimate the values in the vertical plane.

In IR8, the peak radiation dose on the front coils of the short NC compensators, introduced above, is predicted to slightly surpass 10 MGy in proximity to the beam pipe in the vertical plane, after the production of 28 fb^{-1} during Run 3.

As for the ones in IR2, the same upper limit of 1 MGy previously indicated applies.

5 Expected radiation effects on magnet components

5.1 Magnet design criteria

The schematic IT layout is shown in Figure 8. The MQXA and MQXB low-β quadrupole magnets are completed with nested (vertical/horizontal — a_1/b_1) dipole corrector assemblies (MCBX), skew quadrupole (a_2) correctors (MQSX) and higher-order correctors to form the Q1, Q2 and Q3 quadrupoles. The Q1 quadrupole houses an MQXA and an MCBX orbit corrector on the non-IP side, while the Q2 quadrupole includes two MQXB magnets with an MCBX corrector in between. The Q3 quadrupole has an MQXA and an MQSX on the IP side and, on the non-IP side, the assembly MCBXA consisting of a dodecapole (MCTX)/sextupole (MCSX) (b_6/b_3) nested corrector assembly (MCSTX) nested with an MCBX corrector. MCBXA is followed by the skew-octupole (MCOSX)/octupole (MCOX)/skew-sextupole (MCSSX) ($a_4/b_4/a_3$ — MCSOX) nested corrector assembly.

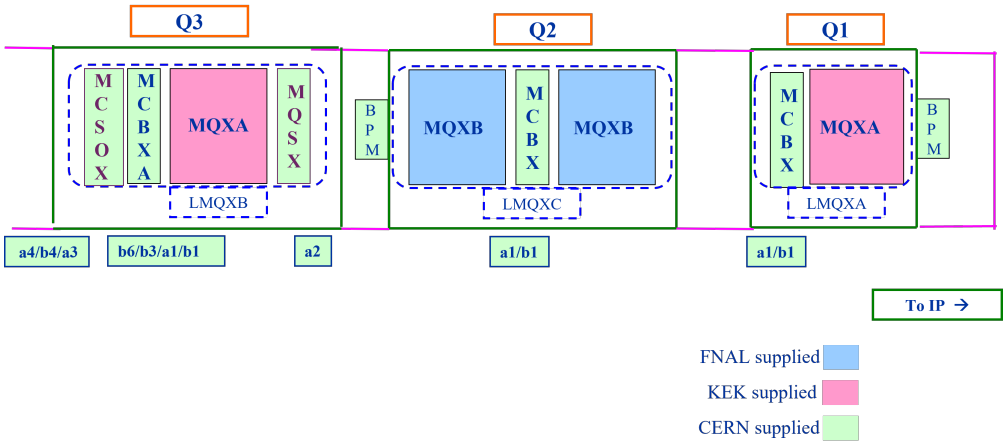

Figure 8: IT Layout. The order of the nested corrector coils is indicated from the innermost to the outermost.

5.1.1 IT Main Quadrupoles

The MQXA and MQXB quadrupoles were produced by KEK and FNAL, respectively. They share common design features relevant for their radiation hardness. The Rutherford-type cables were

insulated with Kapton® along with the multi-layer Kapton®-based ground insulation. The quench-heaters consist of stainless steel strips sandwiched between Kapton® layers. Kapton® is one of the most radiation-resistant insulation materials. Data reported in [27] indicate that Kapton® tape can stand radiation doses exceeding 100 MGy. The wedges in the straight section of the MQXA were made of EP GC3 (also known as G11-CR) along with all the end spacers of both magnet types as illustrated in the Figure 9. The end collets, shown in Figure 10, used for restraining the end regions of the MQXB were made of EP GC3. The main parameters and further construction details can be found in [24]. The IT quadrupoles are expected to withstand accumulated doses larger than 30 MGy estimated from the well documented radiation effects on epoxy and epoxy-glass (coil-end spacers and collets).

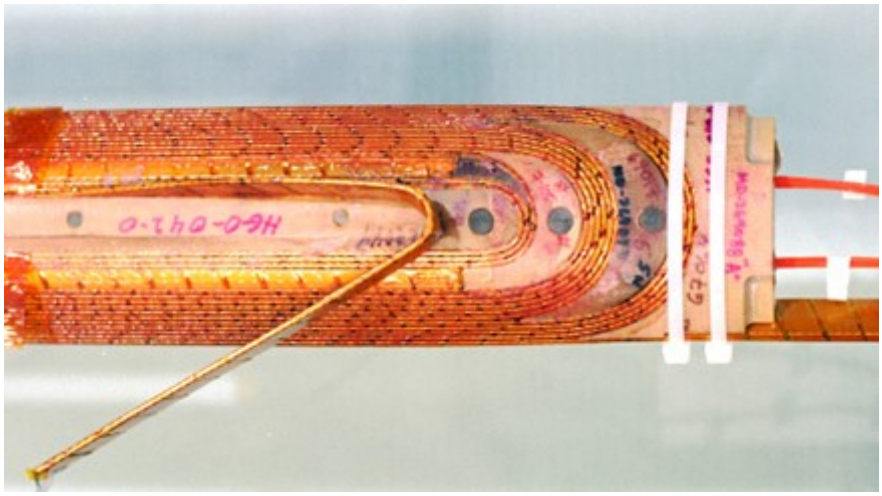

Figure 9: End region of the inner coil layer of the MQXB featuring EPG C3 (G11-CR) end spacers.

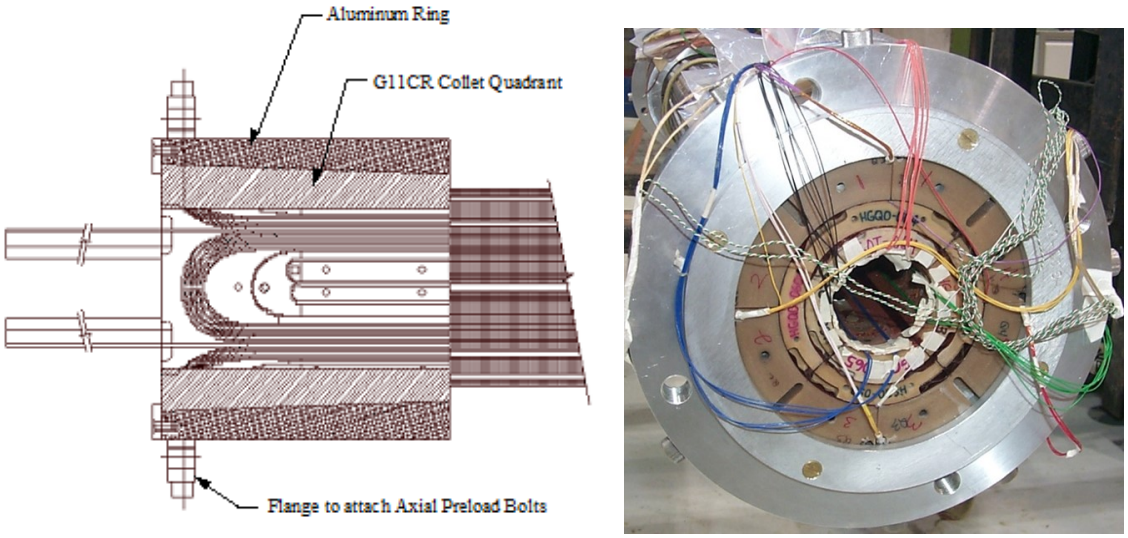

Figure 10: End collet of the MQXB magnets made of EP GC3.

5.1.2 IT CORRECTORS

The SC corrector magnets of the LHC ITs, except the MCSTX that was produced at CERN, were procured through industrial contracts. After acceptance tests at CERN, they were shipped to FNAL for the integration in the cold-masses along with the MQXA and MQXB quadrupoles.

The corrector magnets, whose main parameters are listed in Table 4, share a number of design features relevant for their radiation hardness. The design target in terms of radiation hardness was 7 MGy, a conservative estimate in the absence of experimental data for the polyvinyl acetate (PVA) insulation:

- Coils were wound with single PVA insulated SC strands of three different types. In the case of the MCBX and MQSX the wires were pre-assembled as 8-way or 3-way ribbon, respectively, and bonded together with Epoxy-resin (MCBX: Araldite-F – HY953U – DY026, MQSX: CY1300 – DY026) in a purpose-built machine.
- The thickness of the PVA insulation in the MCBX and MQSX is 60 µm and in all higher order correctors (MCSTX, MCSOX) it is 30 µm.
- In all correctors there is a 0.2-mm-thick EP GC3 protection layer in the bore on which the coils were glued with Epoxy-resin during the coil assembly.
- The four coils of the MCBX were vacuum impregnated with Epoxy resin (GY285 - D400) and cured. The inner coil assembly was then wrapped with dry E-glass, vacuum impregnated and after curing the outer diameter was turned to the specified diameter prior to repeating the same process for the outer layer coils along with the outer ground insulation layer.
- The four coils of the MQSX were wet-wound using Epoxy resin (AW106 – D400) and cured prior to assembling them together and wrapping the assembly with ISOPREG® 2704. The pre-preg[2] layer was cured with spring loaded clamps followed by turning the outer diameter to the specified diameter.
- The coils and the coil assemblies of MCSOX and MCSTX were done in the same way as the MQSX ones.
- The central posts of the MQSX and all higher order coils were made of EP GC3.
- All end-spacers of the corrector coils and end-plates housing the electrical connections were made of EP GC3.

MCBX(A)

The MCBX dipole corrector features an aluminium cylinder around the coil assembly, and it is the primary source of the coil pre-compression. The scissor laminations are assembled in four orientations and surrounded by a stainless steel outer shell to enhance the structural rigidity against the electro-magnetic (EM) forces. The coil pre-stress of the MCSTX insert of the MCBXA-assembly is provided by a thin aluminium cylinder shrink-fitted directly around the coil assembly. The connection plate of the MCSTX is aligned and fastened to the connection plate of the MCBX and radially supported and centred at the non-connection end through an intermediate aluminium disk.

[2]Pre-preg is a composite material made from "pre-impregnated" fibers and a partially cured polymer matrix, such as epoxy or phenolic resin, or even thermoplastic mixed with liquid rubbers or resins.

Magnet Assembly	Number of assemblies in LHC	Aperture [mm]	Corrector	Nominal current [A]
MCBX	16	90	MCBXV MCBXH	550 550
MCBXA	8	70	MCTX MCSX MCBXV MCBXH	80 100 550 550
MQSX	8	70	MQSX	550
MCSOX	8	70	MCOSX MCOX MCSSX	100 100 100

Table 4: Main parameters of the IT correctors. The correctors are listed ordered from the innermost to the outermost.

It shall be noted that, as the field direction is rotated as a function of the powering of the nested MCBXH and MCBXV correctors, the stress distribution within the coils varies. In a cos-theta dipole the assembly tends to slightly ovalize perpendicular to the field direction, which may lead to small conductor movements, which in turn may lead to micro-cracking of the epoxy and training. The bonding strength of the layers between the coils is sufficient to sustain the relative torque and the consequent shear-stress at the inter-layer during the combined powering. The MCBX field plots along with the EM-force vectors for the MCBXA assembly are illustrated in Figure 11.

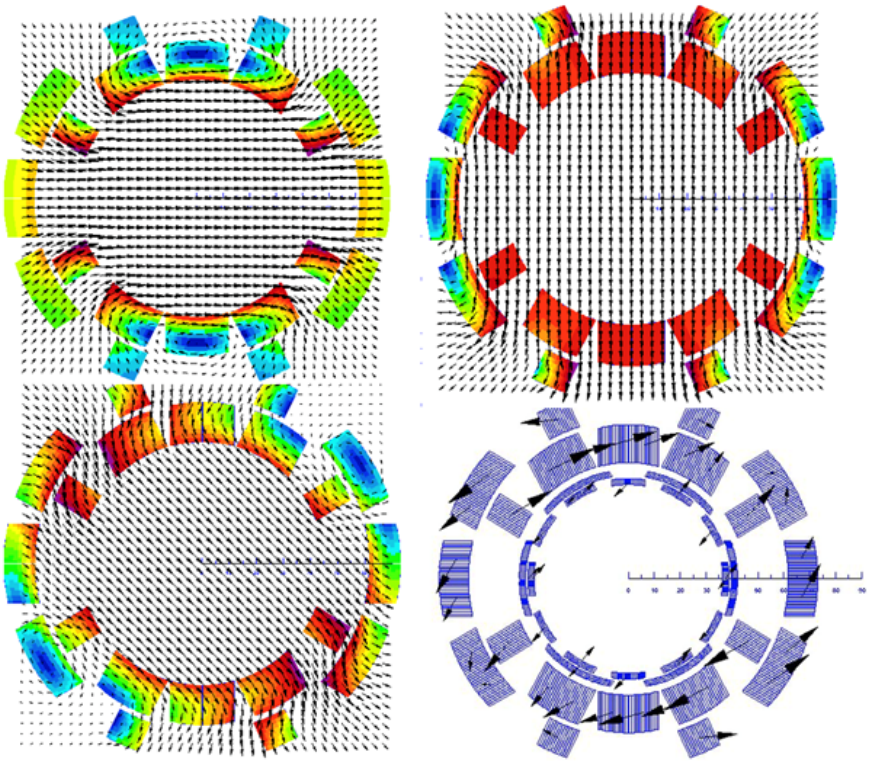

Figure 11: MCBX field plots for individual and combined powering. Top left: MCBXV powering, top right: MCBXH powering, bottom left: combined MCBXH/MCBXV powering, bottom right: EM-force vectors for MCBXH/MCBXV combined powering in an MCBXA magnet assembly.

The criteria for the magnet acceptance are given in Table 5. During the training tests the MCBXH and MCBXV dipoles were first trained individually followed by the combined powering along the diagonals (equal or opposite currents in the MCBXH and MCBXV magnets). After this the field rotated from 0° through to 360° at 50 %, 75 %, and 100 % of the nominal field (vector sum of H and V). The summary of this last and most severe test, is given in Table 6. Non-Conformity Reports (NCR) were produced for those magnets which did not meet the specifications. All MCBXA (with MCSTX) underwent vector powering (as above) with the MCSTX at 100 A.

Criteria	MCBX	
	MCBXH	MCBXV
I_{nom}	550 A	550 A
I_c at 4.3 K	940 A	880 A
Training (Individual and Combined)	Quench 1 > 350 A. Max 10 quenches to reach 650 A	
Re-training	Quench 1 > 600 A	

Table 5: MCBX Acceptance criteria at 4.3 K.

Fraction of operational space reached at 1.9 K	Number and type of magnets
100 %	11 MCBX and 2 MCBXA
95 %	3 MCBXA
90 %	3 MCBX
85 %	1 MCBX
80 %	3 MCBXA
75 %	1 MCBX
rejected	1 MCBX

Table 6: Summary of rotating field tests.

MQSX and MCOSX

The coil configurations and the field plots of these magnets are illustrated in Figure 12.

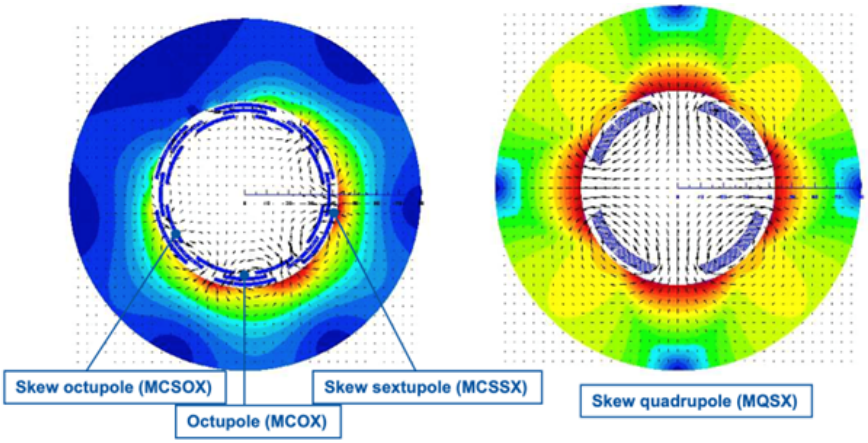

Figure 12: MCSOX (left) and MQSX (right) coil configuration and field vectors.

The MQSX and MCSOX mechanical concept is based on scissor laminations around the coil assembly and the outer aluminium cylinder shrink-fitted around the yoke laminations with a slight interference at ambient temperature.

The acceptance criteria for MQSX and MCSOX at 4.3 K are listed in Table 7. All magnets were conforming with the specification.

Criteria	MQSX	MCSOX		
		MCOSX	MCOX	MCSSX
I_{nom}	550 A	100 A	100 A	100 A
I_c at 4.3 K	940 A	181 A	179 A	176 A
Training	Quench 1 > 350 A. Max 10 quenches to reach 650 A	Max 10 quenches (Individual and Combined) to reach 150 A		
Re-training	Quench 1 > 600 A	Quench 1 > 120 A (Combined powering)		

Table 7: Acceptance criteria for MQSX and MCSOX at 4.3 K.

5.1.3 NC SEPARATION AND COMPENSATOR DIPOLES – MBXW

The experimental insertions of the LHC include NC magnets to separate the beams in IR1 and IR5 and to compensate the effects of the two large ALICE and LHCb spectrometer dipoles in IR2 and IR8, respectively. Each separation dipole D1 on both sides of IP1 and 5 consists of 6 MBXW dipoles. Each of these single aperture magnets have a core length of 3.4 m and a gap height of 63 mm (see Figure 13).

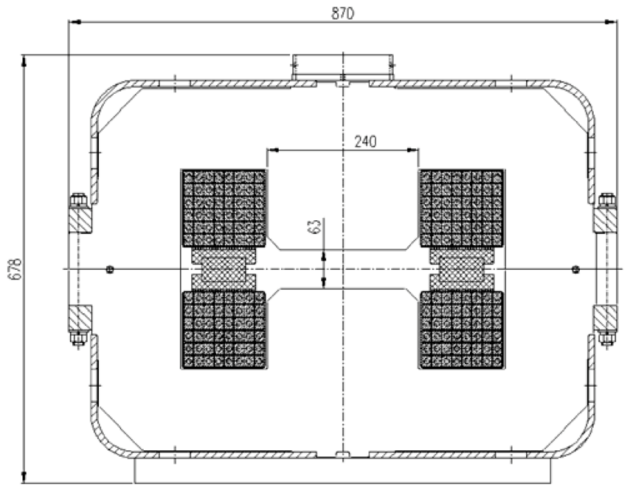

Figure 13: MBXW cross-section.

These dipole magnets comprise two excitation coils composed of three pancakes. Each pancake consists of 2 layers of 8 turns of a hollow copper conductor (18 mm×15 mm with a bore of 8 mm in diameter for water cooling). Each pancake was wound and wrapped separately with a glass fibre tape for electrical insulation. The three pancakes were then assembled together and wrapped with thicker glass fibre tape for the ground insulation. The complete coil was vacuum impregnated with radiation resistant epoxy resin. The impregnating compound was composed of 100 parts of epoxy

resin ED-16, 37 parts of Maleic Anhydride (MA), 20 parts of polyester plasticizer MGF-9 and 0.5 parts of accelerator Triethanolamine (TEA).

The MBXW magnets share the same design concept and technologies of the MBW magnets which are installed and operated around IR3 and IR7. As the design and technological choices were the same, we can estimate that their behaviour vs. accumulated radiation dose would be comparable to the one of the MBW. The MBW have been extensively studied in order to ensure that they can be operated through the whole HL-LHC timespan and the detailed analysis are available in [28, 29]. Following extensive mechanical and electrical tests the following damage limits were estimated:

1. Onset of damage: no bubble in the resin, limited variation of properties: 50–75 MGy.
2. Moderate damage: bubble formation and properties rapid reduction: 75–90 MGy.
3. Failure: extensive bubbles, important loss of properties: >90 MGy.

The ultimate flexural strength shows a decrease of 20 % from 300 to 250 MPa at 50 MGy and the electrical breakdown voltage shows a deterioration at 75 MGy, but it is still of the order of 40 $\mathrm{kV\,mm^{-1}}$.

5.2 Effects of radiation and impact on magnet performance

The main magnet components affected by the radiation degradation are the polymers and polymer composites that are used to build the insulating system of the conductors or mechanical components, generally designed to transfer forces. Normally, two main families of insulation can be identified: impregnated insulating systems or insulation making use of overlapped wrapping of insulating films. The insulation system of the LHC main dipoles and of the arc and IT quadrupoles is based on overlapped polymer layers while that of the correctors and of the NC magnets is built around an impregnation process. Both NC and SC magnets make use of machined pieces made of composites (generally epoxy and glass fibres) as filler pieces or spacers generally transferring compressive loads.

Generally, in polymers and polymer composites, radiation damage manifests itself with a change and/or deterioration of the mechanical and electrical properties, but normally the initial degradation is observable on the mechanical ones while the effect on the electrical properties is measurable only at larger levels of absorbed dose.

As a result of the irradiation, ions or radicals can be generated, the latter being highly chemically reactive. This can lead to the breaking of chemical bonds or breaks in the polymer chains, rearrangements of the polymer structure in the areas affected, and ejection of hydrogen or small molecules. The produced highly chemically reactive radicals are responsible for the degradation of the material properties. Radiation-initiated reactions can be classified in two types [30]:

1. Cross-linking is the inter-molecular bond formation of polymer chains. The commonly accepted mechanism involves the cleavage of a C—-H bond on one polymer chain to form a hydrogen atom, followed by abstraction of a second hydrogen atom from a neighbouring chain to produce molecular hydrogen. Then the two adjacent polymeric radicals combine to form a cross-link.
2. Scission is the opposite process of cross-linking in which the rupturing of C—-C bonds occurs.

Cross-linking increases the average molecular weight, whereas scission reduces it. Cross-linking usually increases tensile strength properties but reduces elongation. Scission results in reduction of tensile strength and increased elongation. In both cross linking and scission there is generation of light molecules that are in gaseous state at room temperature. Via diffusion these molecules tend to coalesce in bubbles that can cause swelling and deformation of the polymeric component. In case of irradiation at cryogenic temperature the diffusion is stopped, and it is enabled again at the moment of the warm-up to room temperature, with the consequent risk (in extreme cases) of the rupture of the composite from the inside (see Figure 14) [31].

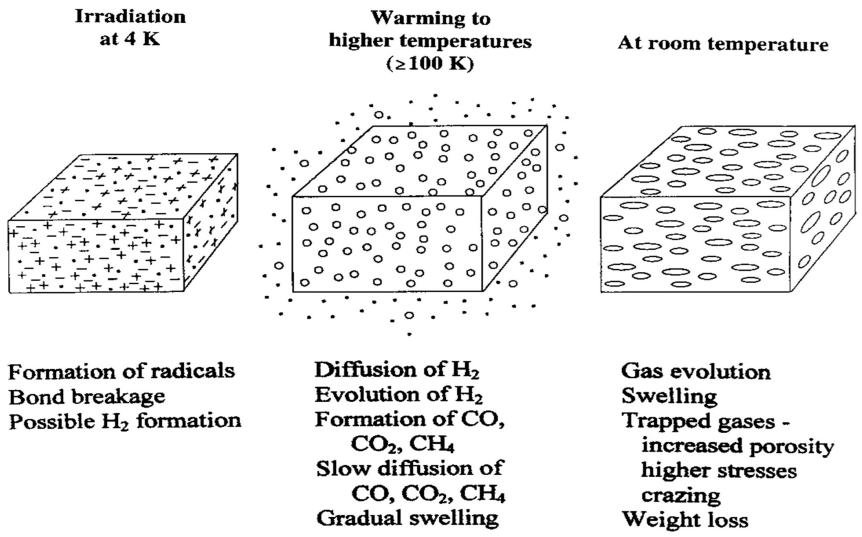

Figure 14: Effect of Radiation [31].

As mentioned before the irradiation process create reactive free radicals that have strong tendence to react with the oxygen of the air. SC magnets are exposed to radiation during operation in the absence of oxygen and therefore the recombination takes places only when the magnet is warmed-up and exposed to air.

In summary, while the degradation of room temperature irradiated component is a continuous incremental process, it is not the case for irradiation in cryogenic conditions (as for the SC magnets) because of the absence of diffusion and of oxygen. Both processes are suddenly activated when the magnets are warmed-up and exposed to oxygen.

It is also worth pointing out that in composites (e.g. G10 and G11 or other fibre + polymer composite) the preferred location for failure is at the interfaces. It is the bonding between the fibre and the matrix that becomes the weak link not allowing any more to redistribute the loads via the fibres.

While radiation induced magnet failure could appear as an electrical problem, it is quite improbable that it would be linked to the loss of electrical properties of the organic material. As observed before, the electrical properties start to degrade after the mechanical ones and it is therefore a radiation mechanical failure that will provoke, as secondary effect, electrical failure. This suggests that likely electrical testing will not evidence the precursors of polymer degradation.

On the other hand, mechanical damage is linked to the failure of a component in a specific load configuration. Therefore, while mechanical tests at various levels of radiation exposure will provide a hint of how the material behaves, it is mandatory to correctly link those mechanical properties to that load configuration. For composites it is relevant also to identify the main direction of the fibres with respect to the load direction which depends on the construction details of the component. Last, but not least, commercial composites like G11 and G10 can receive those qualifications inside a range of material composition, for example volumetric ratio of glass fibre vs. resin. It is therefore evident that a precise prediction of when failure would take place is very difficult and the margin of error very high.

5.3 Radiation resistance measurements

The radiation limits considered for the task force scope are based on literature data, where available, and on on-going tailored measurements campaigns. Most of measurements available in literature have been performed in ambient air. We may assume that, for an SC magnet operating at low temperatures, far away from T_g (glass transition temperature)[3] of organic components, and in absence of oxygen, irradiation tests performed at ambient temperature provide pessimistic limits with respect to the operational conditions. However, we shall be aware that ageing may result from the superposition of combined effects, including mechanical stress-strain under the radiation exposure: for the typical organic components in a magnet these effects have not been studied yet.

Literature data are essentially based on several reports [32, 33]. More recently, new test campaigns, promoted by the HL-LHC project, are being organized to complete the missing information on specific components (in particular the PVA conductor insulation which is also used in the inner triplet correctors) and to explore the influence of environmental conditions on the organic components typically used in accelerator magnets. Here, we describe the ongoing irradiation test program and its relevant preliminary results.

5.3.1 Description of the programme

In the first stage of the CERN polymer laboratory irradiation programme [34] polymers for potential use in SC accelerator magnets are submitted to different irradiation sources and environments to determine:

- the effect of irradiation on thermo-mechanical, thermal and dielectric properties;
- the dependence on radiation type (γ rays, protons and neutrons);
- the dependence on the irradiation atmosphere (ambient air, vacuum/inert gas);
- the dependence on temperature (ambient and cryogenic temperature).

The measurements of irradiation-induced changes of functional material properties are complemented by sophisticated chemical analysis methods with the goal to determine the different aging mechanisms and rates. The materials studied include different constituents of magnets presently installed in the LHC, different epoxy resin systems studied for SC magnet coil impregnation, as well as 3D printable polymers.

[3] The temperature at which an amorphous polymer material turns into a rubbery form when heated is known as the glass transition temperature (T_g). It can also be defined as a temperature at which an amorphous polymer develops the characteristic glassy-state properties such as brittleness, stiffness and rigidity upon cooling.

5.3.2 Preliminary results: irradiation in ambient air

Irradiations in ambient air are performed with four different sources:

- ^{60}Co γ rays at an external company;
- 24 GeV protons at the CERN IRRAD facility;
- thermal and fast neutrons at the research reactor of Vienna Technical University;
- neutrons at the CERN n_TOF NEAR spallation facility.

γ irradiation of different epoxy resins and other polymers with a ^{60}Co source in ambient air has been completed by the beginning of 2023. A new ^{60}Co γ irradiation campaign up to 30 MGy is planned to start in 2023 and to be completed in 2024. The effect of irradiation induced aging has been characterised for instance by Dynamic Mechanical Analysis (DMA)[4] and short beam stress-strain measurements. Proton irradiations are ongoing with the goal to achieve a maximum dose of 30 MGy by the end of 2023.

5.3.3 Preliminary results: influence of the irradiation environment

Irradiations have been performed in:

- ambient air at 20 °C;
- dry air at −20 °C;
- vacuum at ambient temperature;
- liquid helium.

24 GeV proton irradiation at the CERN IRRAD facility in dry air at −20 °C with selected materials with low glass transition temperature was performed in 2022 [35]. 24 GeV proton irradiation in liquid helium to a dose 3 MGy could be achieved at the CERN IRRAD facility [36]. It has been found that the irradiation environment has a strong influence on the aging of the CTD101K epoxy resin after the same absorbed dose. After 3 MGy absorbed dose in liquid helium no measurable difference of T_g between irradiated and non-irradiated samples was observed, while the same dose absorbed in air increases T_g by about 25 °C. In 2023 the irradiation study will be complemented by 24 GeV proton irradiations in inert gas at ambient temperature. This will allow to distinguish between the effects of oxygen and temperature.

5.3.4 Irradiation induced aging of polymer constituents of MCBY correctors

The main goals of this investigation are to verify if there are irradiation induced changes of thermo-mechanical properties of the polymer constituents that could explain changing training behaviour of MCBC and MCBY magnets in the LHC, and if there is an irradiation induced degradation of the dielectric properties of the Nb-Ti wire PVA enamel insulation [37]. Three constituent materials have been studied:

[4] DMA is a technique used to study the viscoelastic behavior of polymers. A sinusoidal stress is applied and the strain in the material is measured, allowing one to determine the storage modulus (G' or E') that is related to sample stiffness, and the loss modulus (G" or E"), which measures the energy dissipated as heat (viscous portion). If during the experiment the temperature of the sample is varied, the resulting changes of the storage modulus and loss modulus can be used to determine T_g of the material, as well as to identify transitions corresponding to other molecular motions.

- PVA enamel (30 µm thickness) insulated MCBY rectangular Nb-Ti wire (also used for the the IT higher order correctors, MCBX and MQSX have a 60 µm thick PVA enamel insulated wire — see Section 5.1.2);
- coil block samples cut from a pre-series MCBC coil impregnated with Araldite GY 285/Texaco D400; the same type of material was used for the impregnation of the MCBX coils;
- ISOPREG® 2704 used for the MCBC/MCBY/MQSX/MCSOX/MCSTX outer insulating layer.

The changes of the dielectric properties of the PVA enamel wire insulation with increasing dose in ambient conditions are shown in Figure 15.

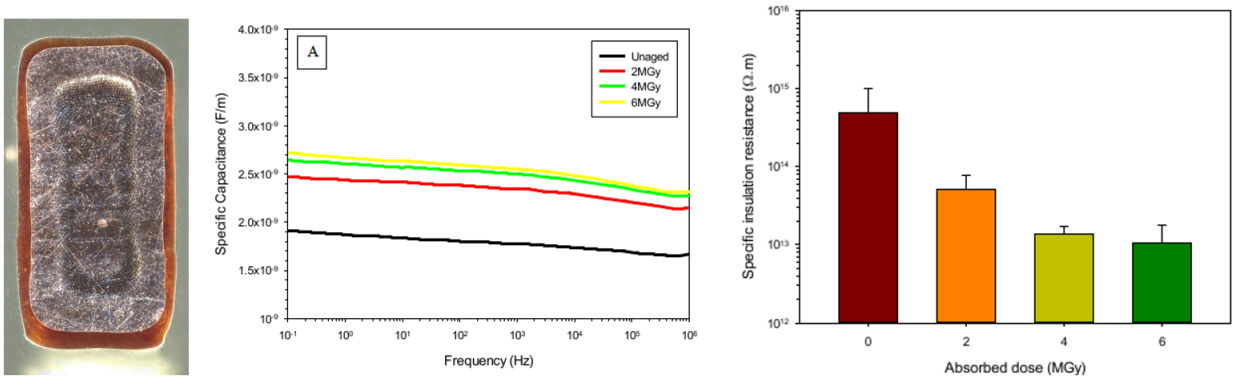

Figure 15: Metallographic cross section of PVA enamel insulated wire (left), specific insulation capacitance (centre) and specific insulation resistance (right) after different ^{60}Co doses.

The thermal analysis and flexural stress-strain results of the ISOPREG® 2704 MCBY outer insulation layer are presented in Figure 16 [38].

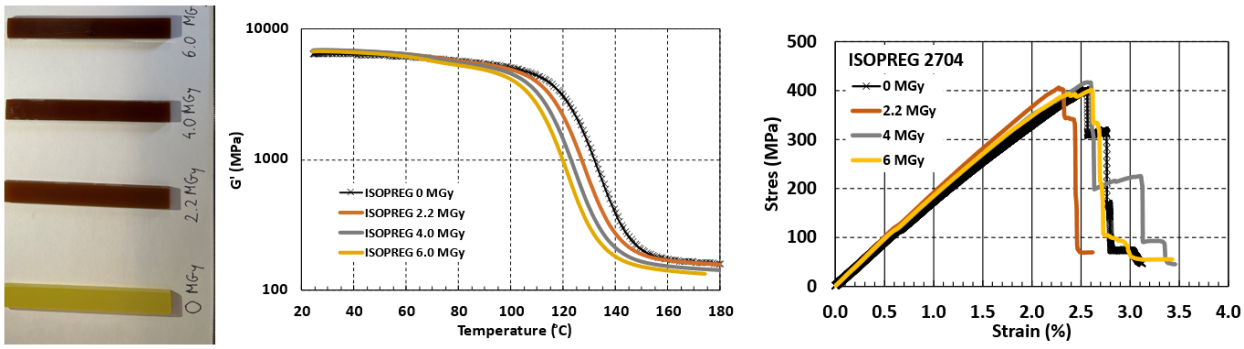

Figure 16: ISOPREG® 2704 samples and test results before and after γ irradiation up to 6 MGy in ambient conditions: (left) visual comparison, (centre) storage modulus G' as a function of temperature, and (right) flexural stress-strain curves.

In the next γ irradiation campaign to 30 MGy other polymer constituent materials of inner triplet magnets presently installed in the LHC will be included, for instance the fibre reinforced epoxy EP GC3 (G11-CR) out of which the end spacers of the MQXA and MQXB magnets have been made (see Figure 9).

Correlating irradiation test results with magnet performance is difficult because:

- Transverse compression is the main load case in the SC magnets, while the irradiated test samples have been characterised in shear or in 3-point bending configuration.
- In the magnets, dielectric insulation is achieved by an insulation system, but the effect of irradiation on dielectric properties has been tested on single constituents of the system.
- The irradiation conditions are not identical (γ irradiation in ambient air of the test samples, and mixed field irradiation in liquid helium of the polymers in SC magnets). Therefore, the aging rates that can be derived from the present irradiation tests are to be considered as pessimistic estimates.

The small effect of γ irradiation up to 10 MGy on the ISOPREG® 2704 composite confirms the robustness of the corrector coil to ground insulation system. Irradiation induced changes of the resistance of the coil to ground insulation system, including the PVA wire insulation, would be revealed by leakage current measurements that are regularly performed by the Electrical Quality Assurance (ElQA) team. A softening of the coil impregnation resin at ambient temperature might change the magnet training behaviour after a thermal cycle.

5.3.5 PLANNED IRRADIATIONS

A new γ irradiation campaign will be started in August 2023. The goal is to achieve a maximum dose of 30 MGy in ambient air within 15 months (with a dose rate of 3 kGy h^{-1}). Thermomechanical properties in tension, compression and shear of the triplet spacer materials (fibre reinforced epoxy resin EP GC3) will be characterised after intermediate dose steps, and results after 10 MGy will be available by February 2024. Results after 30 MGy will be available by November 2024. A proton irradiation run in liquid helium up to 4 MGy is planned at the CERN IRRAD facility in October 2023. In this run inner triplet magnet spacer samples will be included, to verify the effect of the irradiation environment.

6 Observations and possible methods for early detection

6.1 Observations

No non-conformities related to the irradiation from the collision debris generated at the IPs have been observed so far.

6.1.1 MCBX

Since LHC start the 24 MCBX magnets have been trained during the so-called Hardware Commissioning (HWC) campaigns. The majority of training quenches occurred after a thermal cycle (for example after a LS) whereas hardly any training occurred during operation or immediately after a Year-End Technical Stops (YETS), as long as the magnet is maintained at cryogenic conditions. Until 2013 training was performed by powering the horizontal (H) and vertical (V) coils separately. This resulted in a total of 35 quenches in 2008–2009 and 14 quenches in 2013 (pre-LS1 HWC) as shown in Table 8.

As of 2015 an additional test was added, namely by powering the H and V coils together, while keeping the quadratic sum of the currents in the H and V coils ($I_H^2 + I_V^2$) constant (see Figure 17).

	IR1	IR2	IR5	IR8	Total
2008–2009	10	5	13	7	35
2013	3	7	0	4	14
2015 (post LS1)	3	8	8	0	19
2016	1	1	0	0	2
2017	17	0	0	0	17
2018	1	0	0	0	1
2021–2022 (post LS2)	25	2	42	1	70
2023	0	0	0	0	0

Table 8: Number of training quenches in the MCBXH/V magnets during various HWC campaigns for individual powering.

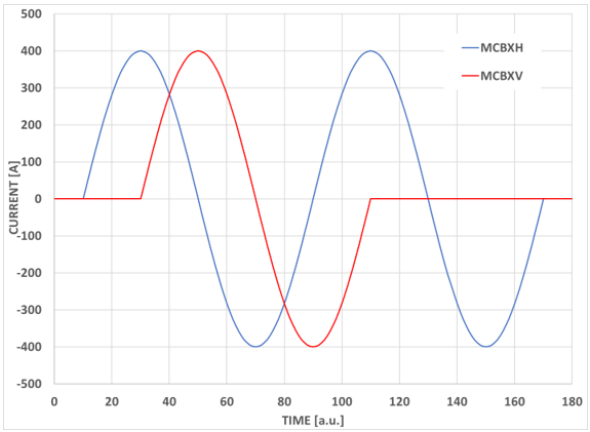

Figure 17: Typical current evolution for the HWC of the MCBX circuits.

In 2015 (post-LS1 HWC) this resulted in 19 quenches in individual powering and 59 quenches in combined powering. The total number of quenches were rather equally distributed between the two *high-radiation regions* (IR1, IR5) and the two *low-radiation regions* (IR2, IR8), namely 36 and 42 respectively (see Table 9). During the Extended Year-End Technical Stop (EYETS) 2016–2017 only sector 12 was warmed up in order to replace one non-conform dipole magnet. After cool-down a significant number of training quenches was observed (15+5) in the MCBX magnets right of IP1. In the HWC after LS2 (2021 and 2022) a strong increase in number of training quenches is observed, namely 70 in individual powering and 45 in combined powering, even though the commissioning currents were reduced for many magnets. After LS2 also a large difference in number of training quenches is observed between the two *high-radiation regions* and the two *low-radiation regions*, namely 108 and 7 respectively. This large imbalance gives a strong indication that the increase in number of training quenches is related to the radiation received during Run 2, although the estimated accumulated dose is by at least a factor two lower than design one (see Tables 18 and 19 in Appendix B). During the YETS 2022–2023 none of the MCBX magnets was thermally cycled, and no training quenches were observed during the HWC campaign early 2023. The distribution of the currents at which training quenches occurred during the periods 2008–2009, 2015 (post LS1) and 2021–2022 (post LS2) are also shown in Figure 18. Virtually no training quench has been observed below 300 A. It is important to mention that we have not observed any permanent degradation of the performance of these magnets. All magnets

still reach the required current for HWC, but often with increased number of training quenches.

	IR1	IR2	IR5	IR8	Total
2015 (post LS1)	18	22	7	12	59
2016	0	0	0	0	0
2017	5	0	0	1	6
2018	2	0	0	1	3
2021–2022 (post LS2)	25	0	16	4	45
2023	0	0	0	0	0

Table 9: Number of training quenches in the MCBXH/V magnets during various HWC campaigns for combined powering, Note that combined powering tests have not been performed before 2015.

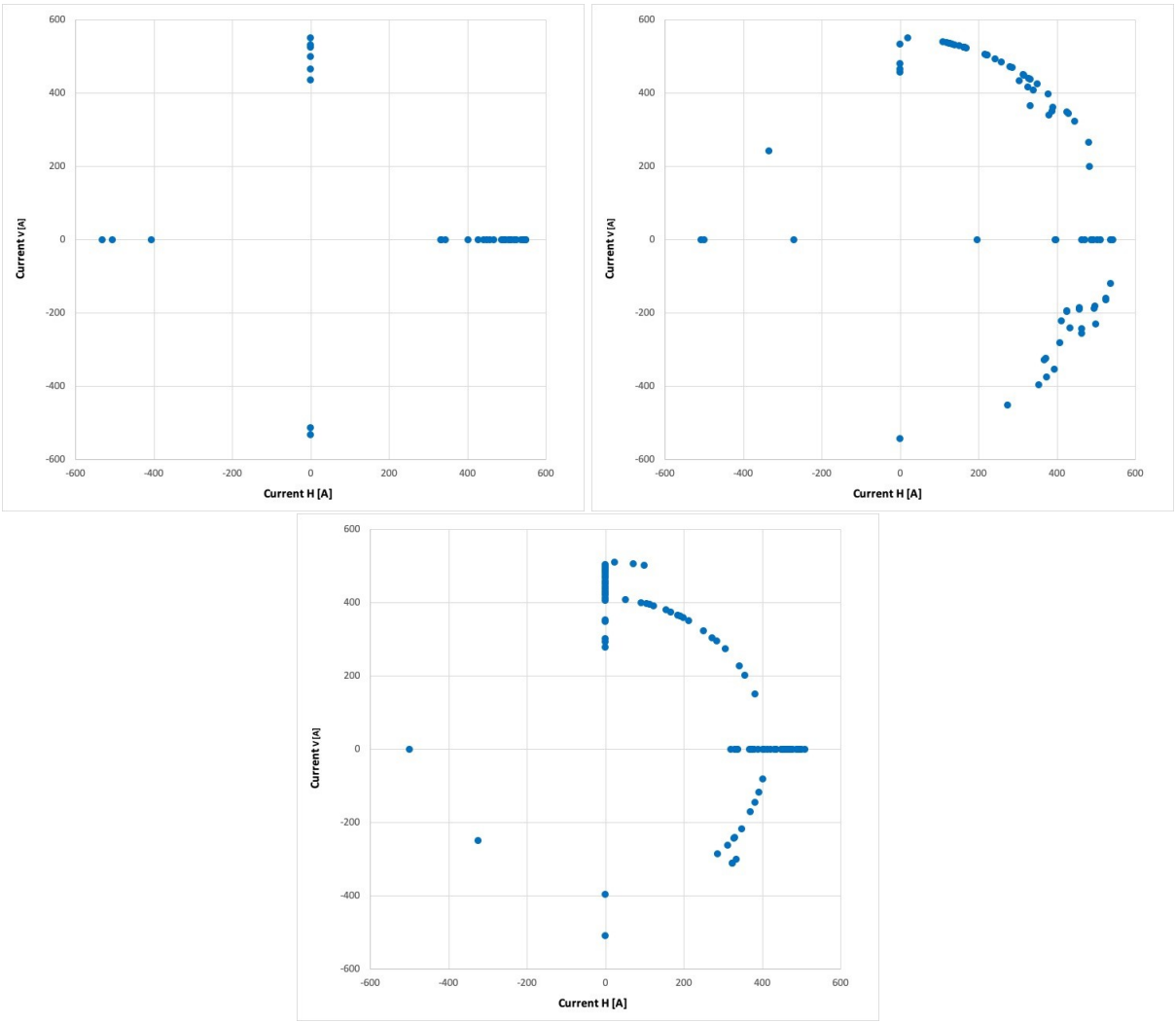

Figure 18: Distribution of the currents at which training quenches in the MCBXH/V magnets occurred in 2008–2009 (top left), 2015 (post LS1 — top right) and 2021–2022 (post LS2 — bottom). Note that the circuits are first individually powered at positive current, and then at negative current.

6.1.2 MQSX

Similar statistics can be made for the training behaviour of the MQSX magnets (see Table 10). Here a clear increase is observed in training quenches after LS1 and after LS2 as compared to the initial HWC in 2008–2009. Although there is a difference between the number of training quenches in *high-radiation regions* as compared to *low-radiation regions*, the difference is not as large as for the MCBXH/V magnets. Radiation might have had a negative impact on training, but the increased training could also be due (completely or partially) to aging and/or fatigue effects. Similarly to the MCBX magnets, no training quenches occurred in 2023 during the HWC after the YETS 2022–2023.

	IR1	IR2	IR5	IR8	Total
2008/9	0	0	0	1	1
2013	0	0	0	0	0
2015 (post LS1)	5	5	7	1	18
2016	0	0	0	0	0
2017	0	0	0	0	0
2018	1	0	0	0	1
2021/2 (post LS2)	6	6	12	4	28
2023	0	0	0	0	0

Table 10: Number of training quenches in the MQSX magnets during various HWC campaigns.

6.1.3 Other IR magnets

In none of the other triplet circuits (including the higher order correctors), neither in the D1 magnets in IR2 and IR8 or in the D2 magnets in the experimental IRs we see any clear statistical sign of degraded quench performance since the start of the LHC. The evolution and distribution of the training quenches of the main IT quadrupoles is shown in Figure 19. Slightly more training quenches have been observed in 2021 as compared to past HWC campaigns, though likely related to the higher post-LS2 HWC current due to the higher energy. No clear correlation with radiation dose has been observed. Furthermore, we have not observed any clear indication of degraded voltage withstand levels of any of the triplet, SC D1 and D2 magnets during the ElQA tests performed since the start-up of the LHC.

6.2 Possible methods for early detection

Two ElQA measurements could possibly indicate a performance degradation of SC coils due to radiation, namely:

a. High Voltage (HV) qualification;

b. Transfer Function Measurement (TFM).

The logged data from the Quench Protection System (QPS) are not useful since they have insufficient resolution and sampling rate.

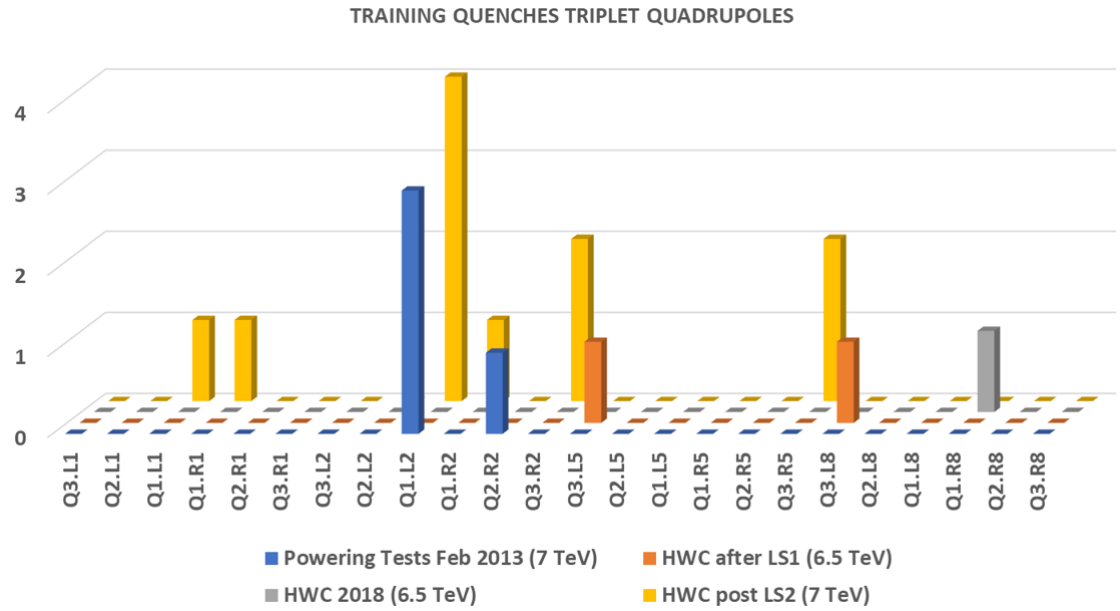

Figure 19: Evolution and distribution of the training quenches of the main IT quadrupoles. Note the different energies for which the magnets have been trained.

6.2.1 HV QUALIFICATION

During this test the leakage current between circuit and ground is measured during typically 3 min at different temperatures (1.9, 4.5 and 300 K):

- the applied test voltage depends on the circuit and the temperature. The maximum voltage for the triplet is 1 kV at cryogenic temperatures;
- the measurement equipment and test voltage have evolved since the start of LHC;
- the measurement cannot distinguish between leakage in the coil, busbars, current leads and measurement equipment connected to the circuit (for example voltage-taps);
- the test is not sensitive to any inter-turn insulation problem;
- only when the test fails (i.e. breakdown or leakage current >1-10 µA) additional diagnostics is performed;
- the measurement accuracy is about 20 nA. However, the measurement variability is much larger, mainly due to humidity variations affecting the NC part of the circuit.

The measured leakage currents in all triplet circuits between 2008 and 2022 have been analysed and one example is shown in Figure 20. The following conclusions can be drawn:

- the leakage currents of all triplet circuits are below 1 µA at cold, a factor of at least 10 smaller than the acceptance criterion of 10 µA;
- no clear trends over the years are visible for any of the circuits;
- no clear difference is visible between *high-radiation* and *low-radiation regions*.

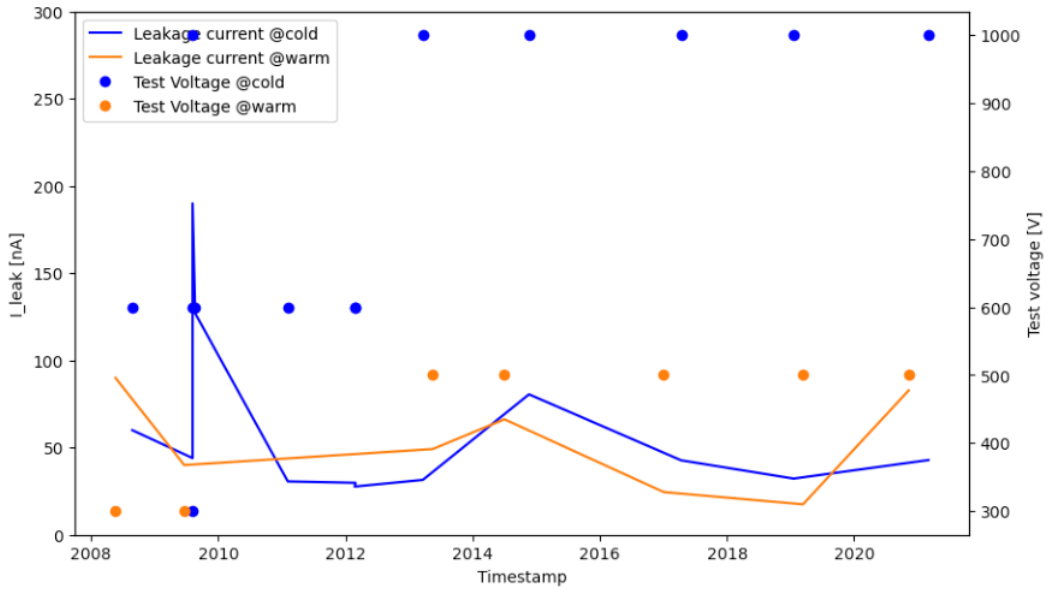

Figure 20: Measured leakage currents in the circuit of MCBXV2.R1 magnet between 2008 and 2022 (*Courtesy of M. Bednarek*).

6.2.2 Transfer Function Measurement (TFM)

This test is performed by applying a sinusoidal voltage between circuit and ground, and across-the-circuit, while sweeping the frequency from 1 Hz to 100 kHz. An example of 7 measured curves between 2008 and 2021 is shown in Figure 21.

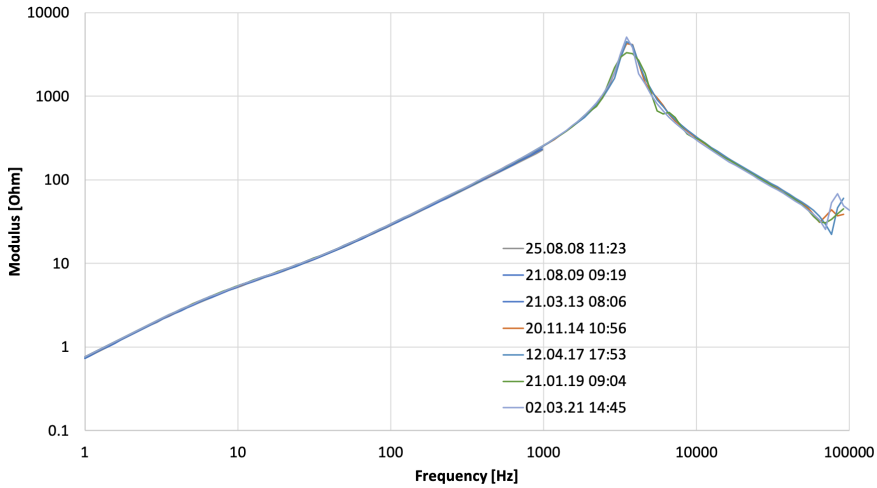

Figure 21: TFM results on the circuit of the MCBXV1.R1 magnet between 2008 and 2021 (*Courtesy of M. Bednarek*).

Some notes concerning this test:

- The TFM is performed at 1.9 or 4.5 K and at 300 K;
- the measurement equipment has evolved since the start of LHC;

- it would be possible to detect an inter-turn short if this reduces the inductance of the circuit by an amount significantly different from the measured inductance in the past;
- it is possible to detect a global change in capacitance between coils and ground.

After analysing the test data since 2008, the following conclusions can be drawn:

- No clear trends in the TF over time are observed.
- Some variations in TF are observed for some circuits, especially at high frequencies >1 kHz, but no correlation is observed with the radiation dose received by the magnets of these circuits. It seems that these changes are partially caused by variations in the capacitance of the NC part of the circuit.

At present the degraded training performance of the MCBX magnets is not correlated with the results of the HV or the TFM tests. There is therefore no proof that such measurements will show in the future possible precursors of degraded magnet performance (see also Section 5.2).

7 Impact of failures in IR1 & 5 and possible mitigation measures

Replacement of an IT cryo-magnet in case of failure is a more complex operation than the replacement of a cryo-dipole in the LHC arcs. In the following some of the main differences are listed [39]:

- A replacement of a Q1 magnet automatically requires the removal of Q2 and in some locations even Q3 for transport reasons. It is required to remove all systems around the cryostats (e.g. survey systems, BLMs, electrical and vacuum equipment, protection gutters).
- Triplet interconnections are more complex than arc dipole interconnections due to the presence of a larger heat-exchanger, larger Plug-In-Modules — PIMs — and Beam Position Monitors — BPMs.
- Instrumentation wires go through the magnet (no IFS box) and shall be identified.
- Tooling (for example orbital cutting machine) shall be adapted to the non-standard inner tubes of the triplet interconnection.
- Handling tools to hold long tubes, like heat-exchangers, shall be made.
- SC splices are more complex and adequate training of the operators is needed prior to an intervention in the tunnel.
- Radiation levels in IR1 and IR5 are high and the intervention is classified as ALARA (As Low As Reasonably Achievable) Level 3.

The replacement of a triplet magnet is expected to take up to 1 year (for comparison the replacement of an arc dipole takes $\approx$ 4 months) though a detailed procedure does not exist yet. The TE/MSC group is in the process of defining it [40].

Different failure scenarios have been studied to determine their impact on machine performance and to identify possible mitigation measures.

7.1 Main IT Quadrupoles

In case of triplet quadrupole failure in IR1 and IR5, it could be possible to operate the machine with an optics not using the triplets and provide collisions for the remaining IPs. Such, so-called *ballistic*, optics has been tested in the machine and was used to calibrate the BPMs in the vicinity of IP1 and IP5 [41] but it does not provide sufficient aperture for the injection of high-intensity beams. However, its design was not optimized for this and further investigations would be required to determine whether solutions exist that are compatible with high-intensity operation. Failure of the triplet quadrupoles in IR2 and IR8 might prevent operation in all cases given the additional optics constraints imposed by the injection in these IRs.

7.2 IT Orbit Correctors (MCBX)

The MCBX correctors were initially planned to be used up to a nominal current of 550 A in both planes and their functionality is twofold:

- correct as locally as possible the transverse misalignment of the IT quadrupoles, up to 0.5 mm, which, in the case of the Q1/3 (L = 6.37 m) and Q2 (L = 11.00 m) cryo-assemblies, demands a current of up to 240 A and 420 A, respectively, when operating the triplet at 205 T m^{-1}.
- participate to the crossing bump generation (crossing angle and parallel separation) at the IP.

During the design phase of the LHC, only the MCBX magnets at Q1 (MCBX1) were dedicated to the crossing bump generation, with optimized settings in the range of 150 A for a typical half-crossing angle of 160 µrad (and sensibly less in the parallel separation plane) aiming at minimizing the strength requirement on the other closed orbit correctors (MCBYS @ Q4, and MCBC @ Q5 and Q6) participating to the parallel separation and crossing angle bumps (see Figure 22). Later on, in view of the poor quenching performance of these magnets, the nominal current of the MCBX circuits was reduced to 400 A, and the MCBX1 contribution to the crossing bumps was then equally shared between the MCBX2 and MCBX3 circuits (i.e. only $\approx$ 50 A required per MCBX to participate to the crossing angle generation in this configuration). Therefore, provided a good alignment of the IT quadrupoles is guaranteed (see hereafter), the availability of at least one MCBX magnet per plane per IP side should preserve the crossing bump functionality in IR1 and IR5, with no particular preference at this stage amongst the MCBX1, MCBX2, or MCBX3 magnets, which would also not necessarily need to be the same between the left and right side of the IP, and between the horizontal and vertical plane. On the other hand, as can be inferred from Figure 22, if all 3 MCBX circuits would be condemned in the crossing plane, on a given side of IR1 or IR5, the crossing angle would be limited to about $\Theta_X/2 \approx 100$ µrad, from the orbit corrector (COD) strength at Q5 and Q6. In this scenario, a more sophisticated crossing bump would then be needed (e.g. extension of the bump up to Q7/Q8 or beyond), in order to recover the necessary crossing angle and collide bunch trains at low β^*.

Thanks to the regular realignment of LSS1 and 5, an excellent flat orbit (i.e. with the crossing bumps switched off) can generally be established with MCBX settings found in the range of 100 A, but with some outstanding outliers essentially in the vertical plane on the right side of IR1 (see the 2022 MCBX settings of the flat machine in Table 21 in Appendix C). In this context, simulations have been performed assuming a random excitation of the MCBXs in IR1 and IR5 by up to $\pm$100 A (100 different seeds generated using a Gaussian distribution with a RMS of 67 A, and truncated at

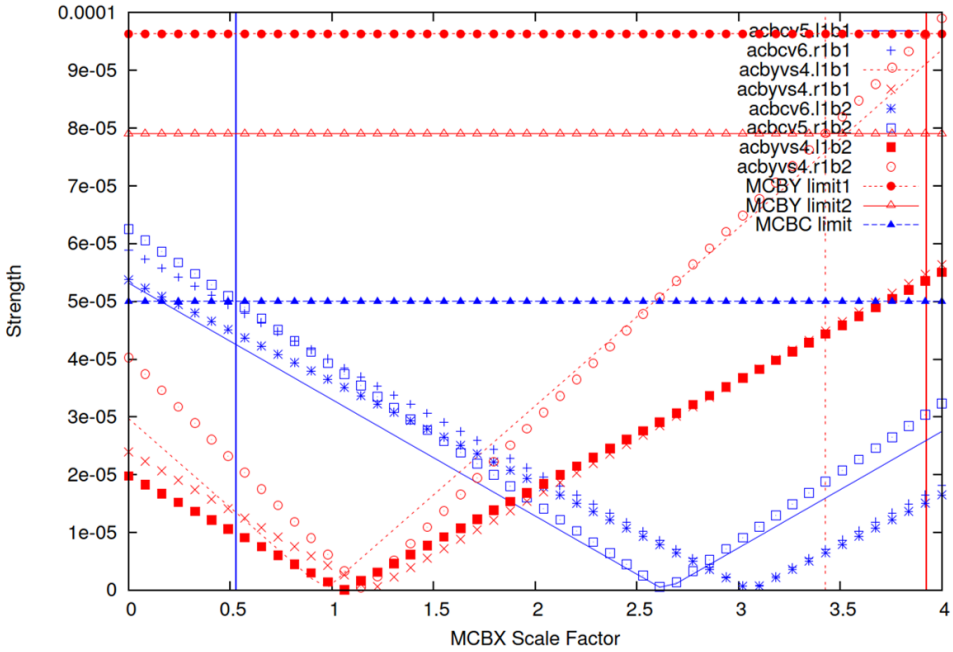

Figure 22: Strength and limits [µrad], given in absolute value, for the orbit correctors at Q4 (MCBYS), and Q5/Q6 (MCBC) which are involved in the crossing bumps, as a function of the MCBX setting [a.u.], in the case of the ATLAS experiment with a vertical crossing angle of $\Theta_X/2$ = 145 µrad. For the MCBYS, exclusively dedicated to the crossing bumps, the limit indicated corresponds to 80 % (recommended) or 100 % of their nominal strength at 7 TeV (see the vertical dotted and solid red lines respectively). For the MCBC, the recommended limit is set at 50 %, because these correctors also participate to the closed orbit correction (and are involved in the luminosity knobs). Without MCBX, this 50 % limit is sensibly exceeded for the assumed crossing angle of 145 µrad. The MCBX settings are then generally chosen to sit at center of the allowed band, which corresponds to the vertical blue and red solid lines of the plot in the present case.

1.5 σ). Starting from the induced closed orbit distortion, 4 different orbit correction schemes have been tested, namely:

- the **MCBX0** scheme: using the CODs at Q4 (except the MCBYS), Q5, Q6, and Q7, but none of the MCBX,
- the **MCBX1** scheme: using the CODs at Q4, Q5, Q6, and MCBX1,
- the **MCBX2** scheme: idem but using MCBX2 instead,
- the **MCBX3** scheme: idem but using MCBX3 instead,

and requesting a perfect orbit correction both at the IP and at the last COD participating to the correction (4+4 orbit constraints per beam). The results obtained are reported in Table 11. An immediate conclusion is that if none of the MCBX magnets was available on a given side of IR1 or IR5, and in a given transverse plane (**MCBX0** scheme), the ability to correct the orbit would be significantly affected (see the 5.7 mm peak orbit reported in bold for the **MCBX0** scheme in Table 11). In this worst case, an improvement by a factor of at least 5 would need to be achieved

Case	MCBX0	MCBX1	MCBX2	MCBX3
CO [mm] before correction	31.4/112.5			
CO [mm] after correction	2.2/**5.7**	0.4/0.9	0.5/1.1	0.9/1.9
MCBC strength [% of max]	24.5/69.5	2.5/14.0	3.0/17.8	5.3/30.5
MCBY strength [% of max]	21.0/77.5	9.0/26.8	10.9/32.2	19.7/61.9
MCBX current [A]	-	67/213	40/131	82/266

Table 11: Closed Orbit (CO) correctability and required corrector strength in LSS1 or LSS5 assuming no, or only one, MCBX magnet available per plane and per IP side. Simulations were done for 100 different seeds, where the non-corrected orbit was induced by a random excitation of up to $\pm$100 A in all the MCBX circuits of IR1 and IR5 (which are virtually kept on for this purpose). The statistics is reported in terms of average over the seeds (first number) and worst seed (second number). The case of the 50 cm RP collision optics (see Section 8.2) is reported on (being said that the injection optics leads to very similar results, except of course for the closed orbit before correction which is not as huge).

in the LSS1/5 realignment to reduce to 20 A the initial 100 A excitation assumed as input to define the perturbed closed orbit. This, in turn, would correspond to prescribed transverse displacements of up to 170 µm and 100 µm to be applied by the survey team to the Q1/3 and Q2 cryo-assemblies, respectively. Very likely, fine-tuning will also be needed later on using a beam-based remote alignment of the IT. On the other hand, if at least one of the 3 MCBX circuits remains available in a given plane on each side of IP1 and IP5, the situation can be greatly improved, both in terms of:

i orbit correctability: peak orbit of about 1 mm reached in the triplet for the worst seed of the **MCBX1** and **MCBX2** cases, doubled in the **MCBX3** case.

ii COD strength in the matching section: about 15 % of their nominal current for the worst seed of the MCBX1 and MCBX2 cases, doubled in the MCBX3 case, but ignoring the higher demand on the MCBYs at Q4 assuming that Q4 is OFF as in the case of the Reverse Polarity (RP) optics (see Section 8.2).

iii current required in the remaining MCBX circuits: namely 213 A, 131 A and 266 A, for the worst seed of the **MCBX1**, **MCBX2** and **MCBX3** cases, respectively, therefore less than, or in the range of 400 A when adding the 150 A contribution for the crossing bumps (up to a half crossing angle of 160 µrad).

In summary, the unavailability of 3 MCBX in a given plane on a given side of IP1 or IP5, will require a dedicated realignment procedure of the inner triplets (and very likely fine-tuning with beam-based alignment) to ensure a decent orbit correctability, and then the possibility to inject high intensity beams in the LHC. The conservation of a sufficiently large crossing angle to collide trains at low β^* will then require a more sophisticate crossing bump (still to be studied, but very likely feasible). On the other hand, if on each side of IP1 and IP5, and in each of the two transverse planes, at least one of the 3 available MCBX magnets is still working, and up to a current of $\approx$ 400 A, the crossing bumps generation should be granted (using the nearly standard crossing scheme), together with the closed orbit correctability, with a maximum degradation of up to 1 mm peak (reached in the IT) if either the MCBX1 or MCBX2 magnet is still working, and twice more if the surviving circuit is MCBX3. In this second case (or in general), a prescribed offset of up to $\pm 100 - 150$ µm

to be applied *à la carte* on Q1, Q2 and/or Q3, should definitely improve the situation. These conclusions are independent on the choice of the IT polarity (since the worst case between the H and V planes have been reported in Table 11). In the nominal (existing) configuration where Q4 is powered, the MCBY available strength may be a concern (see Table 11), in particular for the configuration where only MCBX3 would be available.

7.3 IT Skew Quadrupoles (MQSX)

The MQSX magnets play a fundamental role in correcting both the global and local coupling in the LHC [42, 43]. Their strength (K1S) is constant throughout the LHC cycle and their powering current scales proportionally with the energy. In case of a single failure of an MQSX per IP, it is possible to re-distribute the correction from the MQSX on one side of the IP to the other. This corrects the global coupling well. However, depending on the MQSX that fails this can cause a significant increase in the effective beam size at the IP [42, 44]. The impact of transferring the correction from the MQSX3.L1 to the MQSX3.R1 on luminosity was tested in 2022. The measured luminosity variation is shown in Figure 23 where it is compared to what is expected from simulations.

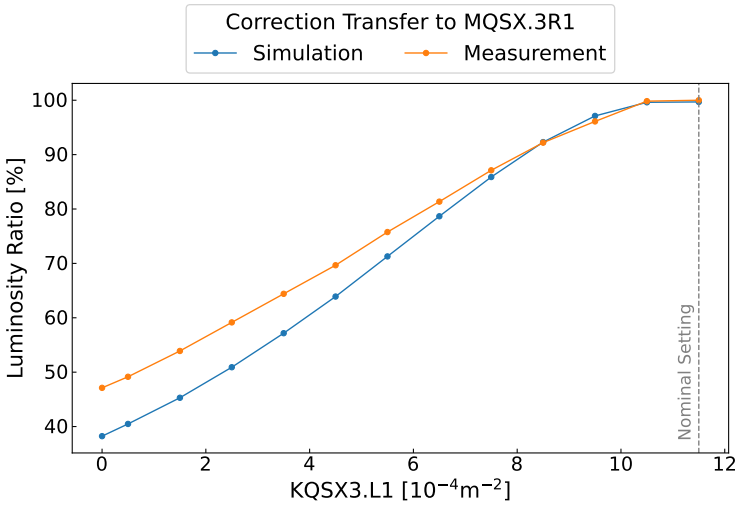

Figure 23: Impact of the transfer of the correction from MQSX3.L1 to MQSX3.R1 on the instantaneous luminosity at $\beta^* = 30\,\text{cm}$. The nominal strength of MQSX3.L1 is $11.5\,\text{m}^{-2}$. After transferring the full correction from MQSX3.L1, MQSX3.R1 has a strength of $15\,\text{m}^{-2}$ (nominal correction for MQSX3.R1 is $3.5\,\text{m}^{-2}$).

The expected relative loss of integrated luminosity in case of failure of an MQSX and compensation by the one located on the other side of the IP is shown in Figure 24 as a function of the unavailable MQSX. The failure of an MQSX in IR2 and IR8 will have a negligible impact on the proton-proton integrated luminosity of ALICE and LHCb. However, correction of the global coupling along the cycle will be needed. For ion operation, the loss of a single MQSX in IR2 would have a significant impact on the peak luminosity due to the increase in the beam size at the IP. Note that the radiation received by the MQSX in IR2 and IR8 is much lower compared to IR1 and IR5.

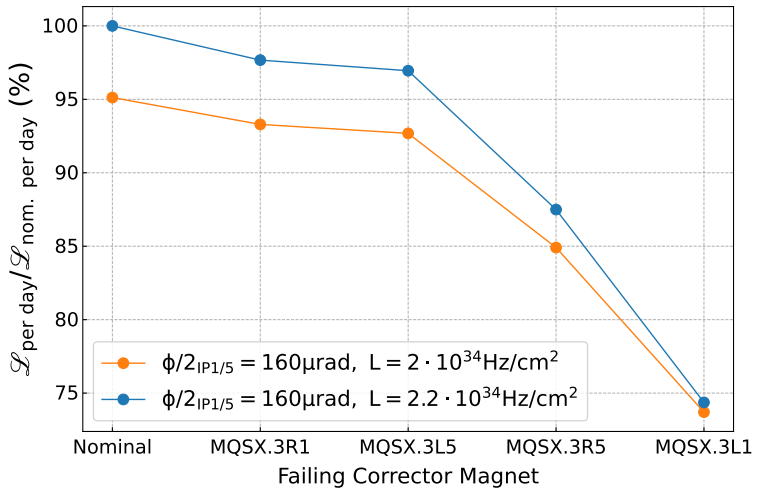

Figure 24: Expected relative loss of integrated luminosity in case of a single MQSX failure as a function of the unavailable MQSX for an initial bunch population of 1.8×10^{11} p and assuming β^* levelling from 1.2 m down to 0.3 m. The value of the levelled luminosity is given in the figure. The turnaround time is assumed to be 4.5 h and the number of bunches 2380. The impact on instantaneous luminosity increases as β^* decreases which means that if we are limited to lower intensities the impact will be bigger since we will be at lower β^* for longer.

In case of a failure of the MQSX on both sides of the IP the impact on the global coupling will be very significant and the strength of the arc skew quadrupoles will not be enough to correct coupling to low β^* values. In addition, the layout of the arc skew quadrupoles is favourable to the correction of the coupling difference Resonance Driving Term (RDT) (f_{1001}) but not of the coupling sum RDT (f_{1010}). The possibility of changing the phase advance between IP1 and IP5 to have a partial self-compensation of the coupling will be tested in a future Machine Development (MD) session. However, it is unlikely that an effective β^* smaller than 85 cm can be reached. This would lead to a reduction of the integrated luminosity by around 30-35% assuming an initial bunch population of 1.8×10^{11} p. This new setup would need new optics measurements and also a potential correction. A new setup of the collimators is most likely not needed but aperture measurements and machine protection tests will be necessary before going to high intensity after such a modification.

An approach to correct the local coupling would be to tilt the Q2 and/or the Q3 IT magnet. Note, that the direction of the tilt would have to be opposite between the two magnets. The needed tilts to fully compensate for the loss of a MQSX are shown in Table 12. In order to replace a single failing MQSX the accuracy of the tilt must be within ± 0.5 mrad (assuming Q3 tilt) of the desired tilt to limit the integrated luminosity loss to less than 1-2 %. However, if the MQSXs on both sides of the IP fail an accuracy of ± 0.2 mrad is needed if we want to reach the β^* of 30 cm and limit the loss in performance. It should be emphasised that the loss of the MQSX is a significant performance limitation but that operation can continue, albeit with a limited β^* reach.

The impact on β-beat and on non-linearities is in the range of 0.1% so no additional correction would be needed [45]. However, considering the challenging procedure to tilt the magnet one can not expect it to reproduce fully the MQSX correction, so a fill for coupling and optics measure-

IR	Failing Magnet	K_{1S} [1×10^{-4} m^{-2}]	Tilt for Compensation	
			Q2 Tilt [mrad]	Q3 Tilt [mrad]
IR1	**MQSX.3L1**	11.5	−1.65	2.325
	MQSX.3R1	3.5	0.5	−0.7
IR5	**MQSX.3R5**	8	−1.15	1.6
	MQSX.3L5	4	0.575	−0.8

Table 12: Necessary tilt angles of either Q2 or Q3 triplet elements to compensate for the loss of the skew quadrupole corrector. A positive sign corresponds to a clockwise rotation in the Beam 1 direction.

ments should be done followed by machine protection checks such as loss maps and asynchronous dump. The tilt is technically a difficult operation and the potential risks need to be considered. A recent analysis [46] has shown that a tilt of Q2 would be possible but, considering that the support of the IT cryo-magnets is statically indeterminate (hyperstatic) and therefore that the response to a rotation is not predictable and considering the low level of mechanical margin on the buckling of the W bellows, it is recommended to perform this operation at room temperature. Given the effect of temperature on irradiated polymeric components, this does not appear to be a viable solution.

Another mitigation method would be to install a warm skew quadrupole close to the failing one. The technical proposal for this is described in Section 8.4. In this case no loss of integrated luminosity is expected. One shift to measuring and validating the correct behaviour of the warm skew quadrupole followed by additional machine protection tests will be needed.

7.4 Higher Order IT correctors

The higher-order correctors refer to the non-linear (NL) correctors available in the ITs. Since 2023 all of the NL correctors are used in IR1 and IR5. The LHC was operated without non-linear IT correctors for β^* larger or equal than 40 cm until 2017. The impact of the NL correctors becomes more important as β^* decreases and it has been shown in MD that the dynamic aperture deteriorates at β^* of 15 cm without the b_4 corrections [47]. NL correctors are not used in IR2 and IR8 because of the larger β^* in the corresponding IPs. The description in the following section is focused on the current baseline scenario of 30 cm.

7.4.1 Skew/Normal Sextupole (MCSX/MCSSX)

Failure of the two b_3 correctors on each side of the IP would lead to a change in the transverse coupling of 2–3$\times 10^{-3}$ and the two a_3 corrector would lead to a β-beat of 2% in IR1. The impact is similar in IR5 but due to the different crossing plane the loss of the b_3 (respectively a_3) correctors will induce β-beating (respectively transverse coupling). A fill for optics and coupling checks might be required before resuming normal operation. In the absence of Skew/Normal Sextupole IT correctors, the change of crossing angle will have a larger impact on tune, coupling and β-beat. This is an operational inconvenience but is not expected to have a direct impact on performance.

7.4.2 OCTUPOLE (MCOX)

The b_4 correctors have a significant impact on the amplitude detuning. If a single MCOX is failing the global amplitude detuning can be compensated by redistributing the powering from IR1 to IR5 (the left of IR1 needs to go to right of IR5). There is sufficient powering margin in all the MCOX to do this operation. This could be done and no need for re-validation would be required to continue operation. If all the MCOX in IR1 and IR5 would be unavailable then this would significantly change the amplitude detuning at β^*=30 cm. This is of importance for beam stability and lifetime but also for the optics commissioning where it has been shown that without the b_4 corrections, the tune signal significantly deteriorates. It is possible to mitigate this effect by powering the Landau Octupoles (MO) in the arcs. In order to reach the same level of residual amplitude detuning as after the corrections with the MCOXs have been applied, MO need to be powered up to ≈200 A (different depending on family and arc). Figure 25 shows the expected residual detuning from simulation when MO powering is applied to compensate for the amplitude detuning induced by the IT b_6 and b_4 errors. The dotted lines show the residual detuning that was measured in 2022 after applying the nonlinear corrections. Note that the figure refers to β^*= 30 cm where the impact of the MCOX is the strongest but the effect of the MOs is also amplified thanks to the Achromatic Telescopic Squeeze (ATS) tele-index of 2 [48, 49]. The powering that would be needed to reach the same residual level of amplitude detuning in the absence of all the b_4 and b_6 correctors is shown in Table 13. MCOX in IR8 (and IR2) are not effective due to the larger β^* and hence smaller β-function at the location of MCOX.

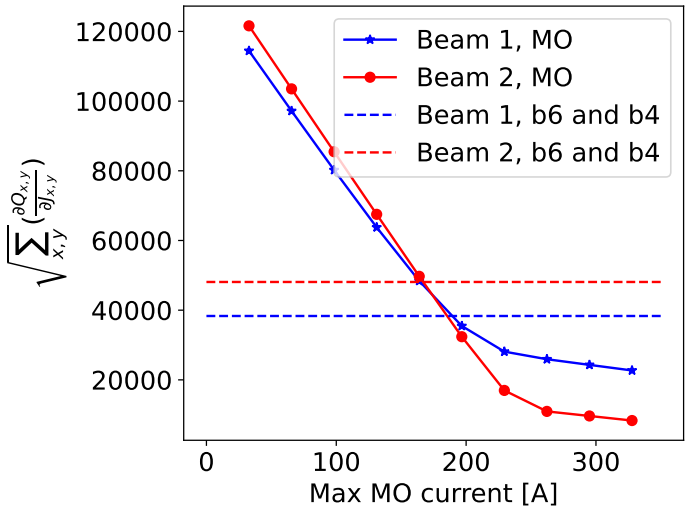

Figure 25: Expected residual amplitude detuning as a function of the maximum MO powering.

In normal operation, amplitude detuning is most crucial to stabilize the bunches before the beams are brought in collision, which in Run 3 is at 1.2 m. Once in collision the beam-beam tune spread will have a stabilizing effect except for the bunches that are non-colliding or only colliding in IP2 and IP8 . At a β^* of 1.2 m the effect of the MCOXs is negligible but it increases at smaller β^* and the powering of the Landau Octupoles will have to change with β^* reaching 500 A for the MOF and 100 A for the MOD at β^*=30 cm. In this case the amplitude detuning would be very similar to what it is today. However, even without compensating for missing MCOX it is likely

Family	Powering [A]
MOD	-200
MOF	200

Table 13: The powering needed to reduce the amplitude detuning to the same level as when using the MCOXs at 30 cm.

that the beam would remain stable due to the negative sign of the cross-term naturally generated by the triplet errors.

7.4.3 SKEW OCTUPOLE (MCOSX)

The LHC was operated in 2022 without any a_4 correctors. In case an a_4 corrector would not be available in IR5 the recommendation would be to move the correction from the corrector on one side of the IP to the other. There is sufficient powering margin and the global effect is very small since the a_4 corrector on the left and right side of the IP have very similar effect on the RDTs. This compensation is not possible in IR1 where there is only a single a_4 corrector functioning. The recommendation would then be to turn them all OFF, including the correctors in IR5. The operation could continue without any mitigation measure but the coupling will change by $1-2\times10^{-3}$ so if this causes any issues for operation, e.g. instabilities, a fill for coupling measurement should be inserted.

7.4.4 DODECAPOLE (MCTX)

The LHC was operated the entire Run 2 without any b_6 correctors and the impact on the amplitude detuning as well as the dynamic aperture is limited so if one of them fails the recommendation is to turn all of them OFF and continue operation. No mitigation is needed and no impact on performance is expected.

7.5 D1 in IR1 and IR5

The separation dipoles D1 in IR1 and IR5 consist each of 6 MBXW magnets. The magnets located left and right of each IP are powered in series by a 850 A/700 V power converter. The possibility of operating with 5 out of 6 MBXW magnets by disconnecting two of them (one magnet on each side of the IP and in symmetric positions with respect to it) has been considered. The scenario of the failure of the MBXW magnet closer to the IP has been studied. The maximum integrated field provided by each of the MBXW magnets when operated at 850 A is 5.12 T m providing a kick angle of 225 µrad at 6.8 TeV, to be compared with the nominal kick of 188 µrad provided by each magnet in the nominal configuration with 6 MBXW magnets. The maximum current could be increased to 900 A by swapping the present power converter with the previous thyristor-bridge power converter that is still installed as "hot spare"; this operation would take of the order of 2-3 hours while the disconnection of one of the MBXW on each side of the IP could be completed in a few hours. The possibility to operate the magnet and the power converter at 900 A should be validated with a heat run but appears to be possible. The MBXW integrated field at 900 A is 5.3 T m corresponding to a kick of 233 µrad at 6.8 TeV (see Figure 26 — left) [50]. The MCBX correctors on each side of

the IP will need to provide a small contribution to the separation with $\approx 0.1\,\mathrm{T\,m}$. The strength of the D2 (MBRC) magnets will have to be increased by 5.22 % from 1129 µrad to 1188 µrad which is within the capability of the magnet and power converter thanks to the operation at 6.8 TeV. No impact on the D2 aperture is expected. Measurements of the field errors have been performed when feeding the MBXW modules at a current of 900 A and compared with those at the present operational current of 685 A showing a significant increase of the b_3 component (see Figure 26 — right) [50]. This systematic b_3 of 1.6 units, integrated over 5 MBX modules corresponds (in integrated strength) to 1.1 units of uncorrected b_3 in Q2, and/or to 30 A in the MCSX corrector, which is significant. The impact on dynamic aperture and possible correction should be further studied.

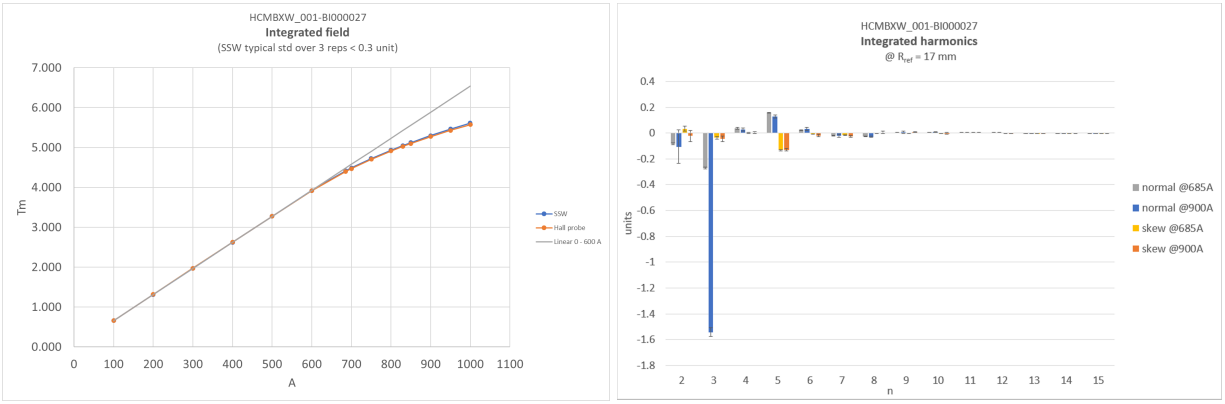

Figure 26: Measured MBXW integrated field vs. current (left) and multipolar errors at 685 A and 900 A (right).

8 Preventive actions

8.1 Operation

As discussed in the previous sections, a failure of a superconducting circuit could lead to performance reduction and/or significant downtime. It is also expected that radiation is responsible for the degradation of the mechanical properties of the polymers used in the construction and insulation of the coils and therefore it could lead to reduced training performance. Reduction of mechanical stresses and of the probability of quenches, that might lead to electrical failure and permanent damage, is therefore recommended. Limitation of the maximum currents at which commissioning and pre-cycle are performed can be beneficial at this scope.

8.1.1 Reduction of HWC currents

LHC operation relies on 1572 superconducting circuits distributed along the eight LHC sectors. Whenever an intervention is carried out on one of these circuits, the functionality needs to be validated to ensure correct and reliable operation. At this purpose, a series of tests (so called powering tests) with progressively increasing current levels is performed. After any interruption of beam operation during which several interventions take place in the LHC tunnel, a campaign of

tests is executed on all superconducting circuits, regardless whether an intervention was performed. Such validation is also taking place whenever a magnet undertake a thermal cycle. The current reached during this validation is the maximum current the circuit was designed for (so called I_PNO). However, especially in the case of corrector circuits, this current value often exceeds substantially the operational needs.

With the goal of reducing the mechanical stress on the corrector magnets located in the IT assembly of IR1 and IR5, it was therefore recommended to reduce the value of I_PNO at least in the *high-radiation regions*. A correct choice of these values would not entail any performance limitation.

The value of 300 A was considered safe for the MCBX and MQSX correctors from the point of view of the corresponding stored magnetic energy (considered sufficiently low to avoid damage in case of quench in presence of a degradation of the insulator electrical properties) and considering the quench performance of these circuits (see Figure 18 in Section 6.1). The values listed in Table 21 in Appendix C have been implemented in the control database and used for the HWC campaign following the YETS 2022–2023. As it can be seen, the values have been chosen allowing some margin with respect to the operational values (I_OP) of Run 2 (2018) and Run 3 (2022). The same logic was applied for the NL correctors and the corresponding I_PNO are listed in Table 22 in Appendix C.

In the case of IR2 and IR8, the situation is slightly different. The required operational current for the MCBX correctors is too high to allow a reduction to 300 A, however they are subject to a lower radiation dose. For that reason no reduction of the HWC currents was implemented in 2023, but it is proposed to reduce I_PNO for the next HWC according to the values listed in Table 23 in Appendix C. The proposal for the NL correctors in IR2 and IR8 is presented in Table 24 in Appendix C.

8.1.2 Reduction of pre-cycle currents

Both superconducting and resistive magnets need a proper pre-cycle to have a reproducible behavior, namely to provide the same field at the same level of current. For the IT correctors, this consists of a bipolar cycle to the nominal current of the magnet. An example is presented in Figure 27. The global pre-cycling strategy was modified in 2015, in order to reduce the global time of the operation, reducing the values of the pre-cycle current to the equivalent energy of 3.5 TeV. However, this reduction was only applied to to the high current magnets as the cycle of the correctors is much quicker and does not impact the overall pre-cycle time.

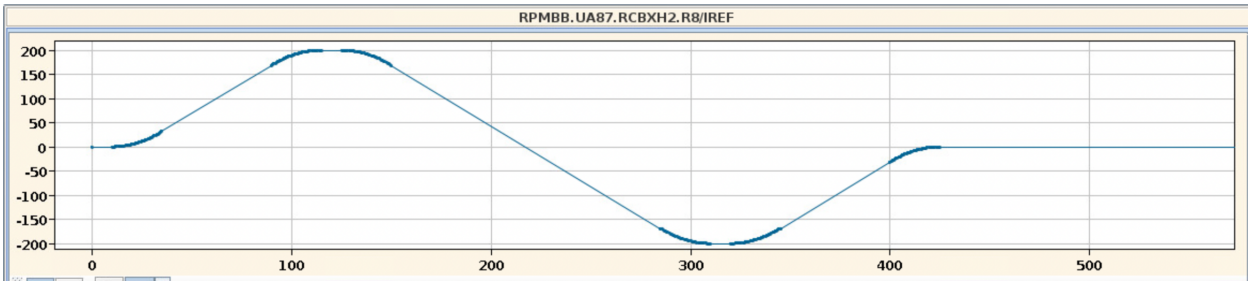

Figure 27: Typical bipolar pre-cycle for IT corrector magnets.

This operation is carried out at each operational cycle. It is therefore of fundamental importance

to also reduce these values to the minimum, to limit stress on the magnets. The values at which the different IT correctors are pre-cycled can be found in Table 25 in Appendix C, together with the new values implemented for the 2023 run.

The residual field of the MCBX magnets could potentially have an effect on the reproducibility of the orbit. However, while the horizontal correctors are pre-cycled at 200 A, the vertical correctors have never been pre-cycled (to avoid powering MCBXH and MCBXV at the same time and limit mechanical stress – see Section 5.1.2) without any noticeable effect on the orbit reproducibility. The MCBX residual magnetization is 2–3 % at 20 A, 3–7 % at 10 A, and 13 % at 5 A [51]. This residual magnetization would produce a kick of up to 1.5 µrad, which corresponds to about 13 % of the typical kick needed from one of this magnets at injection energy. Such a kick would produce an orbit distortion, which would be corrected away by the orbit feedback. The residual RMS would be around 0.01 mm. As the orbit feedback does not use the MCBXs, a local structure around the IR will however remain, but below 0.1 mm (typically about 30% of a sigma). Moreover, as the error is systematic and the current cycle of the correctors is always the same, the effect would be corrected away during the initial commissioning. Absence of pre-cycle would only generate the discussed orbit distortion in the very rare case of an unusual current cycle. Even in the worst case, when all errors sum up, the effect would be negligible at injection and would disappear during the ramp, when the magnet current is increased. It can therefore be considered negligible. As the effect of a residual magnetic field in the MQSX magnets is more difficult to quantify, it was decided to maintain a pre-cycle, but with reduced current. The residual field for the NL correctors is negligible, so the pre-cycle current was set to zero. Following the successful implementation in IR1 and IR5 during the 2023 HWC it is proposed to apply the same criteria for IR2 and IR8 for the 2024 run (see Table 26 in Appendix C).

8.1.3 Possibility of warming-up the arcs and not the triplet area

The largest mechanical stress for a magnet happen during warm-up and cool-down. In addition, getting in contact with air as part of the warm-up is potentially detrimental for magnets which were exposed to radiation as the IT (see Section 5.2). For these reasons, it is recommended to avoid thermal cycles of the IT assemblies as much as possible. No thermal cycle is foreseen until LS3, when the IT assemblies of IR1 and IR5 will be replaced in the frame of HL-LHC project. However, it cannot be excluded that a warm-up will be required in the arc, for example, to intervene on a cryo-magnet. As the cryo-plant used for the arc and for the IT are the same, a warm-up of the arc was always coupled with warm-up of the IT. Some mitigations could be put in place to partially decouple them:

- isolate all valves of the IT and DFBX;
- keep the active cooling of thermal shields as long as possible (until the arc temperature is around 80 K);
- depressurize a few times the IT cold mass towards the Cryogenic Distribution Line (QRL) via the quench valves.

Unfortunately, the DFBX will rapidly warm-up to 300 K, entailing additional heat load on the IT. With the implementation of the above mentioned measures, the IT magnets would naturally warm-up, following the behaviour shown in Figure 28.

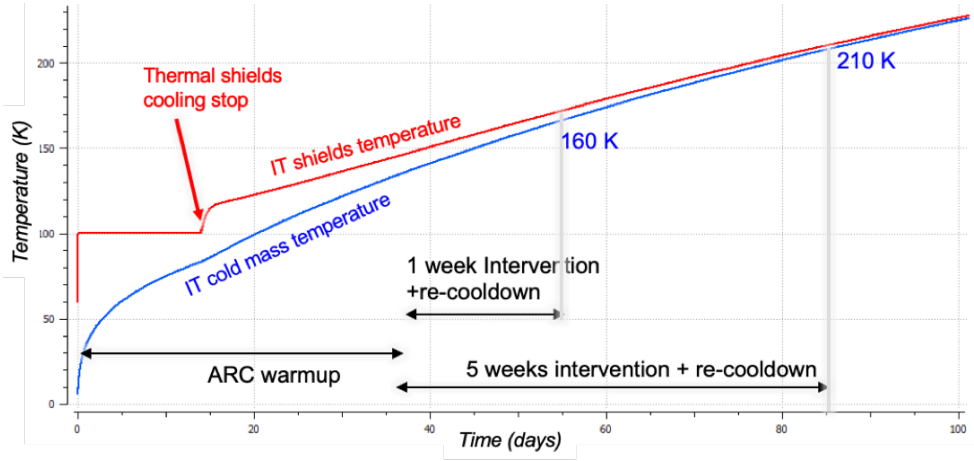

Figure 28: Simulation of natural warm-up of IT assembly as a function of time in case of intervention on a cryo-magnet in the arc.

Counting about 5 weeks to warm-up the arc, assuming optimistically 5 weeks for the intervention for a replacement of a magnet in the arc and about 2 weeks to cool-down the arc to reach the IT temperature, the IT will reach a temperature of about 210 K before its cool-down can restart. This will reduce to 160 K in case of a 1 week intervention (e.g. for a Plug-In Module—PIM—replacement). However, Helium release towards QRL/arc magnets cannot be avoided. As consequence there could be several major issues in case of QRL/magnet opening:

- safety risks to be assessed;
- significant Helium background in the tunnel, with impact on leak tests;
- pollution of the IT Helium circuits without possibility to purge at ambient temperature, entailing risk of clogging the cryo-circuits.

In summary, it might possible to maintain the IT in Helium atmosphere during an intervention in the arc but the IT temperature might approach ambient temperature depending on the duration of the intervention. In addition, the associated safety risks and potential implications for the operation of the IT circuit (e.g. pollution) need to be fully assessed. This situation will change in the HL-LHC era for the IT in IR1 and IR5 (not for those in IR2 and IR8), as independent refrigerators for IT cooling will be installed. As consequence, arc and IT cooling operation will be decoupled, but the IT installed on the left and right side of IP1 and IP5 will be cryogenically coupled (which is not the case today). However, it will be possible to warm-up one IT, while maintaining the other one cold in degraded conditions with the existing LHC refrigerator.

8.2 Triplet Polarity Inversion

8.2.1 Triplet radiation versus optics configuration

The IT peak integrated radiation dose not only depends on the integrated delivered luminosity, but also on other ingredients defining the so-called machine configuration, coming from the fact that the peak dose is reached at a few hot spots located at a few longitudinal positions along the magnet coils and at a few azimuthal angles (see illustrations in Figures 3 and 4 in Section 4). In particular, as pointed out in Section 4, the IT peak integrated radiation dose depends on

- the plane, magnitude and polarity of the crossing angle;
- the beam-screen orientation;
- and the triplet polarity, presently FDF.

Therefore, four different machine configuration can a priori be envisaged for both IR1 and IR5, depending on the triplet polarity (FDF or DFD), and the crossing angle orientation (H or V). Imposing the best possible long-range beam-beam mitigation results in only four combinations between IR1 and IR5, out of the sixteen in principle possible, due to the fact that the crossing plane orientation must be alternated in ATLAS and CMS (H/V or V/H), and the IT polarity should (preferably) be the same in these two experiments[5].

Configuration	ATLAS	CMS	Optics type at the end of levelling
1	FDF-V	FDF-H	Round (nominal configuration)
2	FDF-H	FDF-V	Flat (for maximized performance)
3	DFD-V	DFD-H	Round
4	DFD-H	DFD-V	Flat (for maximized performance)

Table 14: Selected configurations for ATLAS and CMS, with best possible crossing angle reach thanks to a self compensation between IR1 and IR5 of the long-range beam-beam induced b_{4n+2} multipoles (b_2, b_6, ...), exact for round optics, only partial for flat optics.

These four possible combinations are reported in Table 14. The first one corresponds to the nominal (present) LHC configuration; the second and the fourth (with H/V crossing in ATLAS/CMS) are limited to a β^* reach in the range of $\beta^*_\times = 50 - 60$ cm in the crossing plane (see later). On the other hand, these configurations remain competitive, if not superior than the nominal configuration in terms of virtual luminosity reach, provided a flattening of the optics down to $\beta^*_{||} = 15 - 18$ cm is applied in the parallel separation plane, as soon as the IT aperture has been saturated in round optics mode in the crossing plane (see [52] for more details, and [53] for MD results obtained with 60/15 cm flat optics in Run 2). Finally, symmetries exist when exchanging ATLAS and CMS (V $\leftrightarrow$ H beam-screen) and going from the first to the third configuration or from the second to the last configuration (FDF $\leftrightarrow$ DFD triplet polarity) with the V/H and H/V crossing schemes, respectively: the 3D triplet radiation map gets rotated by $\pm 90^\circ$ along the beam axis.

The longitudinal peak dose profile along the triplet at 0, 90, 180 and 270° is shown in Figure 29 for the nominal, and the two possible configurations with reverted triplet polarity, illustrating in particular the above-mentioned symmetries between the first (nominal) and the third configuration of Table 14. The latter can be immediately discarded, for IR5 only, due to the maximum of 30 MGy, reached after only 300 fb^{-1} and found at 0° at the entry of Q2A in IR5, with no possibility to revert year by year the horizontal crossing angle polarity. On the other hand, the RP-V configuration for IR1 (considered separately), would strongly mitigate the Q2 hot spot, at a cost of increasing the radiation rate in Q2B (but for which the integrated dose is presently quite small). Such hybrid configuration, namely RP-V in IR1 and Nominal-H (no change) in CMS, will be discussed in more details in Section 11. The radiation levels are found to be sensibly reduced

[5] At a given β^*, the minimum allowed crossing angle in ATLAS and CMS is known to be very poor in the configuration of a H/H or V/V crossing scheme. However, sticking to the alternated H/V or V/H crossing scheme, but with opposite IT polarity in IR1 and IR5, the possible impact on the crossing angle reach still needs to be quantified to really discard this kind of hybrid machine configuration.

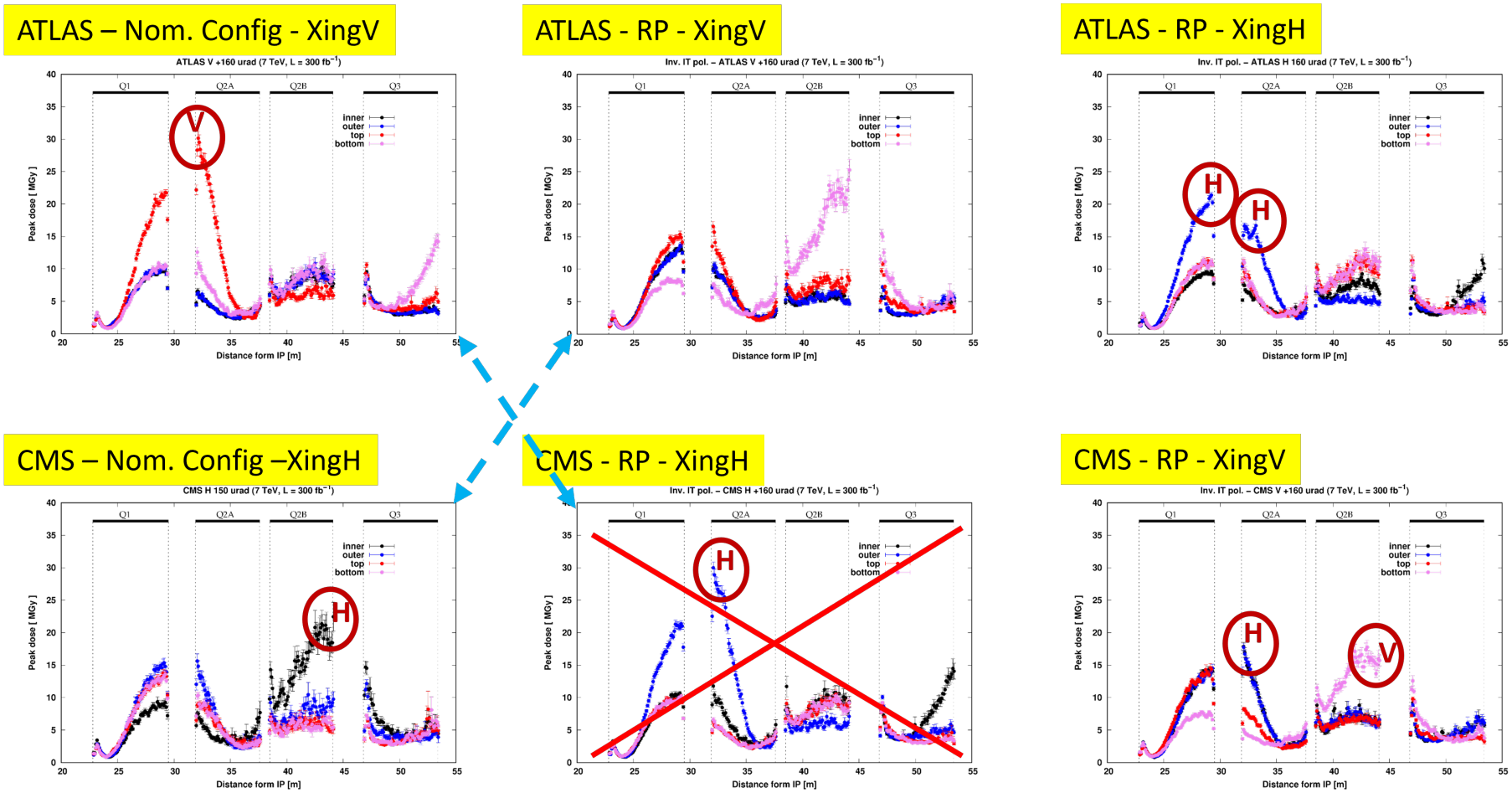

Figure 29: Radial peak dose [MGy] in the coils along the triplet of the ATLAS (top) and CMS (bottom) insertion after 300 fb^{-1}, at an azimuthal angle of 0, 90, 180 and 270° (in blue, red, black and magenta, respectively), for the nominal LHC configuration (left plots) and the two configurations with reversed triplet polarity (RP) optics (middle and right plots with V/H and H/V crossing planes in ATLAS/CMS, respectively). The potential reduction by a regular polarity inversion of the vertical crossing angle is not included. This is not possible in the case of horizontal crossing, which discards the RP-H configuration in IR5.

for both IRs and at all azimuths in the fourth configuration of Table 14 (right plots of Figure 29). Furthermore, compared to the nominal configuration, the hot spots are displaced from Q2A to Q1 in IR1 and from Q2B to Q2A in IR5, and often shifted from the horizontal to the vertical plane, and viceversa. All together, switching to this configuration for the last two years of Run 3 (2024–2025) would lead to a significant peak dose reduction, as detailed in Table 15 (see also Tables 18 and 19 in Appendix B for more details), or, in other terms, to a potential increase of the integrated luminosity after which the peak radiation dose of 30 MGy is reached from $\approx 500\,\text{fb}^{-1}$ up to $\approx 625\,\text{fb}^{-1}$.

Configuration plan	Most impacted magnets	Peak dose [MGy] after $500\,\text{fb}^{-1}$
1 until 2025 end	Q2A in IR1	29.5–32.5
	Q2B in IR5	31–31.5
4 in 2024 and 2025	Q2A in IR1	23.5–25.5
	Q2A in IR5	24

Table 15: Effect of the adoption of the RP optics with H/V crossing in ATLAS/CMS from the beginning of 2024 until reaching $500\,\text{fb}^{-1}$ at the end of 2025. The intervals (see also Figure 5) give the margin between the more favourable configuration, featuring a crossing angle decrease along the fill and – in ATLAS – the upward/downward swap in the middle of 2025 (first row) or 2023 (second row), and the less favourable configuration, with constant crossing angle and ATLAS crossing swap only at the beginning of 2024 (first row) or not anymore (second row).

Moreover, the adoption of the fourth configuration in 2024 and 2025 would yield a remarkable benefit on D1, namely on its hot spot in the magnet heads of the first module after the IT (see Section 4.2), which is predicted to decrease from 120 MGy to 80 MGy in IR1 and from 80 MGy to 60 MGy in IR5 (see Tables 18 and 19 in Appendix B).

8.2.2 Optics

A large variety of possible hardware configurations have been envisaged with the triplet polarity inverted. The latter can be basically classified into two different categories:

- **RP1** Polarity inversion of all quadrupoles till quadrupole Q_n, $n \geq 3$, Q_n and Q_{n+1} with the same polarity, and nominal quadrupole polarity recovered as of quadrupole Q_{n+2}.
- **RP2** Polarity inversion of all quadrupoles till quadrupole Q_n, $n \geq 3$, Q_{n+1} switched off, nominal quadrupole polarity recovered as of quadrupole Q_{n+2}.

The case $n = 3$ of the **RP1** category was investigated, showing the feasibility of matching both injection and collision optics (within the magnet strength and aperture constraints), but with no obvious connection with the telescope and anti-telescope of the nominal ATS optics (with left and right IR phases found to be shifted by $\approx \pi/2$ w.r.t. to the nominal IR1 and IR5 ATS phases in the H plane). Then the "Q4off", "Q5off" and "Q6off" configurations, corresponding to the cases $n = 3, 4, 5$, respectively, of the **RP2** category, were also looked at. In each of these 3 cases, injection and collision optics could be matched, and with the right betatron phases in order to reuse the nominal telescope and anti-telescope of the nominal optics. The "Q6off" configuration showed the best optics flexibility in collision, but a rather tight aperture at injection, with $1.5\,\sigma$ missing at Q5 w.r.t. to a nominal target of $11\,\sigma$ (due to the Q5 beam-screen orientation which is adjusted for the present Q5 polarity). On the other hand, the collision optics was found less flexible for the "Q4off"

and "Q5off" configurations, but with an aperture still within the target at injection, although reduced w.r.t. the nominal injection optics in the matching section. In order to limit the hardware modifications to the triplet only (2 circuits — RQX and RTQX2 — per triplet), the "Q4off" configuration was selected as baseline to fully develop the RP optics. Injection ($\beta^* = 11$ m) and 30 cm optics (using the nominal telescope) are compared in Figure 30 in the nominal and "Q4off" configuration. Within a sign, the triplet gradient are quasi the same between the nominal and RP configuration, together with the peak β-functions reached in the triplet at a given β^*. As previously mentioned, however, to fully profit of the beneficial impact on radiation, mostly in IR5, a rotation of the crossing plane in the RP configuration is necessary, which therefore imposes as well a rotation in IR1 to keep an alternated crossing scheme (H/V or V/H) in ATLAS/CMS, to mitigate the impact of the long-range interactions on beam dynamics. This crossing bump rotation (in both IRs), in turns, limits the β^* reach in the range of 50 – 60 cm in round optics mode, and then requires to flatten the optics to preserve and further maximise the performance reach as soon as this β^* has been reached in the new (rotated) crossing plane In this context, 50/15 cm and 15/50 cm flat optics complement Figure 30 as potential candidate for ATLAS and CMS, respectively, at the end of β^*-levelling.

Comparing Figures 30(a) and 30(b), the β-functions at Q5 and Q6 become sensibly larger at injection, but still in the right plane (with the Q5 and Q6 polarity kept untouched in the "Q4off" configuration) such as the matching section aperture requirements can be preserved at injection: see Figure 31 comparing the nominal and the "Q4off" configuration at injection with $\beta^* = 11$ m) and the nominal crossing plane orientation with $\Theta_X/2$ = 170 µrad in both cases. On the other hand, requesting the crossing plane to be already rotated at injection in ATLAS and CMS, would require to relax β^* in the range of 15– 16 m) to preserve the triplet aperture, which, in the case of the "Q4off" configuration, would induce an aperture bottleneck at Q6, and is therefore excluded. As for the LHCb rotation implemented in 2023 [6], an ATLAS and CMS crossing angle rotation, combined with the former, will take place after the squeeze at flat top energy, just before the tune change.

The nominal and "Q4off" configurations are also compared in terms of aperture at the end of β^*-levelling (EoL) in Figures 32(a) and (b), using two different sets of optics parameters as previously discussed, namely: $\beta^* = 30$ cm in both planes with a half crossing angle of 160 µrad (corresponding to a normalized beam-beam long-range separation of 9.2 beam σ for $\gamma\varepsilon = 2.5$ µm at EoL) for the nominal configuration, and a flat optics in the"Q4off" configuration with $\beta^*_{x/y} = 50/15$ cm at IP1, and $\beta^*_{x/y} = 15/50$ cm at IP5, and $\Theta_X/2$ = 145 µrad (10.7 beam σ at EoL), H in ATLAS and V in CMS. The aperture is found to be a bit tight in IR1 (9.1 σ for the first MBXW (D1) module on the out-going beam side) compared to a minimum target of 9.3 σ (i.e. with a margin of 0.8 σ w.r.t. the nominal TCT settings of 8.5 σ), and the 9.6 σ obtained on paper and actually measured for the ATLAS triplets in the nominal configuration. The situation is a bit better in IR5 where D1 is no longer limiting and a normalized aperture of 9.4 σ is found for the inner triplet. It is then advisable to target a 60/18 cm flat optics in 2024 (and eventually 50/15 cm for 2025), which should definitely improve the triplet aperture by 10 % ($\sim 1\sigma$), out of which, some fraction up to 0.5 σ, might be used, if needed, for pushing the crossing angle up to 160 µrad (10 %), depending on the outcome of ongoing beam-beam simulations [see Figure 32(c)]. To be noted that the 60/18 cm flat optics (with $\Theta_X/2$ = 160 µrad) is still found to be 11 % more performing than the 30 cm nominal optics in terms of virtual luminosity (calculated for an RMS bunch length and normalized beam emittance of 9 cm and 2.5 µm, respectively, at the end of β^*-levelling), while the 50/15 cm (with $\Theta_X/2$ = 145 µrad) is

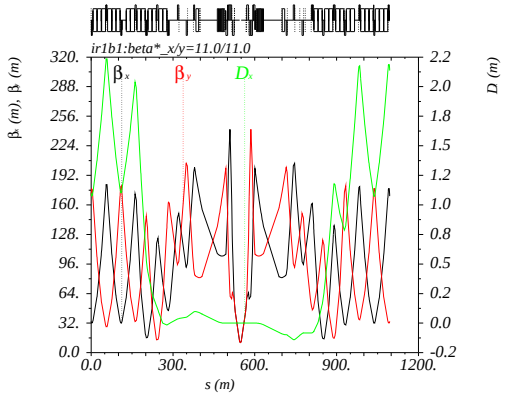

(a) Nom. Config. (IR1b1): $\beta^* = 11\,\mathrm{m}$

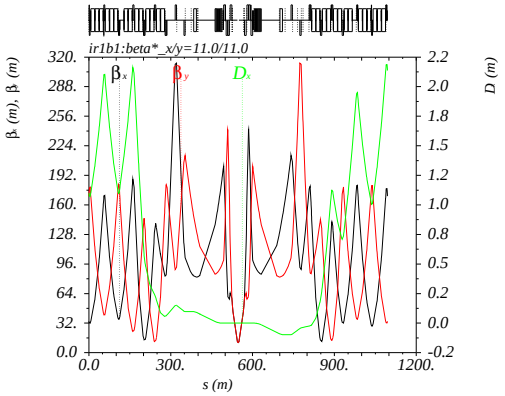

(b) "Q4off" Config. (IR1b1): $\beta^* = 11\,\mathrm{m}$

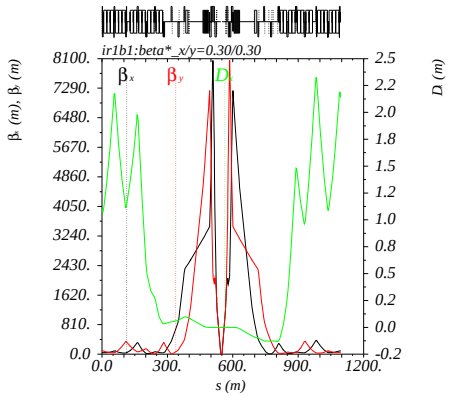

(c) Nom. Config. (IR1b1): $\beta^* = 30\,\mathrm{cm}$

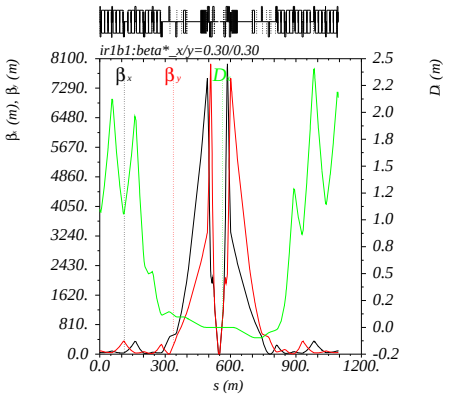

(d) "Q4off" Config. (IR1b1): $\beta^* = 30\,\mathrm{cm}$

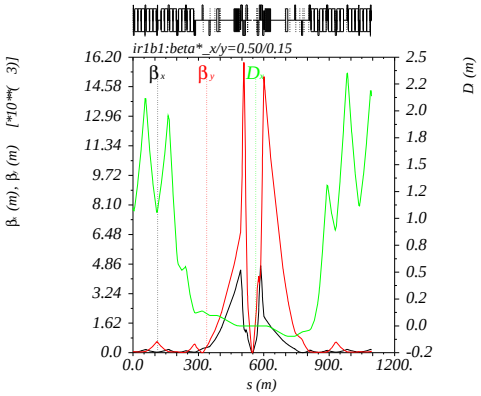

(e) "Q4off" Config. (IR1b1): $\beta^*_{x/y} = 50/15\,\mathrm{cm}$

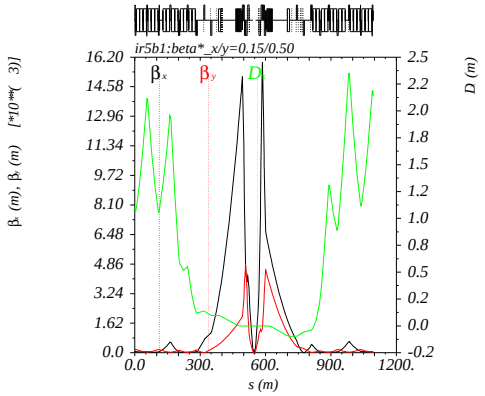

(f) "Q4off" Config. (IR5b1): $\beta^*_{x/y} = 15/50\,\mathrm{cm}$

Figure 30: Optics comparison between the nominal and the "Q4off" configuration for $\beta^* = 11\,\mathrm{m}$ [Figs. (a) and (b)] and 30 cm [Figs. (c) and (d)]. The comparison at 30 cm is academic, in the sense that the β^* reach is limited in the range of 50– 60 cm by the triplet aperture when the crossing plane are rotated in ATLAS and CMS for the "Q4off" configuration, in which case the optics should be flattened when reaching β^* =50– 60 cm in the crossing plane, in order to maximise the performance reach [see flat optics candidates at the end of β^*-levelling in Figures (e) and (f)].

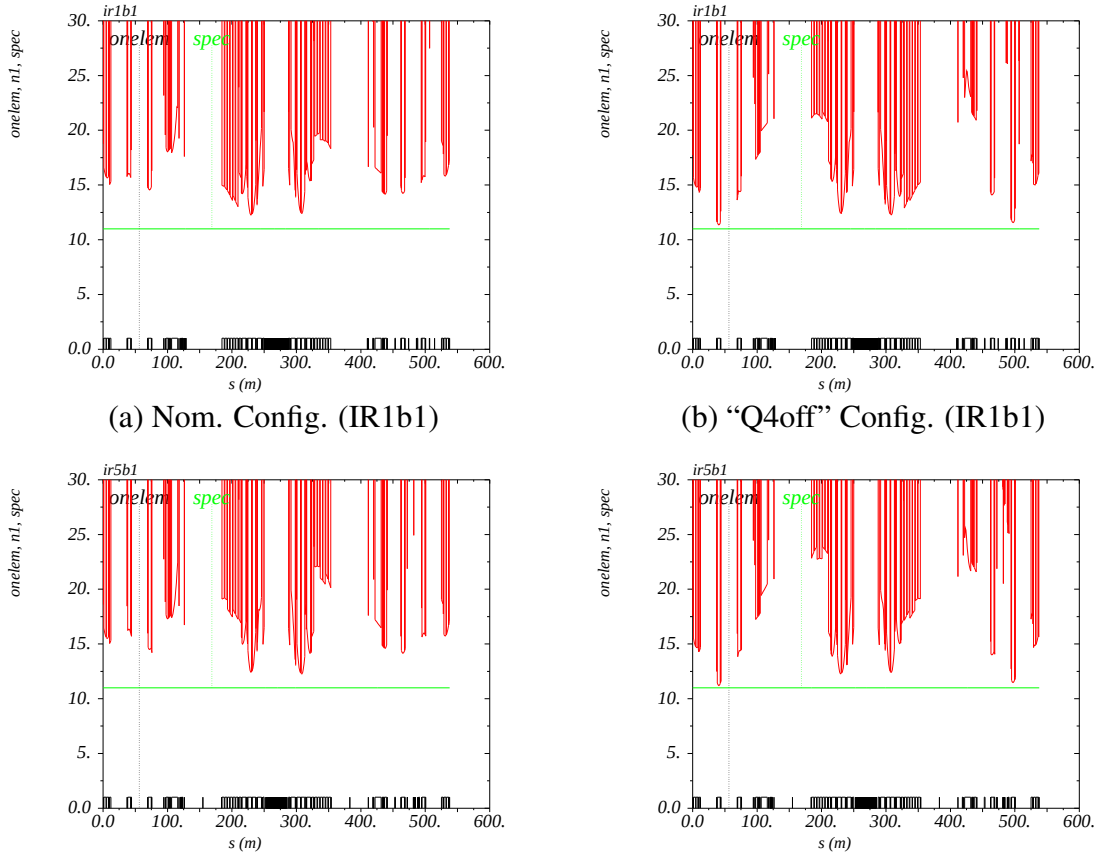

(a) Nom. Config. (IR1b1)

(b) “Q4off” Config. (IR1b1)

(c) Nom. Config. (IR5b1)

(d) “Q4off” Config. (IR5b1)

Figure 31: Normalised aperture [σ] for Beam 1 at injection, calculated for the normalized emittance $\gamma\varepsilon = 3.5\,\mu$m in the nominal (left) and “Q4off” configuration (right), from Q7.L to Q7.R in IR1 (top) and IR5 (bottom). The optics parameters are the same for the two configurations, namely $\beta^* = 11$ m and $\Theta_X/2 = 170\,\mu$rad, vertical in ATLAS and horizontal in CMS. A tolerance budget of 10 % for the β-beating and 2 mm for the closed has been assumed [54], with an aperture requirement of at least $11.0\,\sigma$ at injection (horizontal green bar). The Q6 aperture is sensibly reduced for the “Q4off” configuration, but still meets the requirement.

found to be 34 % more luminous. The corresponding proposed 2024 LHC cycle is then sketched in Figure 33, and compared to 2023.

In case of operation with the RP optics (in IR1 and/or IR5) for proton-proton physics, the ion optics will be based on the 2023 ion optics, simply overwriting the IR1 and/or IR5 settings with those of the new proton cycle (down to a pre-squeezed β^* of 50 cm at IP1 and IP5), with full freedom on the choice of the crossing plane orientation and polarity (in case of vertical crossing) in IR1/5. The same philosophy will be applied to the VdM cycle, for which the 19 m RP optics already exists for IR1 and IR5, but the 11–19 m transition still needs to be redone, though this is expected to be feasible.

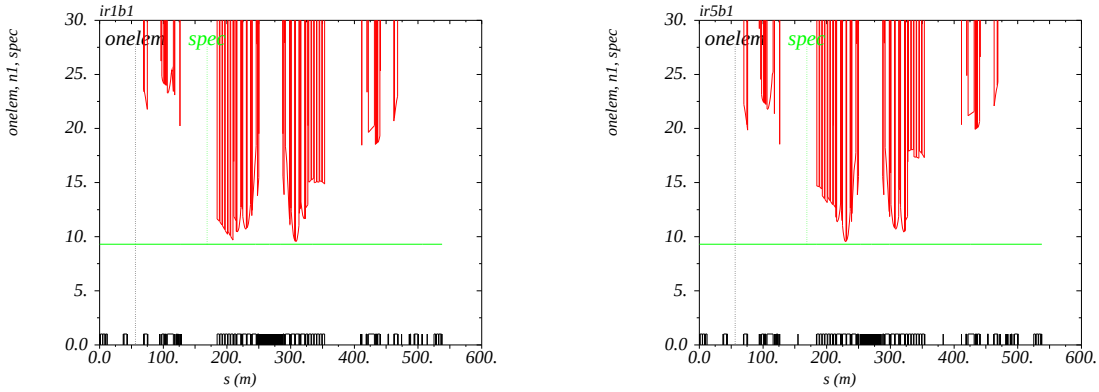

(a) Nom. Config. for IR1b1 (left) and IR5b1 (right) with $\beta^* = 30\,\text{cm}$ and $\Theta_X/2 = 160\,\mu\text{rad}$

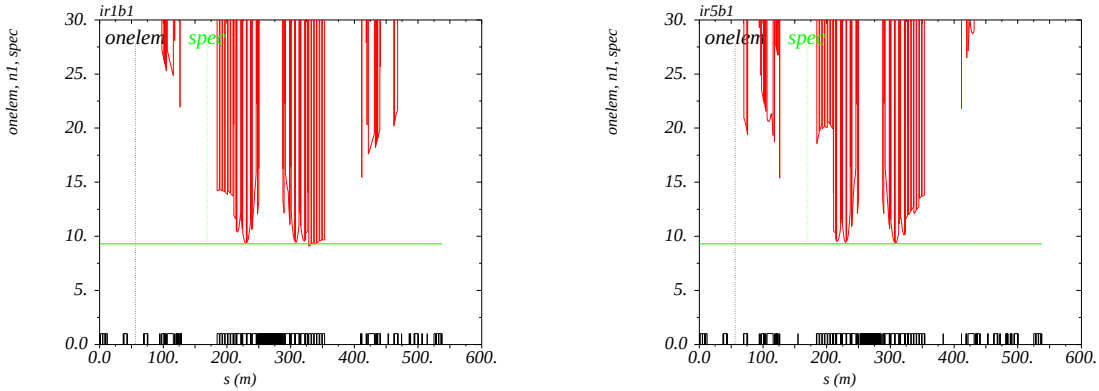

(b) "Q4off" Config. for IR1b1 and (IR5b1 with $\beta^*_\times = 50\,\text{cm}$, $\beta^*_{||} = 15\,\text{cm}$, and $\Theta_X/2 = 145\,\mu\text{rad}$

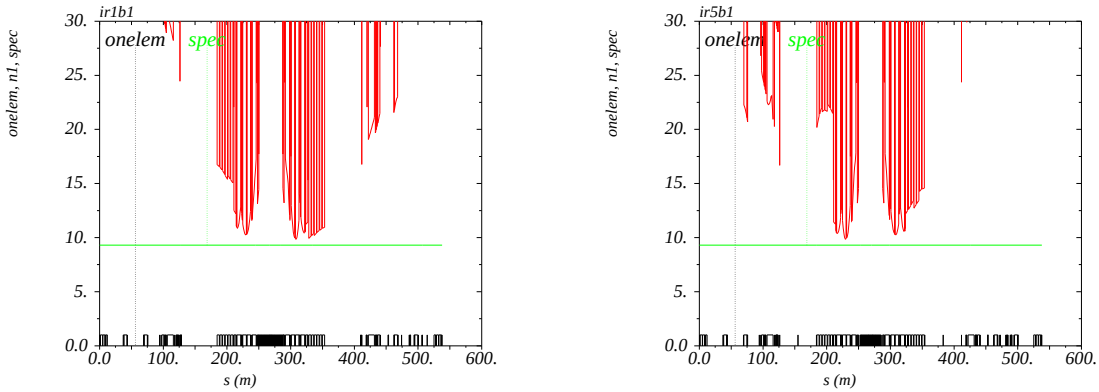

(c) "Q4off" Config. for IR1b1 and (IR5b1 with $\beta^*_\times = 60\,\text{cm}$, $\beta^*_{||} = 18\,\text{cm}$, and $\Theta_X/2 = 160\,\mu\text{rad}$

Figure 32: Normalised aperture [σ] for Beam 1 at EoL, calculated for $\gamma\varepsilon = 3.5\,\mu\text{m}$ in the nominal (top plots) and the "Q4off" configuration with pushed (middle) and relaxed (bottom) optics parameters, from Q7.L to Q7.R in IR1 (left) and IR5 (right). A tolerance budget of 5 % for the β-beating and 0.5 mm for the closed has been assumed [54], with an aperture requirement of at least $9.3\,\sigma$ in collision (horizontal green bar). Within $0.2\,\sigma$, the minimum triplet aperture is similar in the cases (a) and (b), but the D1 aperture is a bit tight in IR1 when the optics parameters are pushed in the "Q4off" configuration [Figure (b)]. Targeting a 60/18 cm flat optics in 2024 [Figure (c)] will definitely improve the situation while giving some margin to the crossing angle, pending 2024 MDs and more experience with flat optics.

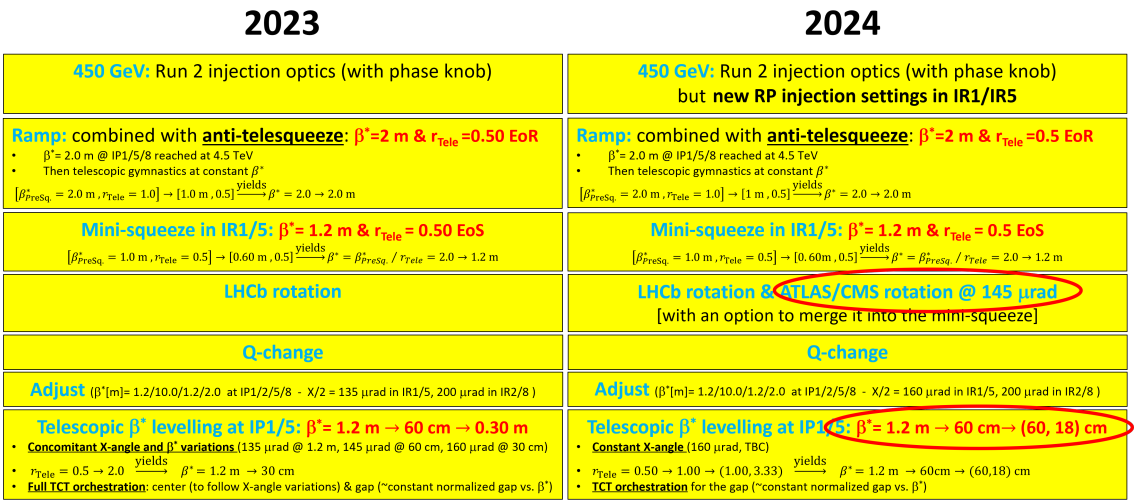

Figure 33: Proposed LHC cycle for the 2024 pp run in the "Q4off" configuration, and comparison with 2023.

8.2.3 Necessary validation steps and time required for the HW modifications

The inversion of the polarity of the triplet quadrupoles is far from being a trivial activity. The water-cooled cables of the RQX (8 kA) and RTQX2 (6 kA) circuits are very heavy and difficult to manipulate. Risks of damaging the cables, the water cooling circuit or the current leads cannot be excluded. A Visite d'Inspection Commune (VIC) was carried out on 14.03.2023 with all relevant teams (EN/CV, SY/EPC, EN/EL, BE/OP) to identify the best way to swap the polarity of the circuit. The report of the visit is summarised in [55]. The identified solution was estimated to be feasible in about 2.5 days in IR1 and about 1 week in IR5, due to the more complex installation. Once the polarity is swapped, some validation tests are needed to verify the correct functionality of the circuit, namely:

- PCC.T4
- PIC2
- PNO.d12
- PNO.d14
- PNO.a9

Execution and validation of these tests would take about 1 shift, assuming no need of magnet training as the magnetic forces are expected to be the same. The validation of the HW modifications required for the IT polarity reversal, at least in IR1, and the corresponding HWC of the circuits above outlined at the beginning of the YETS 2023/2024 is a mandatory pre-condition towards the implementation of the RP optics.

8.2.4 General comments and beam tests

The optics feasibility has been proven in MADX, with a full set of optics already available, even pushed down to 50/15 cm [56], successfully tested in LSA for the power converter limits, and covering all the beam processes described in Figure 33.

In all cases, any significant modifications of the LHC optics needs to be validated with beam tests before implementation; these should cover the following aspects by order of priority:

- aperture measurement at injection after optics correction,
- optics correction and aperture measurement of the round 60 cm (or 50 cm) optics after the IP1/5 crossing plane rotation, to assess the β^* reach in the new (rotated) crossing plane,
- optics correction and aperture measurement of the 60/18 cm (or 50/15 cm) flat optics, to assess the β^* reach in the new (rotated) parallel separation plane.

The validation by additional beam dynamics simulations is ongoing, in particular for beam-beam effects. An improvement of the dynamic aperture has been observed for the proposed RP configuration all along the β^*-levelling beam process, in comparison with the nominal configuration, a fortiori if one works at strictly constant performance, i.e. $\beta^* = 50/30$ cm (in the crossing/parallel separation planes, respectively) @ 145 μrad for a truncated end of levelling of the RP configuration vs. $\beta^* = 30/30$ cm @ 160 μrad for the 2023 configuration [57].

8.3 D1 shielding or replacement

Considering that the expected radiation dose at the first MBXW magnet on the IP-side might reach values beyond the failure limit by the end of Run 3 (see Section 4), if no action is taken, two possible preventive actions to mitigate the risk of MBXW failure have been studied:

a. installation of a protective shielding;

b. magnet swap or substitution;

However, it must be noted though that operation with 5 out of 6 MBXW appears to be possible (see Section 7.5) and the RP optics, if implemented in 2024, provides a considerable reduction of the radiation dose at the first and most irradiated MBXW magnet.

8.3.1 Installation of a protective shielding

One possible approach would be the installation of a tungsten alloy shielding as it has been performed in LS1 and LS2 for the MBW magnets (see [28, 29]). Unfortunately, the formerly designed shielding is not effective, since in IR3 and IR7 the radiation to be attenuated consists of the secondary particle shower resulting from the proton beam halo impacting on the collimators jaws, while in IR1 and IR5 it is represented by the particle debris directly emerging from the collision point. In order to be effective, the installation of a very thick shielding is required. This does not fit either in the very reduced space available between beam pipe and coil, or in the space between the MBXW and the vacuum valve in front of it, shown in Figure 34. As a consequence, this is not a viable option.

8.3.2 Magnet swap or substitution

A possible alternative would be the substitution of the first MBXW with a magnet that has not been accumulating significant radiation dose. Two options have been considered and an estimate of the time required for their implementation has been provided:

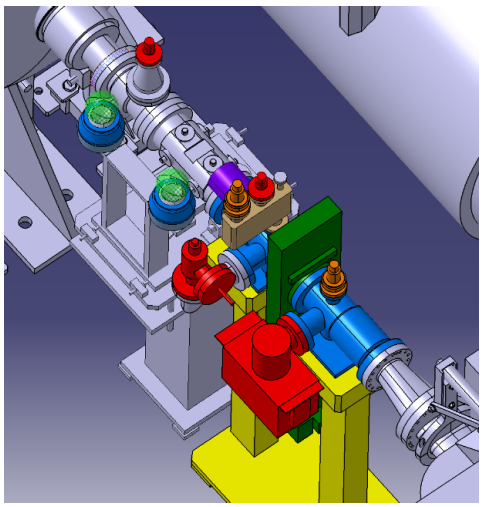

Figure 34: Present layout between DFBX and MBXW

- Removing the presently installed MBXW and swapping it with one of the magnets installed downstream, probably the last of the chain. The list of activities necessary for this type of intervention is presented in Table 27 in Appendix D and requires approximately a total of 6 to 7 weeks for each IP side.
- Removing the presently installed MBXW and substituting it with a spare. The list of activities necessary for this type of intervention can be found in Table 28 in Appendix D and require approximately a total of 6 to 7 weeks for each IP side.

It must be noted that the sequence and possible cohabitation of activities has not been optimized yet and this could lead to a reduction of the overall duration of the intervention.

8.4 NC skew quadrupole installation

The installation of NC skew-quadrupoles in IR1 and IR5 has been considered and studied as part of the possible preventive measures to be implemented to mitigate the effect of the failure of an MQSX corrector if the less demanding mitigation measure of tilting the Q3 and/or Q2 magnets could not be implemented. After an analysis of the main HW and infrastructure requirements three possible scenarios are presented:

- installation between D1 and the DFBX without MBXW removal;
- installation between D1 and the DFBX with MBXW relocation;
- installation on the non-IP side of D1.

The required activities and their expected duration have been sketched and all of them will require the creation of a detailed Work Dose Plan. It must be noted that the sequence and possible cohabitation of activities has not been optimized yet and this could lead to a reduction of the overall duration of the intervention.

8.4.1 D1 LAYOUT IN IR1 AND IR5

Figure 35 shows the configuration at the left side of IP1, the same is featured in the other three IP sides. A sector valve, a warm BPM and the DFBX are visible on the IP side of the magnet. The sector valve delimits the vacuum sector that includes the IT. The D1 vacuum sector includes, in addition to the D1 modules, the absober for neutrals (TAN), the vertical and horizontal tertiary collimators (TCTPV and TCTPH) and the collimator for debris (TCL) positioned in front of the D2 recombination dipole. The sector has a total length of about 90 m.

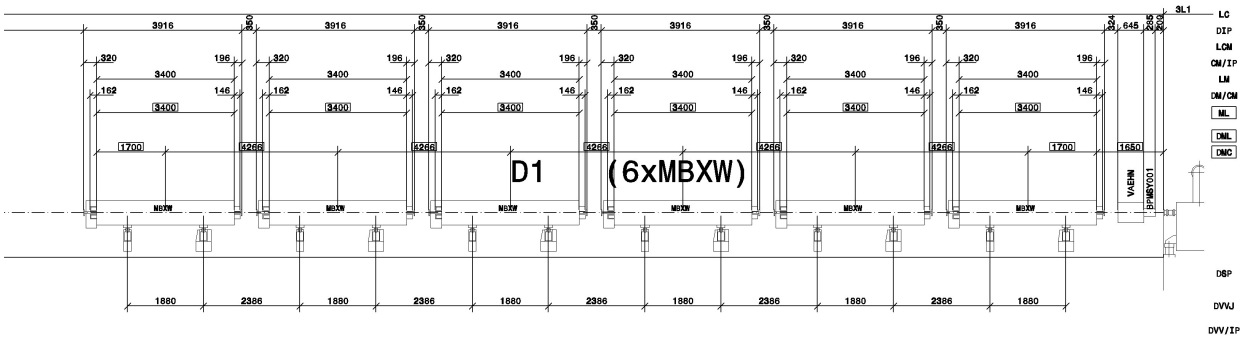

Figure 35: Layout of the D1 area in left side of IR1

8.4.2 NC SKEW QUADRUPOLE MAGNET CHOICE

The SPLQS__NWP (LQS) magnet shown in Figure 36 was found to be a suitable candidate. Six of these magnets are currently used in the SPS and nine spares are available. Using some of these spares for the LHC would not be critical for SPS operation.

Figure 36: LQS skew-quadrupole.

The LQS design is based on a low-carbon steel laminated yoke and water-cooled coils with radiation-hard Mica (inorganic) inter-turn insulation. The main characteristics of the magnet are listed in Table 16.

The quadrupole was originally designed to work up to 120 A, but after inspection of coil design, cooling parameters and yoke cross-section it was suggested that the quadrupole could easily work at higher current. A test campaign was organized to confirm that:

Parameter	Value
Name	SPLQS__NWP
Family	Quadrupole
Cooling system	Water
Aperture diameter [mm]	90
Iron Length [mm]	500
Total Length [mm]	750
Total Width [mm]	550
Total Height [mm]	750
Weight [kg]	575
Peak current [A]	180
RMS current [A]	180
Resistance at 20 °C [mΩ]	198
Inductance at 20 Hz [mH]	75
Power [kW]	6.4
Nominal ΔP [bar]	10
Nominal ΔT [°C]	28
Integrated gradient at Peak Current [T]	7.07

Table 16: LQS main characteristics.

- Powering and cooling: the quadrupole was tested up to 240 A. A pressure drop ΔP of 12 bar on the demineralized water circuit would be required to maintain the maximum coil temperature elevation ΔT below 30 °C. When the current is limited to 180 A (maximum current available with the Power Converter — PC — proposed by SY-EPC) and ΔP is limited to 10 bar, ΔT on the quadrupole reached a maximum of 28 °C, which is acceptable for long term operation. It is nevertheless recommended to connect the thermal switches installed on the magnet coils to the Warm Interlock Controller (WIC) in order to be able to stop the powering in case of coil overheating.
- Magnetic measurements: a magnetic measurement campaign was performed by TE-MSC-TM [58]. The integrated gradient was measured up to 200 A with a Single Stretched Wire and it is shown in Figure 37 (left). The saturation of the quadrupole yoke is relatively mild up to 180 A. The field multipoles were evaluated at 120, 150 and 180 A at a 30 mm radius and are plotted in Figure 37 (right). The strength of these multipoles is, in the worst case, a few percent of the NL triplet correction. They will therefore not cause any issues for operation. Both yoke saturation conditions and field quality appear compatible for an operation of the quadrupole up to 180 A.

8.4.3 Installation feasibility and options

For the installation of the NC skew quadrupole there are two possible options:

- installation between D1 and DFBX;
- installation on the non-IP side of D1.

Below we discuss the issues common to both solutions and then the ones specific to each of the two possible locations.

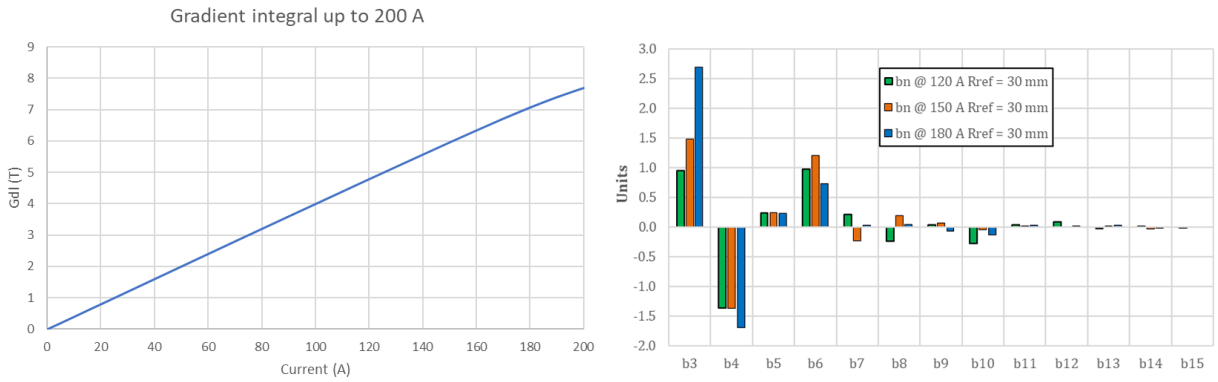

Figure 37: Gradient integral measured up to 200 A (left). Field multipoles measured at 120, 150 and 180 A at a 30 mm radius (right).

Availability of cooling water

The demineralized cooling water circuits available in IR1 and IR5 are able to sustain pressure drops larger than 10 bar allowing to operate the magnet at 180 A with a corresponding integrated gradient of 7.07 T.

Powering

SY-EPC has identified a suitable PC able to operate at 180 A with the following characteristics:

- single-quadrant 200 A/60 V, recommended for continuous operation up to 190 A;
- 100 part per million (ppm) stability at 200 A;
- time constant $\leq$0.4 s;
- the volume taken by one PC is one rack 42 Rack Units (RU) high and 80 cm wide;
- one rack would contain one operational and one spare unit, the front and rear access would be needed, the DC connections would be placed at the bottom of the rack;
- the requested ramp rate of +2 A s^{-1} can be provided, and it would be possible to reach a maximum ramp rate of +5 A s^{-1};
- possible to regulate around 2 A, i.e. at $\approx$ 1 % of the nominal current.

Each PC rack would be installed together with a second rack containing the FGC3 gateway with LHC timing. The cabling for the WIC should also be pulled. SY-EPC has identified possible installation slots in the UL14, UL17, UL557, USC55. The proposed locations in UL14, UL17 and UL557 could partially enter in the magnet transport volume, therefore it would be necessary to disassemble these units in case of transport of large equipment. The cabling study and the related integration has not been carried out yet.

Installation between D1 and the DFBX without MBXW removal

The LQS magnet requires a space of about 800 mm along the beamline. Presently, the following components are installed between the DFBX and the first MBXW magnet (from the IP towards the arc): 1 warm Beam Position Monitor (BPM — BPMSY), 1 sector valve with two Penning

gauges installed on each side of the valve, 1 ion pump (for CH_4 pumping) and 2 Non-Evaporable Getter (NEG) cartridges (for H_2 pumping), 1 pressure relief valve, 2 bellows.

In order to create the space for the LQS magnet installation, it would be necessary to remove the BPM and to displace part of the vacuum components in the interconnect between the first and the second MBXW as shown in Figure 38.

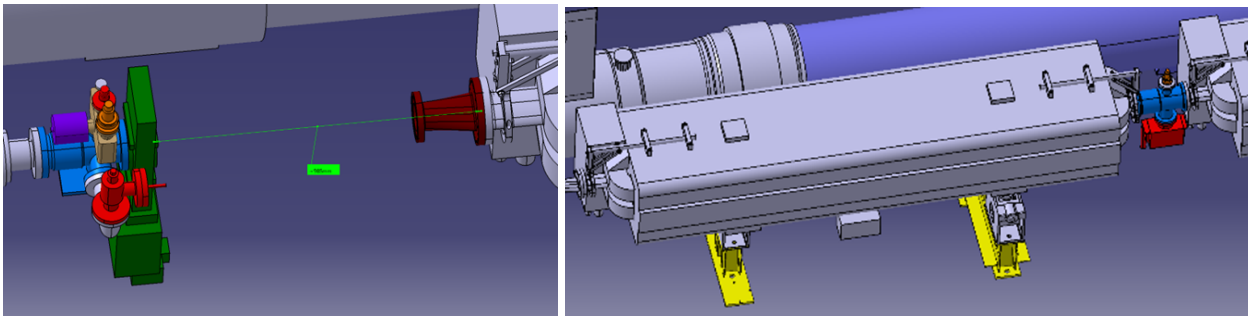

Figure 38: Reorganization of the vacuum components on the IP side of the first MBXW module to create space for the LQS magnet (left) and vacuum components moved between the first and second MBXW units (right).

The first vacuum group on the IP side of the first MBXW would be made by the assembly of: 1 module with bellow, 1 penning gauge, 1 valve for rough pumping, 1 NEG cartridge, 1 sector valve. The second module between the first and second MBXW would be composed of the second required penning gauge and the ion pump. This solution would provide the necessary space (also taking into account the transitions), but the installation would impose the warm-up of the triplet as the sector valve has to be displaced and the BPM removed. In addition, the following integration aspects must be considered for both IR1 and IR5:

a. temporary removal of the Wire Positioning System (WPS) reference and of a radiation monitor during the installation;

b. one Beam Loss Monitor (BLM) shall be permanently relocated;

c. a detailed on-site analysis of the cabling should take place: there are many cables and the possibility to move them without disconnection should be investigated (see Figure 39);

d. the DFBX ancillaries have supports that could partially interfere with the new magnet installation. Therefore, it would be necessary to analyze whether they could be changed or moved in order to free the space for the LQS. From available data, 5R and 1L would almost certainly require this type of changes;

e. design and production of special vacuum supports would be required.

As can be seen, this proposed installation option requires important modifications in a very complex area and the warm-up of the triplet, an operation that this task force recommends avoiding. Moreover, in the considered location, the newly installed LQS magnet will be exposed to a radiation load requiring the assessment of the peak dose reached in its coils as a function of the integrated luminosity production.

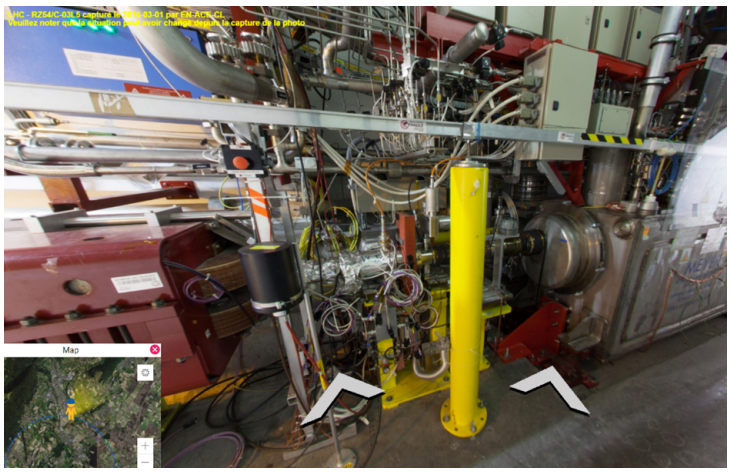

Figure 39: Example of the complexity of the area between D1 (first MBXW module on the left) and DFBX (on the right). The black cylinder is the radiation monitor, while the BLM is not visible.

Installation between D1 and the DFBX with MBXW relocation

Sufficient space for the installation of the LQS magnet on the IP side of D1, without removal of the sector valve installed between the DFBX and D1, could be liberated by removing the first MBXW on the IP side and by relocating it after the last one (module F) on the non-IP side. This is possible due to the space available on the non-IP side of the last of the 6 MBXW and the modularity of the large diameter vacuum chamber that follows it. As a result, the D1 would have its magnetic center moved by about 3.9 m towards the arc requiring an increase in the operational field of the D1 and D2 magnets. A preliminary analysis indicated that this is consistent with the aperture requirements and magnet strength for operation up to 6.8 TeV.

Figure 40 (left) illustrates a proposal for the vacuum layout between the DFBX and the second MBXW after removal of the first one. Figure 40 (right) shows the layout on the non-IP side of the D1 where the displaced MBXW is indicated in yellow. All re-used elements are in yellow, new ones in green.

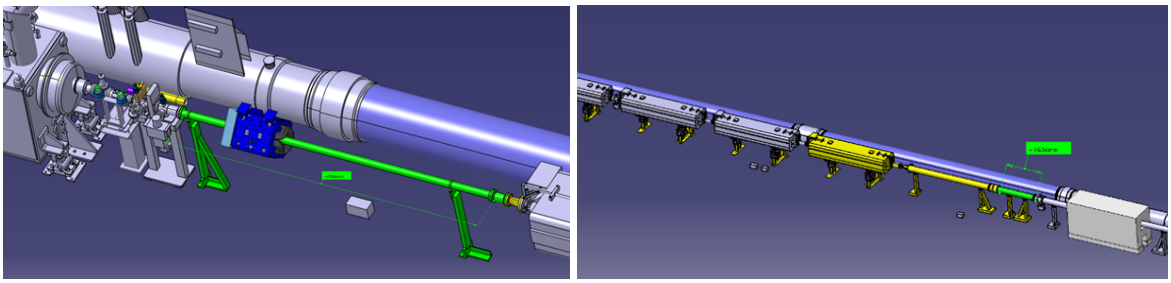

Figure 40: Schematic layout proposal: DFBX/LQS/MBXW (left), MBXW and vacuum transition towards the TAN (right).

The relocation of the installed MBXW is quite a complex operation:

- the Invar rod coming from the underground survey gallery (UPS) and connecting for alignment purposes the left and the right side of the IP is supported on the first MBXW;

- the space available between the MBXW and the surrounding equipment is very limited especially in height.

Table 29 in Appendix E presents a very preliminary and non-exhaustive list of the interventions and of the involved actors with the corresponding duration considering possible parallelism in the different areas. The total duration of the interventions is estimated to 8.5 to 9.5 weeks for each of the IP sides.

In this case, the impact of the collision debris on the LQS quadrupole is expected to be more severe, due to the longer drift from the triplet extremity, and shall be evaluated with respect to the insulator damage limit. The length of the elements to be installed should be less than 2.2 m to ease transport avoiding the need to disassemble the chicane in the LHC tunnel, namely in IR5.

Installation on the non-IP side of D1

Another option would be to modify only the vacuum layout after the last MBXW on the non-IP side moving the transition between the small and large diameter chamber by about 1.5 m towards the arc. The advantage is a much simpler activity as the list of interventions would be strongly simplified. A layout proposal is shown in Figure 41. The following elements should be produced for each installation.

- two amorphous-Carbon (a-C) coated Stainless Steel transition chambers with maximum transition angle 15° between different apertures;
- one a-C coated Stainless Steel Chamber ∅ 84/88 (ID84) 1000 mm-long to be installed inside the LQS.

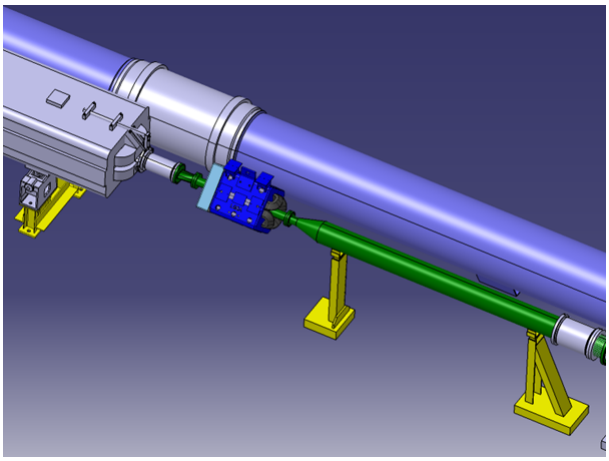

Figure 41: Preliminary layout proposal for the LQS installation on the non-IP side of D1

Table 30 in Appendix E presents a very preliminary and not exhaustive list of the interventions and of the involved actors with the corresponding duration considering possible parallelism in the different areas. A total of 4.5 weeks would be required for the installation of the skew quadrupoles for each of the IP sides.

In this location, the skew quadrupole coils are expected to be subject to a maximum dose of 8 MGy per 200 fb^{-1}, well below their critical limit. On the other hand, the radiation levels in the

proximity of the magnet, in terms of prompt dose to equipment and high-energy hadron fluence, would roughly double as a consequence of its presence, but this is not expected to be of concern.

The circuit would consist of two branches, each 100 m long, using a cable of 120 mm^2 cross-section. The circuit resistance at 90 °C would be 36 mΩ, to be compared with 200 mΩ of the magnet at room temperature.

The availability of resources to carry out the modifications in both IRs in the same (E)YETS shall be verified for all the options. All the options shall be checked for machine impedance.

8.4.4 Correction capabilities as a function of the skew quadrupole position

The LQS location is important for the capability to correct the coupling. The effectiveness of the correction depends on $\sqrt{\beta_x \beta_y}$ and on $\phi_x \pm \phi_y$ where β_x, β_y, ϕ_x, ϕ_y are the horizontal and vertical Twiss beta functions and MQSX to LQS phase advances, respectively. However, due to the large β functions in these regions, the phase advance is not significantly changing between the proposed options. The MQSX strengths used for correcting the coupling in 2022 and 2023 are shown in Table 12 in Section 7.3. They remained relatively constant during the LHC operation, so far. The strongest is located in L1 and requires an integrated gradient of 5.8 T at 6.8 TeV. LQS has a maximum integrated gradient of 7.07 T at 180 A meaning that it would be able to correct the strongest error (L1), and still have a margin, if it would have been located at the same location as the MQSX. Figure 42 shows the ratio of the correction that can be achieved with the LQS magnet to the one needed as a function of its distance from the IP. Moving away from the IP the efficiency goes down because of the reduction of $\sqrt{\beta_x \beta_y}$. For the observed strengths of the MQSX correctors in 2022–2023 the LQS installed on the IP side of the D1 can fully compensate the loss of the corresponding MQSX while if the LQS is placed on the non-IP side it can provide around 90 % of the MQSX correction in the worst case (L1). This can be compensated with the skew quadrupole on the other side of the IP (R1) with the effect that the correction will be less local and as a consequence, the beam size at the IP will be slightly increased. The effect is more pronounced as β^* is decreased. The impact on the integrated luminosity from this is expected to be in the 1–2 % range for the current optics configuration. This might change for the RP optics depending on the exact distribution of the errors.

8.4.5 Summary

The installation of the LQS magnet on the non-IP side of D1 appears to be the less invasive intervention on the existing HW and the preliminary studies indicate that it is compatible with the aperture requirements and with the expected radiation levels. It does not require any movement of the D1 magnets that is not without risks because of the significant irradiation of the coils of the MBXW magnet on the IP side. Because of the fragilization of the MBXW coil insulation resulting from the large radiation dose it might be damaged during the HW intervention. The possibility of operating without one of the MBXW magnet identified in Section 7.5 and the significant reduction of the radiation dose on the first MBXW magnet (IP side) that could be obtained with the implementation of the RP optics in 2024 imply that a preventive relocation of the MBXW magnets is not justified and therefore does not favour the installation of the LQS magnet on the IP side after the relocation of the corresponding MBXW magnet. A preventive installation of the LQS magnet is not justified, in particular in case of implementation of the RP optics in 2024, though

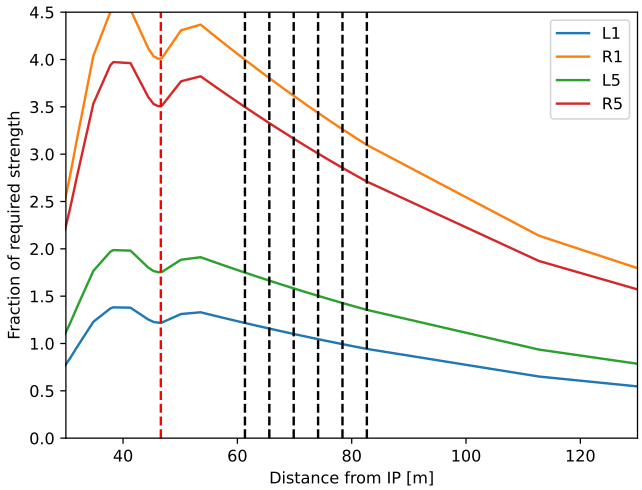

Figure 42: Ratio of the correction that can be achieved with the LQS magnet to the one needed (assuming the values observed in 2022–2023) as a function of its distance from the IP. The dotted red line shows the location of the current MQSX and the black dotted lines show the centre of the different D1 modules

the preparation of two magnets (to replace the function of the two MQSX magnets powered at the highest current) and the necessary vacuum chambers, power converters and controls for a possible installation in case of failure should be pursued to minimize the amount of time required for the installation in case of MQSX failure.

9 Radiation levels in IR2 and IR8 during the HL-LHC operation and implications for magnet performance

9.1 Mode of operation and expected performance

Since the start of Run 3 LHCb can operate at a levelled luminosity of $2 \times 10^{33}\,\mathrm{cm}^{-2}\mathrm{s}^{-1}$, and it is considering a possible additional upgrade of the detector for operation at a levelled luminosity of $1.5 \times 10^{34}\,\mathrm{cm}^{-2}\mathrm{s}^{-1}$ after LS4 [59]. The expected integrated luminosity by the end of the HL-LHC operation without and with the above-mentioned upgrade is shown in Figure 43.

After its upgrade during LS2 ALICE is capable to operate at proton-proton luminosities of $6 \times 10^{30}\,\mathrm{cm}^{-2}\mathrm{s}^{-1}$ and at luminosities of $6.4 \times 10^{27}\,\mathrm{cm}^{-2}\mathrm{s}^{-1}$ with Lead-Lead collisions [60] and it will collect $0.2\,\mathrm{fb}^{-1}$ and $13\,\mathrm{nb}^{-1}$ (corresponding to an integrated nucleon-nucleon luminosity of $0.56\,\mathrm{fb}^{-1}$), respectively, by the end of Run 4. It has been proposed to upgrade the ALICE detector during LS4 [61] to continue operation until the end of the HL-LHC programme at proton-proton luminosities of $3 \times 10^{32}\,\mathrm{cm}^{-2}\mathrm{s}^{-1}$ and at nucleon-nucleon luminosities by more than a factor 5 higher than those achieved with Lead-Lead collisions, possibly with Xenon ions. By the end of Run 6 ALICE could achieve nucleon-nucleon integrated luminosities of $\approx 18\,\mathrm{fb}^{-1}$ with proton-proton collisions and 2.5–3 fb^{-1} with ion-ion collisions.

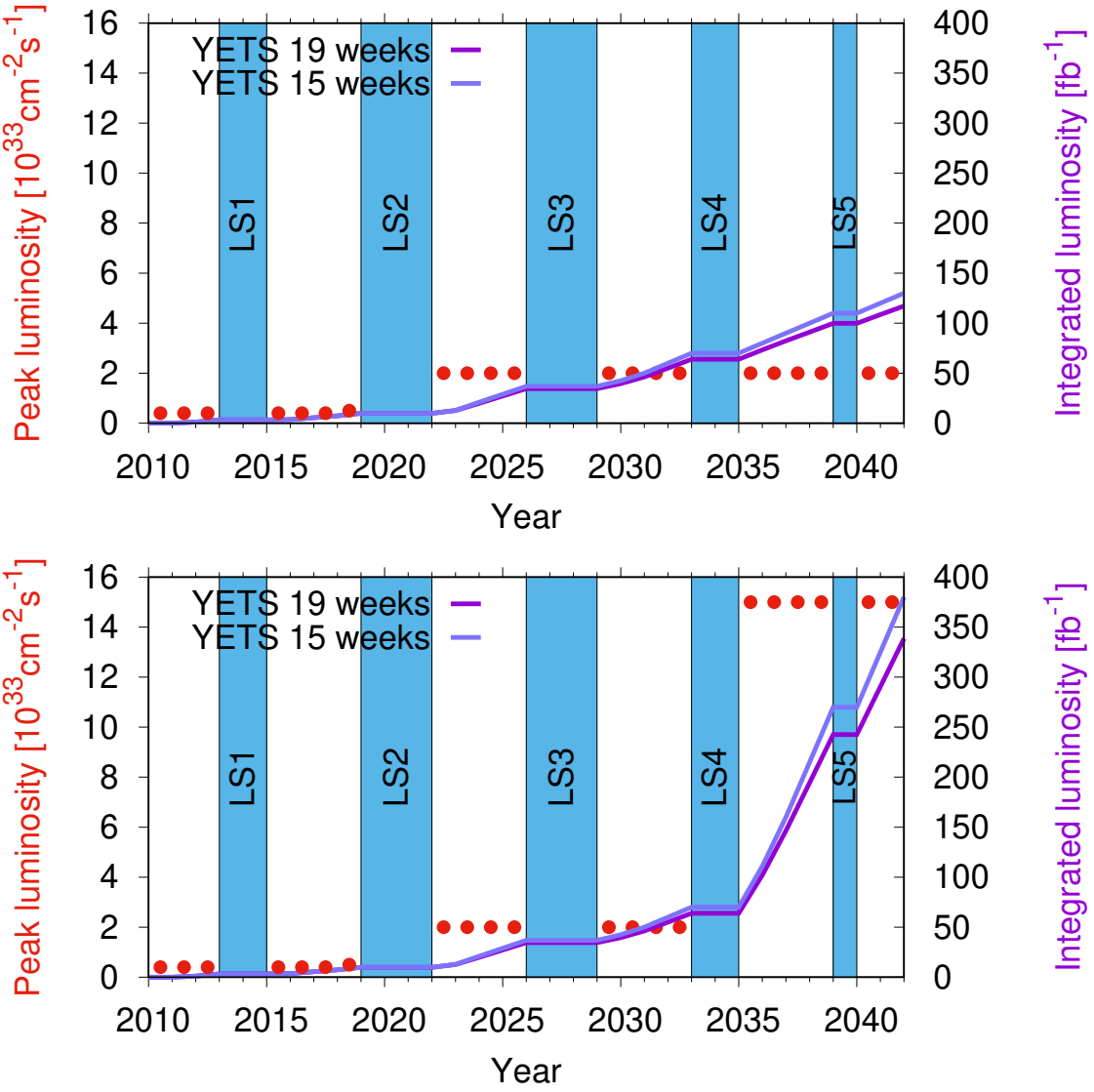

Figure 43: Expected integrated luminosity evolution in IR8 until the end of the HL-LHC operation without LHCb detector upgrade (top) and with LHCb detector upgrade (bottom) (*Courtesy of R. Tomàs*).

9.2 Expected radiation levels and proposed mitigation measures

In the scenario disregarding the additional LHCb upgrade and thereby featuring a final proton–proton luminosity of about 130 fb^{-1} (see the top frame of Figure 43), the most impacted superconducting magnet of IR8 is the first main quadrupole on the right of IP8 (Q1.R8), which is expected to reach 17 MGy (half integrated luminosity is here assumed to be produced with either LHCb spectrometer polarity). Then, the separation dipoles D1 would get 14 MGy, while among the correctors a maximum of 6 MGy is predicted for the skew octupole (MCOSX3), with the dipole orbit corrector and the skew quadrupole remaining below 3 MGy. For the short normal-conducting compensator, the peak dose would be around 40 MGy, almost three times higher than for the long compensator on the left of IP8. A detailed list can be found in Table 20 in Appendix B.

On the other hand, the LHCb upgrade, aiming at an integrated luminosity approaching 400 fb^{-1} (see the bottom frame of Figure 43), would require the implementation of a few measures to protect the most impacted magnets. First, considering the lack of room for the installation of additional elements, the short compensator should be transformed, such as to provide the function of the TAS absorber, by embedding a suitably shaped tungsten block between its yoke and the vacuum chamber. This would allow for the fulfillment of a twofold objective, dropping the dose peak on the IP side of Q1 and reducing to a sizeable extent the total load on the cryogenic system. Moreover, a pronounced dose peak is generated at the non-IP extremity of D1 with one of the two LHCb spectrometer configurations (namely with downward polarity) and calls for the design of an internal shielding along the superconducting dipole. Profiting from the larger coil aperture of the latter, one could replace its present beam screen with a new one identical to the Q2–Q3 beam screen (if the corresponding mechanical aperture reduction is confirmed not to compromise future injection optics scenarios) providing in this way the margin for increasing the thickness of the enclosing stainless steel cold bore wall. This protection scheme was already adopted since the LHC design stage for the present Q1, which hosts an even narrower beam screen. Finally, the front coils of the short compensator shall be shielded by tungsten pieces at least 7 cm long. With these measures in place by the end of LS4 [62], the Q1 and D1 hot spots turn out to be kept below 20 MGy and only slightly above 15 MGy, respectively. In this scenario, the most impacted superconducting magnet of IR8 becomes Q2A, with 22 MGy after 370 fb^{-1}, while the first orbit corrector (MCBX1) and the skew quadrupole reach 7 MGy and the skew octupole displays a peak of 17.5 MGy. Thanks to the envisaged shields, the maximum dose on the short compensator coils barely exceeds 50 MGy, which represents a reduction of more than a factor of two with respect to the value in the absence of a specific protection (see Table 20 in Appendix B for more details).

The radiation levels expected in IR2 in case of upgrade of ALICE will depend on the selected ion specie and will require additional studies once the operational scenario has been defined.

9.3 Magnet design criteria

The IT in IR2 and IR8 have an identical HW configuration to those in IR1 and IR5 although they are powered with opposite polarity. The main difference in the IR magnetic layout is due to the presence of SC separation dipoles D1 (MBX) and the presence of NC dipoles installed on the IP side of the triplets and used to compensate the effect of the magnetic field of the ALICE and LHCb dipole spectrometers.

9.3.1 IR2 AND IR8 SPECTROMETER COMPENSATORS

The effect of spectrometer dipoles in ALICE and LHCb experiments on the beam is compensated in each case with three dipoles installed between the left and right ITs, one placed symmetrically to the spectrometer with respect to the IP and two weaker dipoles placed next to the IT. The dipole field of the ALICE spectrometer, which produces a vertical kick on the beam, is compensated with a MBWMD and two MBXWT magnets. The MBWMD is a 2.6 m-long magnet from the SPS complex, originally built for the ISR beam lines (type HB2 turned vertical). The LHCb dipole, which produces a horizontal kick on the beam, is compensated by an MBXWH magnet and two MBXWS magnets. The MBXWH is in fact a MBXW separation dipole, and the MBXWT and MBXWS magnets share the same cross-section, shown in Figure 13, with the MBXW magnet, but

the core length is 1.5 and 0.75 m, respectively.

9.3.2 MBX MAGNET (IR2 & IR8 D1 MAGNET)

The design of the 80 mm aperture coils of the MBX magnets is similar to that of the coils of the arc dipoles operating at the Relativistic Heavy Ion Collider (RHIC). No specific information could be retrieved about possible manufacturing differences in the coils, if any [63]. So, we assume the coil construction is also the same. The single layer coil consists of 32 turns with three copper wedges. The cable insulation is a double wrap of Kapton® CI tape with polyimide adhesive. As for the RHIC dipoles, the D1 cold iron yoke is separated from the coil by injection molded phenolic spacers. The spacers used for RHIC have been manufactured by Rogers Corp. and were made of a RX® 630 glass-filled phenolic resin.

9.4 Effects of radiation and impact on magnet performance

9.4.1 IR2 AND IR8 SPECTROMETER COMPENSATORS

The same considerations as for the MBXW magnets apply for the MBXWH, MBXWS, MBXWT and MBWMD compensator magnets (see Section 5.1.3).

9.4.2 MBX MAGNET (IR2 & IR8 D1 MAGNET)

RX® 630 is a short glass fiber phenolic molding compound based on Phenolic Epoxy Novolac. Glass filled Phenolic Epoxy Novolac compounds are very robust to radiation: early studies in 1970 showed no mechanical degradation at least up to 40 MGy [64]. More recent studies [33] on similar compounds did not observe any mechanical degradation up to 100 MGy. The choice of RX® 630 in terms of good radiation resistance was based on previous work performed at CERN on materials of the same generic composition as RX® 630 [65]. There are therefore good reasons to believe that the phenolic spacers used for D1 will resist well beyond 30 MGy, and possibly up to 100 MGy.

Concerning the other components of D1, the end spacers and saddles are made in Ultem 6200, and the cable insulation has similar characteristics of the one used in the triplet quadrupoles: for these components no degradation is expected below 30 MGy.

10 Spares situation

10.1 IT spare cryo-magnets

One complete set of inner triplet cryo-magnets (Q1, Q2 and Q3) is available at CERN. The reference of these spare assemblies is the following:

- HCLQXA_001-FL000008 (short name: LQXA-08 for Q1);
- HCLQXB_001-FL000001 (short name: LQXB-01 for Q2);
- HCLQXC_001-FL000009 (short name: LQXC-09 for Q3).

The main quadrupole magnets of these cryo-assemblies were measured at FNAL [66] and KEK [67]. The quench performance of inner triplet magnets production is given in Figure 44. The current targets were 7730 A for MQXA magnets (Q1 and Q3) and 13 000 A for MQXB magnet (Q2).

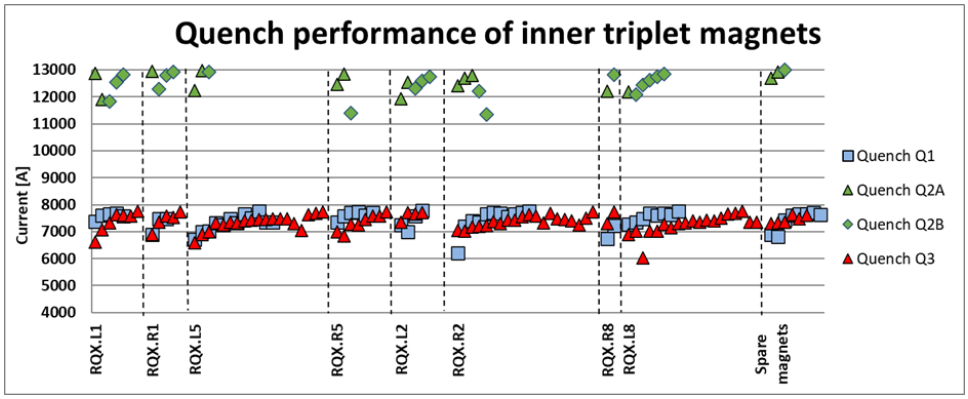

Figure 44: Quench performance of inner triplet magnets installed in LHC and spare magnets. Measurement done at KEK and FNAL.

LQXB-01 presents a non-conformity in one of the quench-heater circuits which was found open [68], nevertheless the remaining quench heaters provide a full magnet protection, but with reduced redundancy. In 2007, LQXB-01 was installed in the LHC in left of the IP5, but had to be exchanged because of damage occurred during the pressure test. Following the incident, all cryo-magnets were consolidated [69], except this one. The cryo-magnet LQBX-01 is currently in the Large Magnet Facility for consolidation to be completed by the end of summer 2023.

Magnetic measurements were also performed. The transfer function and multipole harmonic coefficients are given in the ID cards, which are available in the MTF database. Measured in 2002 in KEK, the LQXA-08 was retested in May 2018 on one of the SM18 test stations confirming the performance of the main quadrupole and corrector magnets. LQXB-01 and LQXC-09 have not been retested at CERN.

10.2 IT spare magnets

Spare magnets are stored at CERN to build Q1 or Q3 cryo-magnets:

- 2 MQXA (MQXA-11 and MQXA-20);
- 3 MCBX (MCBX-32, MCBX-35, and MCBXA-33);
- 2 MCSTX (MCSTX-05 and MCSTX-12);
- 5 MCSOX (MCSOX-09, MCSOX-10, MCSOX-11, MCSOX-20, and MCSOX-21);
- 3 MQSX (MQSX-09, MQSX-10 and MQSX-11).

There are no MQXB spare magnets to build a Q2 cryo-magnet.

The quench performance data for MQXA-11 and MCBX-35 show a long training to reach the ultimate current. To create a new assembly, it would require at least 2 years with sufficient and experienced resources: 6 months would be needed to determine and procure the components and the necessary tooling; assembly, cryostating and testing at 1.9 K is expected to take at least 1.5 years.

10.3 SC separation cryo-dipole (IR2 & IR8 D1)

Two spare cryo-assemblies are available at CERN for four units installed in the LHC:

- HCLBX__001-BL000006 (LBX-106);
- HCLBX__001-BL000007 (LBX-107).

The two units were measured at CERN and reached 6100 A without quenching [70, 71].

11 Update on luminosity evolution, possible stepwise implementation of RP optics and impact of extended operation

In this Section the updated radiation estimates considering the reduced integrated luminosity in 2023 ($\approx 32\,\text{fb}^{-1}$) are briefly presented and a stepwise implementation of the RP configuration, also considering the implications that the associated crossing angle plane rotation in IR1 and IR5 has on the AFP and CMS-PPS acceptance for Forward Physics, is proposed. The expected radiation dose at the triplet quadrupoles is estimated for this scenario and the impact of a possible extended operation in 2026 is assessed.

11.1 Impact on Forward Physics of the RP configuration with rotated crossing planes

The impact of the RP configuration proposed in Section 8.2 on Forward Physics experiments has been studied [72], showing unfortunately the incompatibility of the DFD-H configuration proposed for IR1 (RP optics with horizontal crossing) with acceptable running conditions in AFP. A similar impact is observed for CMS-PPS in the DFD-V configuration proposed for IR5, but, in this case, a physical rotation of some roman pots might restore a full acceptance. The above-mentioned incompatibilities are more related to the rotated crossing planes than to the RP optics proper. In that respect, a hybrid configuration with DFD-V (RP) in ATLAS and FDF-H (no change) in CMS, therefore with no change in terms of crossing planes, optics flatness, telescope, .., with respect to 2023, could (i) provide acceptable (or unchanged) operating conditions for AFP and CMS-PPS with no required HW modification; (ii) reduce the peak radiation dose in IR1 with respect to the present triplet configuration, though not improving that in IR5; (iii) open the possibility of MDs (with no HW modification) during the 2024 run to validate the RP flat optics in IR1, a non-RP flat optics in IR5, and crossing plane rotation for both. This configuration could provide a stepwise approach (being validated with beam-beam simulations) to the full implementation of the RP optics with horizontal and vertical crossing angles in IR1 and IR5, respectively, in 2025. This may require the rotation of some roman pots of CMS-PPS during the EYETS2024-2025.

11.2 Updated peak radiation dose

The expected radiation dose at the IT quadrupoles has been estimated assuming integrated luminosities in IR1 and IR5 of 80 and $90\,\text{fb}^{-1}$ in 2024 and 2025 and $100\,\text{fb}^{-1}$ during an hypothetical operation in 2026. The following scenarios have been considered:

- Present optics configuration assuming regular inversion of the vertical crossing angle every year in IR1 and starting with **positive** polarity in 2024;

- Reverse Polarity configuration with horizontal and vertical crossing planes in IR1 and IR5, respectively;
- Stepwise implementation of the RP optics described above with positive polarity of the IR1 vertical crossing angle in 2024 and full implementation of the RP configuration in IR1 and IR5 starting in 2025.

Configuration	Peak dose [MGy] at the end of 2025 ($430\,\mathrm{fb}^{-1}$)	Peak dose [MGy] for extended operation ($530\,\mathrm{fb}^{-1}$)
Present	26.5–27 (Q2A in IR1) 26.5–27 (Q2B in IR5)	33–33.5 (Q2A in IR1) 33–33.5 (Q2B in IR5)
RP configuration	20.5 (Q2A in IR1) 20.5 (Q2A in IR5)	25 (Q1 in IR1) 26 (Q2A in IR5)
Stepwise implementation	20.5 (Q2A in IR1) 22.5 (Q2B in IR5)	23 (Q1 and Q2A in IR1) 25.5 (Q2A in IR5)

Table 17: Peak radiation doses expected by the end of 2025 and after an additional hypothetical run in 2026.

In addition to the above-mentioned implementation advantages of the stepwise approach, Table 17 shows its neutrality in terms of radiation increase, with respect to a direct implementation of the RP configuration in 2024, for IR1 already at the end of 2025 and an improvement for both IR1 and IR5, should Run 3 be extended by an additional year.

Acknowledgments

We would like to thank M. Bednarek, C.-N. Droin, E.H Maclean, F. Soubelet, E. Todesco and R. Tomàs for their input.

References

[1] G. Arduini *et al.*, "First input from LHC Triplet Task Force," Presented at the 2023 Chamonix Workshop, 2023. [Online]. Available: https://indico.cern.ch/event/1224987

[2] ——, "LHC triplet Task Force Meetings," 2023, Presentations and minutes of the LHC Triplet Task Force Meetings. [Online]. Available: https://indico.cern.ch/category/16000/

[3] F. Moortgat, "Physics expectations and wishes for Run 3," Presented at the 2023 Chamonix Workshop, 2023. [Online]. Available: https://indico.cern.ch/event/1224987

[4] B. Petersen, "Feedback from experiments from 2022 run," Presented at the 2023 Chamonix Workshop, 2023. [Online]. Available: https://indico.cern.ch/event/1224987

[5] L. Mether, "e-cloud constraints on machine and beam configuration," Presented at the 2023 Chamonix Workshop, 2023. [Online]. Available: https://indico.cern.ch/event/1224987

[6] S. Fartoukh, S. Kostoglou, M. Solfaroli Camillocci, G. Arduini, H. Bartosik, C. Bracco *et al.*, "LHC Configuration and Operational Scenario for Run 3," CERN-ACC-2021-0007, CERN, Tech. Rep., 2021. [Online]. Available: https://cds.cern.ch/record/2790409

[7] G. Bregliozzi, "Report on 4L1 Issues and RF Fingers," Presented at the 466th LHC Machine Committee meeting (28 June 2023), 2023. [Online]. Available: https://indico.cern.ch/event/1298988/

[8] S. Fartoukh, "Machine configuration and performance reach for the rest of Run 3," Presented at the 2023 Chamonix Workshop, 2023. [Online]. Available: https://indico.cern.ch/event/1224987

[9] "LHC Program Coordination Web Pages." [Online]. Available: https://lpc.web.cern.ch/

[10] R. Ferreira, "Analysis of the LHCb VELO RF Foils Incident and First Actions," Presented at the 456th LHC Machine Committee meeting (8 February 2023), 2023. [Online]. Available: https://indico.cern.ch/event/1241460/

[11] E. Thomas, "LHCb Velo Report," Presented at the 456th LHC Machine Committee meeting (8 February 2023), 2023. [Online]. Available: https://indico.cern.ch/event/1241460/

[12] N. Mokhov, I. Rakhno, J. Kerby, and J. Strait, "Protecting LHC IP1/IP5 Components Against Radiation Resulting from Colliding Beam Interactions," LHC Project Report 633, CERN, Tech. Rep., 2003. [Online]. Available: https://cds.cern.ch/record/613167

[13] C. Hoa, N. Mokhov, F. Cerutti, and A. Ferrari, "Inter-comparison of MARS and FLUKA: Predictions on Energy Deposition in LHC IR Quadrupoles," LHC Project Note 411, CERN, Tech. Rep., 2008. [Online]. Available: https://cds.cern.ch/record/1091189

[14] https://fluka.cern.

[15] C. Ahdida, D. Bozzato, D. Calzolari, F. Cerutti, N. Charitonidis, A. Cimmino *et al.*, "New Capabilities of the FLUKA Multi-Purpose Code," *Frontiers in Physics*, vol. 9, 2022. [Online]. Available: https://www.frontiersin.org/article/10.3389/fphy.2021

[16] G. Battistoni, T. Boehlen, F. Cerutti, P. W. Chin, L. S. Esposito, A. Fassò *et al.*, "Overview of the FLUKA code," *Ann. Nucl. Energy*, vol. 82, pp. 10–18, 2015. [Online]. Available: http://cds.cern.ch/record/2162467

[17] A. Lechner, B. Auchmann, T. Baer, C. Bahamonde Castro, R. Bruce, F. Cerutti *et al.*, "Validation of energy deposition simulations for proton and heavy ion losses in the CERN Large Hadron Collider," *Phys. Rev. Accel. Beams*, vol. 22, p. 071003, 2019. [Online]. Available: https://link.aps.org/doi/10.1103/PhysRevAccelBeams.22.071003

[18] S. Yang, M. Sabate Gilarte, A. Tate, N. Santiago, R. Longo, S. Mazzoni *et al.*, "^{22}Na activation level measurements of fused silica rods in the LHC target absorber for neutrals compared to simulations," *Phys. Rev. Accel. Beams*, vol. 25, p. 091001, 2022. [Online]. Available: https://journals.aps.org/prab/abstract/10.1103/PhysRevAccelBeams.25.091001

[19] S. Roesler, R. Engel, and J. Ranft, "The Monte Carlo Event Generator DPMJET-III," in *Proceedings of the Monte Carlo 2000 Conference*, A. Kling, F. Barao, M. Nakagawa, L. Tavora, and P. Vaz, Eds. Springer-Verlag Berlin, 2001, pp. 1033–1038.

[20] A. Fedynitch, "Cascade equations and hadronic interactions at very high energies," Ph.D. dissertation, 2015. [Online]. Available: https://cds.cern.ch/record/2231593/files/CERN-THESIS-2015-371.pdf

[21] https://github.com/DPMJET/DPMJET.

[22] N. Mokhov, I. Rakhno, I. Tropin, F. Cerutti, L. Esposito, and A. Lechner, "Energy deposition studies for the high-luminosity Large Hadron Collider inner triplet magnets," *Phys. Rev. Accel. Beams*, vol. 18, p. 051001, 2015. [Online]. Available: https://journals.aps.org/prab/abstract/10.1103/PhysRevSTAB.18.051001

[23] F. Cerutti and S. Fartoukh, "LHC triplet lifetime versus operational scenario in ATLAS and CMS," 2015, Presented at the 225th LHC Machine Committee meeting, 8 July 2015, CERN, Geneva, Switzerland. [Online]. Available: https://indico.cern.ch/event/406858/contributions/966580/attachments/813759/1115142/LMC_IR1sign.pptx

[24] O. S. Brüning, P. Collier, P. Lebrun, S. Myers, R. Ostojic, J. Poole, and P. Proudlock, *LHC Design Report*, ser. CERN Yellow Reports: Monographs. Geneva: CERN, 2004. [Online]. Available: https://cds.cern.ch/record/782076

[25] V. Baglin and N. Kos, "Beam screens for the LHC Long Straight Sections ," CERN, Geneva, Tech. Rep. EDMS #334961, 2007. [Online]. Available: https://edms.cern.ch/document/334961/1.3

[26] A. Ciccotelli, R. Appleby, F. Cerutti, K. Bilko, L. Esposito, R. Garcia Alia *et al.*, "Energy deposition studies for the LHCb insertion region of the CERN Large Hadron Collider," *Phys. Rev. Accel. Beams*, vol. 26, p. 061002, 2023. [Online]. Available: https://journals.aps.org/prab/abstract/10.1103/PhysRevAccelBeams.26.061002

[27] H. Schönbacher, K. Humer, B. Szeless, M. Tavlet, and H. W. Weber, *Results of radiation tests at cryogenic temperature on some selected organic materials for the LHC*,

ser. CERN Yellow Reports: Monographs. Geneva: CERN, 1996. [Online]. Available: https://cds.cern.ch/record/309447

[28] P. Fessia, P. Thonet, and E. Skordis, "Radiation Shielding Installation for the MBW and MQW Magnets in IR 3 and 7 of the LHC. First phase during LS1," CERN, Geneva, Tech. Rep. EDMS #1321044, 2013. [Online]. Available: https://edms.cern.ch/document/1321044/1.0

[29] P. Fessia, I. S. Fernández, P. Schwarz, P. Thonet, R. Bruce, and E. Skordis, "Radiation Shielding Installation and Possible Optics Change for the MBW and MQW Magnets in IR 3 and 7 of the LHC. Second phase LS2, LS3 and HL-LHC," CERN, Geneva, Tech. Rep. EDMS #1321045, 2018. [Online]. Available: https://edms.cern.ch/document/1321045/2.0

[30] L. W. McKeen, *The Effect of Radiation on Properties of Polymers*, ser. Plastics Design Library. Elsevier, 2020.

[31] D. Reed, "Radiation Tolerance of Resins," April 2007, Presented at the Rad-Hard Insulation Workshop, , 20 April 2007, Fermilab, Batavia, USA.

[32] G. Pluym and M. H. van de Voorde, "Radiation resistance of glass reinforced epoxy-resins," CERN, Geneva, Tech. Rep., 1967. [Online]. Available: https://cds.cern.ch/record/1216824

[33] M. Tavlet, A. Fontaine, and H. Schönbacher, *Compilation of radiation damage test data. Index des résultats d'essais de radiorésistance; 2nd ed.*, ser. CERN Yellow Reports: Monographs. Geneva: CERN, 1998. [Online]. Available: http://cds.cern.ch/record/357576

[34] C. Scheuerlein, "Radiation tests program of the CERN Polymer Laboratory ," CERN, Geneva, Tech. Rep. EDMS #2563597, January 2023. [Online]. Available: https://edms.cern.ch/document/2563597/2

[35] D. M. Parragh, C. Scheuerlein, F. Ravotti, and G. Pezzullo, "DMA temperature sweeps of polymers before and after 24 GeV proton irradiation in dry air at $-20\,^{\circ}$C," CERN, Geneva, Tech. Rep. EDMS #2823296, April 2023. [Online]. Available: https://edms.cern.ch/document/2823296/1

[36] D. M. Parragh and C. Scheuerlein, "DMA temperature sweeps of polymers before and after 24 GeV proton irradiation in liquid helium," CERN, Geneva, Tech. Rep. EDMS #2823288, April 2023. [Online]. Available: https://edms.cern.ch/document/2823288/1

[37] C. Scheuerlein, "Radiation test results on cables for orbit correctors (MCBY, MCBC,..)," CERN, Geneva, Tech. Rep. EDMS #2861509, March 2023. [Online]. Available: https://edms.cern.ch/document/2861509/1

[38] D. M. Parragh and C. Scheuerlein, "Effect of gamma irradiation on the thermomechanical properties of MCBY corrector magnet constituent material ISOPREG 2704," CERN, Geneva, Tech. Rep. EDMS #2816963, February 2023. [Online]. Available: https://edms.cern.ch/document/2816963/1

[39] C. Adorisio, S. Le Nour, and L. R. Williams, "Implications of replacing a Q1 magnet," 2017, Presented at the MSC Technical Meeting, 20 June 2017, CERN, Geneva, Switzerland. [Online]. Available: https://indico.cern.ch/event/647021/

[40] S. Le Nour, "Situation of spare for IT magnets and cold D1s," 2023, Presented at 12^{th} Meeting of the LHC Triplet Task Force, 8 June 2023, CERN, Geneva, Switzerland. [Online]. Available: https://indico.cern.ch/event/1281364/

[41] A. Garcia-Tabares Valdivieso, L. Malina, B. M. Salvachua Ferrando, P. K. Skowronski, M. Solfaroli Camillocci, R. Tomas Garcia, J. Wenninger, and J. M. Coello De Portugal Martinez Vazquez, "MD Test of a Ballistic Optics," CERN, Tech. Rep., 2016. [Online]. Available: https://cds.cern.ch/record/2120149

[42] F. Soubelet, T. Persson, R. Tomás, O. Apsimon, and C. P. Welsch, "Rigid Waist Shift: A New Method for Local Coupling Corrections in the LHC Interaction Regions," *Phys. Rev. Accel. Beams*, vol. 26, May 2023. [Online]. Available: https://link.aps.org/doi/10.1103/PhysRevAccelBeams.26.051001

[43] F. Soubelet, O. Apsimon, T. Persson, R. Tomás García, and C. Welsch, "First Interaction Region Local Coupling Corrections in the LHC Run 3," in *Proceedings of the 13th International Particle Accelerator Conference*, vol. IPAC2022. JACoW Publishing, Geneva, Switzerland, 2022.

[44] F. Soubelet, "Prospect of Operating with Limited Skew Quadrupole Corrector Availability in the LHC Interaction Regions," in *Proceedings of the 14th International Particle Accelerator Conference (IPAC'23), Venice, May 7-12, 2023*, vol. IPAC2023. JACoW Publishing, 2023, paper MOPL044.

[45] F. Soubelet, "Local Interaction Region Coupling Correction for the LHC," Ph.D. dissertation, University of Liverpool, 2023.

[46] C. Garion and S. Le Nour, "Roll application on Q3 or Q2 to compensate a MQSX Failure," 2023, Received on 10 July 2023. [Online]. Available: https://indico.cern.ch/event/1326841/

[47] E. H. Maclean, R. Tomás, F. S. Carlier, M. S. Camillocci, J. W. Dilly, J. Coello de Portugal, E. Fol, K. Fuchsberger, A. Garcia-Tabares Valdivieso, M. Giovannozzi, M. Hofer, L. Malina, T. H. B. Persson, P. K. Skowronski, and A. Wegscheider, "New approach to LHC optics commissioning for the nonlinear era," *Phys. Rev. Accel. Beams*, vol. 22, no. 6, p. 061004, Jun. 2019. [Online]. Available: https://link.aps.org/doi/10.1103/PhysRevAccelBeams.22.061004

[48] S. Fartoukh, "Achromatic Telescopic Squeezing Scheme and Application to the LHC and its Luminosity Upgrade," *Phys. Rev. ST Accel. Beams*, vol. 16, Nov. 2013.

[49] S. Fartoukh *et al.*, "Round Telescopic Optics with Large Telescopic Index," CERN, Geneva, Tech. Rep., 2018. [Online]. Available: https://cds.cern.ch/record/2643258

[50] G. Deferne, "Results of the magnetic measurements performed on the HCMBXW_001-BI000027 dipole for the study of LHC D1 reconfiguration in case of a magnet failure," CERN, Geneva, Tech. Rep. EDMS #2953929, 2023. [Online]. Available: https://edms.cern.ch/document/2953929/1.0

[51] The Fidel team, "MCBX Fidel magnet report," Aug. 2009. [Online]. Available: https://lhc-div-mms.web.cern.ch/tests/MAG/Fidel/

[52] S. Fartoukh *et al.*, "About flat telescopic optics for the future operation of the LHC," CERN-ACC-2018-0018, CERN, Tech. Rep., 2018. [Online]. Available: https://cds.cern.ch/record/2622595

[53] ——, "First High-Intensity Beam Tests with Telescopic Flat Optics at the LHC," CERN-ACC-2019-0052, CERN, Tech. Rep., 2019. [Online]. Available: https://cds.cern.ch/record/2687343

[54] R. Bruce *et al.*, "Updated parameters for HL-LHC aperture calculations for proton beams," CERN-ACC-2017-0051, CERN, Tech. Rep., 2017. [Online]. Available: https://cds.cern.ch/record/2274330

[55] M. Solfaroli *et al.*, "Report on the VIC on IR1 IT polarity inversion," CERN, Geneva, Tech. Rep. EDMS #2900264, March 2023. [Online]. Available: https://edms.cern.ch/document/2900264/0.1

[56] S. Fartoukh, "First RP optics version for the 2024 pp run," /afs/cern.ch/eng/lhc/optics/runIII/RunIII_dev/Proton_2024/V0, 2023.

[57] C. Droin, "Beam-beam effects with RP round and flat optics," September 2023. [Online]. Available: https://indico.cern.ch/event/1322290/

[58] R. Chritin and C. Petrone, "Magnetic measurements of the SPS Main Ring quadrupole SPLQS__NWP-00000028," CERN, Geneva, Tech. Rep. EDMS #2869015, 2023. [Online]. Available: https://edms.cern.ch/document/2869015/1

[59] LHCb Collaboration, "Framework TDR for the LHCb Upgrade II — Opportunities in flavour physics, and beyond, in the HL-LHC era," CERN, Geneva, Tech. Rep., 2021. [Online]. Available: https://cds.cern.ch/record/2776420

[60] ALICE Collaboration, "ALICE upgrades during the LHC Long Shutdown 2," CERN, Geneva, Tech. Rep., 2023, 151 pages, 110 captioned figures, 10 tables, submitted to JINST, figures at http://alice-publications.web.cern.ch/node/8965. [Online]. Available: https://cds.cern.ch/record/2847599

[61] ——, "Letter of intent for ALICE 3: A next generation heavy-ion experiment at the LHC," CERN, Geneva, Tech. Rep., 2022, 202 pages, 103 captioned figures, 19 tables. [Online]. Available: https://cds.cern.ch/record/2803563

[62] A. Ciccotelli, R. Appleby, F. Cerutti, K. Buffet, F. Butin, G. Corti *et al.*, "Energy deposition studies for the Upgrade II of LHCb at the CERN Large Hadron Collider," *Phys. Rev. Accel. Beams*, to be submitted.

[63] E. Todesco, Private communication upon contacts with K. Amm, M. Anarella and R. Gupta, July 2021.

[64] D. Evans, J. T. Morgan, R. Sheldon, and G. B. Stapleton, "Post Irradiation Mechanical Properties of Epoxy Resin Glass Composites," Rutherford Laboratory, Chilton, Tech. Rep. RHEL/R 200, 1970. [Online]. Available: https://epubs.stfc.ac.uk/manifestation/33237024/RHEL-R200.pdf

[65] R. LeRoy, "Radiation Resistance of Rogers RX 630," Brookhaven National Laboratory, Tech. Rep. BNL-218926-2020-TECH, 1986.

[66] D. Bossert *et al.*, "Test Results of LHC Interaction Regions Quadrupoles Produced by Fermilab," FNAL, Tech. Rep. FERMILAB-CONF-04-255-TD, 2004. [Online]. Available: https://lss.fnal.gov/archive/2004/conf/fermilab-conf-04-255-td.pdf

[67] A. Yamamoto, Y. Ajima, T. Fujii, E. Hashiguchi, N. Higashi, M. Iida, T. Kanahara, N. Kimura, S. Murai, T. Nakamoto, W. Odajima, T. Ogitsu, K. Ohhata, N. Ohuchi, T. Orikasa, T. Shintomi, S. Sugawara, K. Sugita, K. Tanaka, A. Terashima, and K. Tsuchiya, "Production and measurement of the MQXA series of LHC low- beta insertion quadrupoles,"

IEEE Trans. Appl. Supercond., vol. 15, no. 2 pt.2, pp. 1084–1089, 2005. [Online]. Available: https://cds.cern.ch/record/912250

[68] R. Mompo, "Strip heater YT1142 circuit is open," CERN, Geneva, Tech. Rep. EDMS #555602, 2005. [Online]. Available: https://edms.cern.ch/document/555602/1

[69] A. Yamamoto *et al.*, "Inner Triplet Review," 2007, Presentations at the Inner Triplet Review, 24–25 April 2007, CERN, Geneva, Switzerland. [Online]. Available: https://indico.cern.ch/event/15267/

[70] G. Ninet, "Cold power tests - HCLBX__001-BL000006 ," CERN, Geneva, Tech. Rep. EDMS #1709956, 2016. [Online]. Available: https://edms.cern.ch/document/1709956/1

[71] ——, "Cold power tests - HCLBX__001-BL000007 ," CERN, Geneva, Tech. Rep. EDMS #2038642, 2018. [Online]. Available: https://edms.cern.ch/document/2038642/1

[72] S. Fartoukh, "RP optics and impact on forward physics," September 2023. [Online]. Available: https://indico.cern.ch/event/1318307/

A Definition of acronyms

Below a list of the acronyms used in the report. The magnets are to be intended as super-conducting unless indicated differently.

a-C: amorphous-Carbon
ALARA: As Low As Reasonably Achievable
ATS: Achromatic Telescopic Squeeze
BLM: Beam Loss Monitor
BPM: Beam Position Monitor
COD: Closed Orbit Dipole corrector
D1: separation dipole
D2: recombination dipole
DFBX: electrical distribution feed-box for the Inner Triplet circuits
DFD: configuration of the Q1-Q2-Q3 IT quadrupoles, defocusing-focusing-defocusing in the the horizontal plane for the outgoing proton beam.
DMA: Dynamic Mechanical Analysis
ElQA: Electrical Quality Assurance
EM: Electro-Magnetic
EoL: End of β^*-levelling
EYETS: Extended Year-End Technical Stop
FDF: configuration of the Q1-Q2-Q3 IT quadrupoles, focusing-defocusing-focusing in the the horizontal plane for the outgoing proton beam.
HV: High Voltage
HW: Hardware
HWC: Hardware Commissioning
IP: Interaction Point
IR: Insertion Region
IT: Inner Triplet
HL-LHC: High-Luminosity LHC
LHC: Large Hadron Collider
LMC: LHC Machine Committee
LQS: Normal-conducting SPS Skew-Quadrupole
LS: Long Shutdown
LSS: Long Straight Sections
MA: Maleic Anhydride
MBRC: D2 recombination dipole in the IRs
MBW: Normal-conducting magnet composing the D3/D4 separation/recombination dipoles in the collimation regions IR3 and IR7
MBWMD: Normal-conducting compensator dipole for the ALICE spectrometer in IR2
MBX: D1 separation dipole in IR2 and IR8
MBXW: Normal-conducting magnet composing the D1 separation dipole in IR1 and IR5
MBXWH: Normal-conducting compensator dipole for the LHCb spectrometer in IR8 (long)
MBXWS: Normal-conducting compensator dipole for the LHCb spectrometer in IR8 (short)

MBXWT: Normal-conducting compensator dipole for the ALICE spectrometer in IR2
MCBC: Twin Aperture IR Orbit Corrector
MCBX: IT Nested (vertical/horizontal — a_1/b_1) dipole corrector assembly
MCBXA: IT Dodecapole/sextupole (b_6/b_3) nested corrector assembly (MCSTX) nested with an MCBX corrector
MCBXH: IT Horizontal dipole (b_1) corrector
MCBXV: IT Vertical dipole (a_1) corrector
MCBY: Twin Aperture IR Orbit Corrector (large aperture)
MCBYS: Twin Aperture IR Orbit Corrector (large aperture) used for the separation and crossing bumps.
MCOSX: IT Skew-octupole (a_4) corrector
MCOX: IT Octupole (b_4) corrector
MCSOX: IT Skew-octupole/octupole/skew-sextupole ($a_4/b_4/a_3$) nested corrector assembly
MCSSX: IT Skew-sextupole (a_3) corrector
MCSX: IT Sextupole (b_3) corrector
MCSTX: IT dodecapole/sextupole (b_6/b_3) nested corrector assembly
MCTX: IT Dodecapole (b_6) corrector
MD: Machine Development
MKI: LHC Injection Kicker
MO: Landau Octupoles (arc)
MQSX: IT Skew-quadrupole (a_2) corrector
MQXA: IT Low-β quadrupole magnet supplied from KEK, Japan
MQXB: IT Low-β quadrupole magnet supplied from FNAL, USA
NC: Normal-Conducting
NCR: Non-Conformity Report
NEG: Non-Evaporable Getter
NL: Non-Linear
PC: Power Converter
PIM: Plug-In Module
ppm: part per million
PVA: Polyvinyl Acetate
QPS: Quench Protection System
QRL: Cryogenic Distribution Line
RDT: Resonance Driving Term
RF: Radio-Frequency
RHIC: Relativistic Heavy Ion Collider
RP: Reverse Polarity
RQX: Main IT powering circuit
RTQX2: Trim circuit for the Q2 IT quadrupoles
RU: Rack Unit (unit of height of equipment mounted in a rack frame 1 RU=44.45 mm)
SB: Stable Beam
SC: Super-conducting
TAN: Target Absorber Neutrals (for neutral particles leaving the IP)
TANB: Target Absorber Neutral for IR8
TAS: Target Absorber Secondaries (for particles leaving the IP at large angles)

TCL: Target Collimator for physics debris
TCTP:Target Collimator Tertiary, with BPM pick-up (P)
TEA: Triethanolamine
TFM: Transfer Function Measurement
UPS: Underground survey gallery
VdM: Van der Meer
VIC: Visite d'Inspection Commune
WIC: Warm Interlock Controller
WPS: Wire Positioning System
YETS: Year-End Technical Stop

B Expected Radiation Doses

Element	Maximum dose [MGy] at the end of		
	Run 2	Run 3	Run 3 if RP optics from 2024
Q1.IR1	8.5	23.5	
MCBXV1.IR1	4.0	11.0	9.5
Q2A.IR1	11.0	29.5	23.5
MCBXV2.IR1	1.5	4.0	
Q2B.IR1	5.5	16.0	
MQSX3.IR1	3.5	9.5	8.0
Q3.IR1	5.0	14.0	
MCTX3.IR1	8.5	23.5	16.5
MCSX3.IR1	3.0	7.5	
MCBXV3.IR1	2.5	6.0	
MCOSX3.IR1	7.5	19.0	
MCOX3.IR1	6.5	17.5	
MCSSX3.IR1	4.5	11.5	
MBXW.IR1	50	120	80

Table 18: Maximum radiation dose in the IR1 single bore magnets. Run 3 projections assume: 1) a p–p integrated luminosity production of 80, 90 and 100 fb^{-1} for 2023, 2024 and 2025, respectively; 2) the crossing angle decrease along the fill; 3) the upward/downward crossing swap in ATLAS in the middle of 2025 or, in the case of RP optics adoption from 2024 (where estimates are provided only for a significant subset of magnets), in the middle of 2023. The dose on the MCBXH correctors (outer coil layer — see Section 5.1) is significantly lower than that on the MCBXV (inner coil layer).

Element	Maximum dose [MGy] at the end of		
	Run 2	Run 3	Run 3 if RP optics from 2024
Q1.IR5	7.5	22.5	
MCBXV1.IR5	3.0	9.0	9.0
Q2A.IR5	7.5	22.5	24.0
MCBXV2.IR5	2.0	5.5	
Q2B.IR5	10.5	31.0	
MQSX3.IR5	3.5	10.0	8.0
Q3.IR5	7.5	21.5	
MCTX3.IR5	4.5	13.0	
MCSX3.IR5	2.0	5.5	
MCBXV3.IR5	1.0	3.5	
MCOSX3.IR5	4.0	11.5	
MCOX3.IR5	3.5	10.0	
MCSSX3.IR5	2.0	6.5	
MBXW.IR5	30	80	60

Table 19: Maximum radiation dose in the IR5 single bore magnets. Run 3 projections assume: 1) a p–p integrated luminosity production of 80, 90 and 100 fb^{-1} for 2023, 2024 and 2025, respectively; 2) the crossing angle decrease along the fill. In the case of RP optics adoption from 2024, estimates are provided only for a significant subset of magnets.

Element	Maximum dose [MGy] at the end of		
	Run 3	HL-LHC if no LHCb upgrade	HL-LHC if LS4 LHCb upgrade
MBXWH.1L	4	15	40
MBXWS.IR8	11	40	50
Q1.IR8	4.5 / 6.0	15.0 / 17.0	19.0 / 19.0
MCBXV1.IR8	< 1	2.5	7.0
Q2A.IR8	2.0	7.0	22.0
MCBXV2.IR8	< 1	1.0	2.5
Q2B.IR8	1.0	3.5	12.0
MQSX3.IR8	< 1	2.5	7.5
Q3.IR8	1.0	4.0	12.0
MCTX3.IR8	1.0	4.0	12.5
MCSX3.IR8	< 1	2.5	7.5
MCBXV3.IR8	< 1	1.0	3.5
MCOSX3.IR8	1.5	6.0	17.5
MCOX3.IR8	1.0	4.0	11.5
MCSSX3.IR8	< 1	2.5	7.5
MBXW.IR8	3.0	14.0	16.5

Table 20: Maximum radiation dose in the IR8 single bore magnets according to the p–p integrated luminosity forecasts of Figure 43 for YETS of 15 weeks and assuming that half integrated luminosity is produced with either LHCb spectrometer polarity. For Q1, the values on the left and right of IP8 are separately reported (L/R). In the case of LHCb upgrade during LS4, the implementation of the related mitigation measures described in Section 9.2 is assumed to take place at the same time.

C Proposed currents for HWC and pre-cycle

Circuit	2018		2022			Proposal 2023
	I_OP	I_PNO	I_OP	I_OP (NO IP bumps)	I_PNO	I_PNO
RCBXH1.L1	109.7	500	85.8	85.8	500	300
RCBXH2.L1	122.0	500	83.5	83.4	500	300
RCBXH3.L1	4.1	500	68.3	68.3	500	300
RCBXV1.L1	94.8	500	-81.3	-32.6	500	300
RCBXV2.L1	93.0	500	-78.4	-34.7	500	300
RCBXV3.L1	0.5	500	-23.4	25.2	500	300
RCBXH1.R1	-80.7	500	53.1	53	500	300
RCBXH2.R1	215.8	500	38.6	38.5	500	300
RCBXH3.R1	-81.1	500	81.0	81	500	300
RCBXV1.R1	-258.4	500	-145.2	-193.8	500	300
RCBXV2.R1	-220.4	500	-169.4	-218	500	300
RCBXV3.R1	-218.8	500	-125.1	-177.7	500	300
RCBXH1.L5	255.7	490	103.3	57.4	490	300
RCBXH2.L5	228.8	500	60.0	14.8	500	300
RCBXH3.L5	-103.2	500	29.1	-16.8	500	300
RCBXV1.L5	16.4	500	-38.6	-47	500	300
RCBXV2.L5	-94.0	500	-155.6	-171.2	500	300
RCBXV3.L5	113.0	500	93.2	114.6	500	300
RCBXH1.R5	44.0	500	88.6	134.5	500	300
RCBXH2.R5	7.6	500	52.8	98.7	500	300
RCBXH3.R5	56.4	500	24.8	70.7	500	300
RCBXV1.R5	-33.0	500	17.8	20.3	500	300
RCBXV2.R5	-58.2	500	-117.6	-117.6	500	300
RCBXV3.R5	122.4	500	100.9	100.9	500	300
RQSX3.L1	162.2	550	177.4		550	300
RQSX3.R1	88.5	550	54		550	300
RQSX3.L5	103.2	550	61.7		550	300
RQSX3.R5	103.2	540	123.4		540	300

Table 21: Proposal of modification of the powering test current values (I_PNO) for the IT 600 A correctors in IR1 and IR5 implemented for the 2023 HWC. The operational currents (I_OP) used in 2018 and 2022 are also listed together with the values of the currents (I_OP (NO IP bumps)) at which the MCBX circuits were operated when the crossing/separation bumps were not activated. As an example it must be noted that in the LHC naming convention RCBXH1.L1 is the circuit corresponding to the magnet MCBXH1.L1 - i.e. the horizontal orbit corrector installed in Q1 at the left of IP1.

Circuit	2018		2022		Proposal 2023
	I_OP	I_PNO	I_OP	I_PNO	I_PNO
RCSX3.L1	7.7	100	2.24	100	50
RCSX3.R1	3.2	100	-6.7	100	50
RCSX3.L5	6.4	100	7.4	100	50
RCSX3.R5	16.5	100	11.8	100	50
RCSSX3.L1	-9.9	15	-11.5	15	15
RCSSX3.R1	-15.7	100	-14.8	100	50
RCSSX3.L5	6.1	100	7.2	100	50
RCSSX3.R5	15.1	100	14.2	100	50
RCOX3.L1	33.4	100	33.4	100	70
RCOX3.R1	-43.2	100	-43.2	100	70
RCOX3.L5	33.9	100	33.9	100	70
RCOX3.R5	-25.4	100	-25.5	100	70
RCOSX3.L1	NC 948545: circuit open below the cold V-taps of the current leads				
RCOSX3.R1	19.8	100	0	0	50
RCOSX3.L5	-10	100	0	0	50
RCOSX3.R5	-10.4	100	0	0	50
RCTX3.L1	0	80	-1.3	-1.3	50
RCTX3.R1	0	80	-5.6	-5.6	50
RCTX3.L5	0	80	10.5	10.5	50
RCTX3.R5	0	80	-10.6	-10.6	50

Table 22: Proposal of modification of the powering test current values for the NL IT correctors in IR1/IR5 implemented for the 2023 HWC.

Circuit	2018		2022			2023 Ions	Proposal 2024
	I_OP	I_PNO	I_OP	I_OP (NO IP bumps)	I_PNO	I_PNO	I_PNO
RCBXH1.L2	-20.4	500	NC 2439965				
RCBXH2.L2	-92.1	500	-108.2	13.6	500	-144.7	400
RCBXH3.L2	-192.1	500	-294.5	13.6	500	-293.9	400
RCBXV1.L2	8.8	500	20.1	123.2	500	25.3	400
RCBXV2.L2	241.1	500	202.3	123.2	500	127.9	400
RCBXV3.L2	-129.4	500	-34.3	123.2	500	-53.7	400
RCBXH1.R2	139.2	500	52.1	9.1	500	207.6	400
RCBXH2.R2	155.6	500	89.1	9.1	500	265.8	400
RCBXH3.R2	-68.8	500	0.6	9.1	500	155.4	400
RCBXV1.R2	-214.7	500	-87.8	-123.2	500	-117.6	400
RCBXV2.R2	-241.9	500	-147.1	-123.2	500	-90.5	400
RCBXV3.R2	15.8	500	-134.4	-123.2	500	-72.5	400
RCBXH1.L8	-150.4	500	84.1	-116.2	500	137.6	400
RCBXH2.L8	-378.5	500	-181.9	-116.2	500	-85.5	400
RCBXH3.L8	-141.4	500	68	116.2	500	165.2	400
RCBXV1.L8	-4.7	500	-38.2	-3.8	500	-189.6	400
RCBXV2.L8	-1	500	-62.4	-3.8	500	-261.8	400
RCBXV3.L8	-53.7	500	-4.3	-3.8	500	-235.2	400
RCBXH1.R8	58.5	500	236.6	116.2	500	205.7	400
RCBXH2.R8	-86	500	-92.7	116.2	500	-85.7	400
RCBXH3.R8	343.4	500	133.2	116.2	500	62.7	400
RCBXV1.R8	29.7	500	56.8	-3.8	500	96.3	400
RCBXV2.R8	190.3	500	120.7	-3.8	500	126.6	400
RCBXV3.R8	-16.5	500	22.8	-3.8	500	-225.2	400
RQSX3.L2	-206.4	550	-216		550	-300.9	400
RQSX3.R2	-206.4	550	-216		550	-154.3	400
RQSX3.L8	-73.7	550	-77		550	-77.1	300
RQSX3.R8	-73.7	550	-77		550	-77.1	300

Table 23: Proposal of modification of the powering test current values (I_PNO) for the IT 600 A correctors in IR2 and IR8. The operational currents (I_OP) used in 2018, 2022 and during the ion run in 2023 are also listed together with the values of the currents (I_OP (NO IP bumps)) at which the MCBX circuits were operated when the crossing/separation bumps were not activated in 2022.

Circuit	2018		2022		Proposal 2024
	I_OP	I_PNO	I_OP	I_PNO	I_PNO
RCSX3.L2 (IONS)	-50.7	100	0	100	70
RCSX3.R2 (IONS)	8.9	100	0	100	50
RCSX3.L8	0	100	0	100	50
RCSX3.R8	0	100	0	100	50
RCSSX3.L2	NC 1203479				
RCSSX3.R2	0	100	0	100	50
RCSSX3.L8	0	100	0	100	50
RCSSX3.R8	0	100	0	100	50
RCOX3.L2	NC 1203478				
RCOX3.R2	0	100	0	100	50
RCOX3.L8	0	100	0	100	50
RCOX3.R8	0	100	0	100	50
RCOSX3.L2	NC 1203477				
RCOSX3.R2	0	100	0	100	50
RCOSX3.L8	0	100	0	100	50
RCOSX3.R8	0	100	0	100	50
RCTX3.L2	0	80	0	80	50
RCTX3.R2	0	80	0	80	50
RCTX3.L8	0	80	0	80	50
RCTX3.R8	0	80	0	80	50

Table 24: Proposal of modification of the powering test current values for the NL IT correctors in IR2/IR8

Circuit	Pre-cycle	
	2022	New proposal
RCBXH1.L1	200	0
RCBXH2.L1	200	0
RCBXH3.L1	200	0
RCBXV1.L1	0	0
RCBXV2.L1	0	0
RCBXV3.L1	0	0
RCBXH1.R1	200	0
RCBXH2.R1	200	0
RCBXH3.R1	200	0
RCBXV1.R1	0	0
RCBXV2.R1	0	0
RCBXV3.R1	0	0
RCBXH1.L5	200	0
RCBXH2.L5	200	0
RCBXH3.L5	200	0
RCBXV1.L5	0	0
RCBXV2.L5	0	0
RCBXV3.L5	0	0
RCBXH1.R5	200	0
RCBXH2.R5	200	0
RCBXH3.R5	200	0
RCBXV1.R5	0	0
RCBXV2.R5	0	0
RCBXV3.R5	0	0
RQSX3.L1	200	100
RQSX3.R1	200	100
RQSX3.L5	200	100
RQSX3.R5	200	100

Circuit	Pre-cycle	
	2022	New proposal
RCSX3.L1	0	0
RCSX3.R1	0	0
RCSX3.L5	0	0
RCSX3.R5	0	0
RCSSX3.L1	78	0
RCSSX3.R1	100	0
RCSSX3.L5	100	0
RCSSX3.R5	100	0
RCOX3.L1	0	0
RCOX3.R1	0	0
RCOX3.L5	0	0
RCOX3.R5	0	0
RCOSX3.L1	NC 948545	
RCOSX3.R1	0	0
RCOSX3.L5	0	0
RCOSX3.R5	0	0
RCTX3.L1	0	0
RCTX3.R1	0	0
RCTX3.L5	0	0
RCTX3.R5	0	0

Table 25: Proposal of modification of the pre-cycle currents for the IT correctors in IR1 and IR5 implemented for the 2023 HWC.

Circuit	Pre-cycle	
	2022	New proposal
RCBXH1.L2	NC 2439965	
RCBXH2.L2	200	0
RCBXH3.L2	200	0
RCBXV1.L2	0	0
RCBXV2.L2	0	0
RCBXV3.L2	0	0
RCBXH1.R2	200	0
RCBXH2.R2	200	0
RCBXH3.R2	200	0
RCBXV1.R2	0	0
RCBXV2.R2	0	0
RCBXV3.R2	0	0
RCBXH1.L8	200	0
RCBXH2.L8	200	0
RCBXH3.L8	200	0
RCBXV1.L8	0	0
RCBXV2.L8	0	0
RCBXV3.L8	0	0
RCBXH1.R8	200	0
RCBXH2.R8	200	0
RCBXH3.R8	200	0
RCBXV1.R8	0	0
RCBXV2.R8	0	0
RCBXV3.R8	0	0
RQSX3.L2	200	100
RQSX3.R2	200	100
RQSX3.L8	200	100
RQSX3.R8	200	100

Circuit	Pre-cycle	
	2022	New proposal
RCSX3.L2 (IONS)	0	0
RCSX3.R2 (IONS)	0	0
RCSX3.L8	0	0
RCSX3.R8	0	0
RCSSX3.L2	NC 1203479	
RCSSX3.R2	100	0
RCSSX3.L8	100	0
RCSSX3.R8	100	0
RCOX3.L2	NC 1203478	
RCOX3.R2	0	0
RCOX3.L8	0	0
RCOX3.R8	0	0
RCOSX3.L2	NC 1203477	
RCOSX3.R2	0	0
RCOSX3.L8	0	0
RCOSX3.R8	0	0
RCTX3.L2	0	0
RCTX3.R2	0	0
RCTX3.L8	0	0
RCTX3.R8	0	0

Table 26: Proposal of modification of the pre-cycle currents for the IT correctors in IR2 and IR8.

D Breakdown of the activities required for the D1 magnets replacement or displacement in IR1/5

	Working zones		
	DFBX-MBXW	Distributed over the area DFBX-TAN	MBXW-TAN
1 week	Removing equipment around the first MBXW (TE-MPE, BE-GM, HSE-RP. . .)		Vacuum de-interconnection (TE-VSC)
	MBXWs water and cable disconnection (TE-MSC)		MBXWs water and cable disconnection (TE-MSC)
	Vacuum de-interconnection (TE-VSC)		
1 week+*1 week(IP1)*	*Disassembly shielding wall IP1 (EN-HE)*		
	Exchange 2 MBXWs	Exchange 2 MBXWs	Exchange 2 MBXWs
	Re-installation shielding (EN-HE)		
2 weeks	Vacuum interconnections (TE-VSC)		Vacuum interconnections (TE-VSC)
	Preparation of the bake-out installation and cabling (TE-VSC)	Preparation of the bake-out installation and cabling (TE-VSC)	Preparation of the bake-out installation and cabling (TE-VSC)
	Re-calibration WPS (BE-GM)		
	Cable and water hoses connection, purge (TE-MSC)	Cable and water hoses connection, purge (TE-MSC)	Cable and water hoses connection, purge (TE-MSC)
2.5 days	Alignment (BE-GM)	Alignment (BE-GM)	Alignment (BE-GM)
10 days	Bake out	Bake out	Bake out
3 days	Re-installation ancillaries (TE-MPE, BE-GM)		

Table 27: List of the activities for removing the presently installed first MBXW on the IP side and swapping it with one of the magnets installed downstream. The duration is estimated in case of a planned intervention during a YETS.

	Working zones		
	DFBX-MBXW	Distributed over the area DFBX-TAN	MBXW-TAN
1 week	Removing equipment around the first MBXW (TE-MPE, BE-GM, HSE-RP...)		
	MBXWs water and cable disconnection (TE-MSC)		
	Vacuum de-interconnection (TE-VSC)		
1 week+*1 week (IP1)*	*Disassembly shielding wall IP1 (EN-HE)*		
	Replacement of the MBXW		
	Re-installation shielding (EN-HE)		
2 weeks	Vacuum interconnections (TE-VSC)		
	Preparation of the bake-out installation and cabling (TE-VSC)	Preparation of the bake-out installation and cabling (TE-VSC)	Preparation of the bake-out installation and cabling (TE-VSC)
	Re-calibration WPS (BE-GM)		
	Cable and water hoses connection, purge (TE-MSC)		
2 days	Alignment (BE-GM)	Alignment (BE-GM) only D1 area	
10 days	Bake out	Bake out	Bake out
3 days	Re-installation ancillaries (TE-MPE, BE-GM)		

Table 28: List of the activities for replacing the first MBXW on the IP side with a spare. The duration is estimated in case of a planned intervention during a YETS.

E Breakdown of the activities required for the installation of warm skew quadrupoles in the IR

Duration	Working zones		
	DFBX-MBXW	Distributed over the area DFBX-TAN	MBXW-TAN
1.5 week	Removing equipment around the first MBXW (TE-MPE, BE-GM, HSE-RP. . .)	MBXWs water and cable disconnection (TE-MSC)	Disassembly of the present vacuum line (TE-VSC)
	Vacuum de-interconnection (TE-VSC)	Cable elongation (EN-EL)	Tracing of new equipment position (BE-GM-ASG)
			Installation of the new supports (EN-ACE)
			Preparation new water connections (EN-CV)
			Preparation of the new vacuum system (TE-VSC)
1 week+*1 week (IP1)*	*Disassembly shielding wall IP1 (EN-HE)*		
		Displacement of the first MBXW (EN-HE)	
	Tracing new equipment on the floor (BE-GM-ASG)		Installation MBXW new position (EN-HE)
	Installation new cables for warm skew quadrupole		
	Re-installation shielding (EN-HE)		
2 weeks	Installation new supports in newly freed area DFBS/MBXW (EN-ACE, TE-VSC, BE-GM)		Vacuum mechanical installation and connection of the displaced MBXW (TE-VSC)
	Re-calibration WPS (BE-GM)		Preparation of the bake-out installation and cabling (TE-VSC)
	Installation new warm skew quadrupole		
	Cable and water hoses connection, purge (TE-MSC)	Cable and water hoses connection, purge (TE-MSC)	Cable and water hoses connection, purge (TE-MSC)
1.5 weeks	Alignment (BE-GM)	Alignment (BE-GM)	Alignment (BE-GM)
	Vacuum closure (TE-VSC)		
	Bake-out preparation (TE-VSC)		
10 days	Bake out	Bake out	Bake out
3 days	Re-installation ancillaries (TE-MPE, BE-GM)		

Table 29: List of the activities for the LQS installation between the MBXW and the DFBX with MBXW relocation, provided the relevant equipment is available.The duration is estimated in case of a planned intervention during a YETS.

	Working zones		
	DFBX-MBXW	Distributed over the area DFBX-TAN	MBXW-TAN
1 week			Disassembly of the present vacuum line (TE-VSC)
			Tracing of new equipment position (BE-GM-ASG)
			Installation of the new supports (EN-ACE)
			Preparation new water connections (EN-CV)
	Bake out preparation (TE-VSC)	Bake out preparation (TE-VSC)	Preparation of the new vacuum system (TE-VSC)
2 weeks		Installation new DC cables	Installation new DC cables
			Installation new warm skew quadrupole
			Cable and water hoses connection, purge (TE-MSC)
			Vacuum closure (TE-VSC)
			Preparation of the bake-out installation and cabling (TE-VSC)
		Cable and water hoses connection, purge (TE-MSC)	Cable and water hoses connection, purge (TE-MSC)
	Alignment (BE-GM)	Alignment (BE-GM)	Alignment (BE-GM)
10 days	Bake out	Bake out	Bake out

Table 30: List of the activities for the LQS installation on the non-IP side of the D1, provided the relevant equipment is available. The duration is estimated in case of a planned intervention during a YETS.